# MICROFACIES AND RELATED DIAGENESIS OF THE TUWAIQ MOUNTAIN FORMATION, CENTRAL SAUDI ARABIA

BY

**MAHMOUD MOHAMMED SAMIR DESOUKY NOUR EL YAMANI**

A Thesis Presented to the
DEANSHIP OF GRADUATE STUDIES

**KING FAHD UNIVERSITY OF PETROLEUM & MINERALS**

DHAHRAN, SAUDI ARABIA

In Partial Fulfillment of the
Requirements for the Degree of

## MASTER OF SCIENCE

In

**GEOLOGY**

**JANUARY 2017**

KING FAHD UNIVERSITY OF PETROLEUM & MINERALS

DHAHRAN- 31261, SAUDI ARABIA

**DEANSHIP OF GRADUATE STUDIES**

This thesis, written by Mahmoud Mohammed Samir Desouky Nour El-Yamani under the direction by his thesis advisor and approved by his thesis committee, has been presented and accepted by the Dean of Graduate Studies, in partial fulfillment of the requirements for the degree of Master of Science in Geology

Dr. Khalid Al Ramadan
(Advisor)

Dr. Abdulaziz Al-Shaibani
Department Chairman

Dr. Dave Cantrell
(Co-Advisor)

Dr. Salam A. Zummo
Dean of Graduate Studies


Prof. Dr. Axel Munnecke
(Member)

6/6/17
Date

Dr. Abdullah Sultan
(Member)

Dr. Waleed Abdulghani
(Member

## Dedication

This thesis would not have been possible without the support, guidance and pray of my family. Therefore, my humble efforts I dedicated to

My Mother

The person that is like no other. The person who feels what I am thinking of without talking. She gave me life, taught me, held me, shouted at me but most importantly loved me unconditionally.

My Father

The person who spent days and nights to facilitate everything to me. The person who gave me the greatest gift anyone could ever give another person. He believed in me!

My brother and sisters

The persons who are ready to face with me whatever life sends. Joy, laughter or tears and strife, holding hands tightly as we face life together

My beloved country Egypt

# ACKNOWLEDGMENTS

I would like to thank Geosciences Department and King Fahd University of Petroleum & Minerals (KFUPM) for giving me the scholarship to study Master of Science in geology. Special thanks go out to my advisor Dr. Khalid Al Ramadan for his support, patience, help, guidance and effort throughout my life in KFUPM. Thanks are extended to my co-advisor Dr. Dave Cantrell for his support and fruitful discussion. Also, I want highly to express my gratitude to the support and guidance from Prof. Axel Munnecke. Moreover, I would like to thank Dr. Abdullah Sultan and Dr. Waleed Abdulghani for his their help and support during my work

Special thanks are forwarded to Geology Department at Ain Shams University and its faculty for their support to allow me to have a short leave vacation to complete my Masters at KFUPM. I want to express my gratitude to Prof. Yasser el Safori, Prof. Abdelmohsen, Prof. Adel Ramadan, Prof. Baher el Kaliouby, Prof. Hafez Shamseldin, Prof. Mahmoud Abouzaid and Dr. Ashraf Baghdady.

For the people who helped me through my work, I would like to thank you all, especially; Dr. Abduljamiu Amao for his help during doing SEM. Assistance in the field by Abdulkarim Al-Hussaini, Mohammad Al-Sadah and Mohammad Malik is gratefully acknowledged. Also, I would like to thank; Mr. Mushabab, Mr. Aziz, Mr. Abdulrahman El Ghamdi, Mr. Louie, Mr. Abbas and Mr. Abdulmalik for helping me in lab work. Special thanks to Centre of Nanotechnology, Dr. Zain Yamani and Dr. Abbas Hakim for allowing me to do XRD analysis.

Thanks are extended to my friends; Pradipta, Septriandi, Lukas, Omar Radwan, Mohammed Mahrous, Ahmad Al-Rashidy and Dr. Ammar for their help. Also, I would

like to thank all my friends and especially the Egyptian community who made me feel being in my home country.

# TABLE OF CONTETNS

# LIST OF TABLES

# LIST OF FIGURES

# ABSTRACT

Full Name : Mahmoud Mohammed Samir Desouky Nour El Yamani

Thesis Title : Microfacies and Related Diagenesis of The Tuwaiq Mountain Formation, Central Saudi Arabia

Major Field : Geosciences

Date of Degree : January 2017

The Tuwaiq Mountain Formation (TMF) represents one of the most important intervals within the Jurassic succession in Saudi Arabia because it encompasses two hydrocarbon reservoirs in the Khurais and Ghawar fields (Upper Fadhili reservoir and Hadriya reservoir), one source rock interval, and one unconventional reservoir interval in the Jafura basin. Compared with other intervals within the Jurassic succession in Saudi Arabia, little studies and publications encountered the TMF, especially with respect to microfacies, depositional environment, digenesis and controls on petrophysical properties. Therefore, this study aims to integrate field work, petrography, X-ray diffraction technique, X-ray fluorescence, cathodluminescence and scanning electron microscopy in order to determine the different microfacies and their depositional environment, build a 3D conceptual depositional model, define different diagenetic alterations and their environment and finally determine the controls on petrophysical properties.

Eight microfacies types are identified in the TMF in the Shaqra quadrangle (MF 1 coral rudstone, MF 2 coral rudstone with intraclsts and coated grains, MF 3 coral floatstone, MF4 spiculitic wackstone, MF 5 worn and coated foraminiferal wack/pack-stone, MF 6 non laminated peloidal grainstone, MF7 peloidal packstone and MF 8 peloidal grainstone). The microfacies analysis showed that it was deposited in the interior part of a rimmed

carbonate platform. These facies were deposited in several depositional environments including; deep lagoon, shallow lagoon and shoal. In addition to carbonate sedimentation, XRF results show a signature of siliciclastic input which may be attributed to a tidal channel and/or windblown dust as shield derived siliciclastic input.

The facies stacking pattern of the TMF in the study area shows a general shallowing upward in which deep lagoonal sediments are overlain by shallow lagoon and finally shoal derived sediments. This trend represents a major regressive cycle within the TMF. This major cycle can be further subdivided into medium and small scale cycles. The cyclicity analysis suggests that the scale of small scale and medium scale cycles are probably of $4^{th}$ and $5^{th}$ order, respectively, which may be accounted for by orbitally driven high frequency eustatic fluctuations (Milankovitch cycles).

The TMF has a complex diagenetic history as it includes; micritization, mechanical compaction, dissolution, recrystallization, meteoric cementation, evaporite precipitation and dolomitization, silicification, fracturing, evaporite dissolution and dolomite calcitization. The geochemical analysis using X-ray diffraction technique and X-ray fluorescence reveals that meteoric diagenesis have left a severe signatures on the studied interval. The lack of early marine cementation allowed slight compaction (interpenetrating grain contact and concavo-convex boundaries) to occur but these rocks were never deeply buried (as evidenced by the lack of stylolitization and burial cements). By integrating XRD, XRF and petrography, the dolomitization mechanism may be attributed to hypersaline fluids based on texture, association with evaporites and Sr concentration of 800-1200 ppm. On other hand, silicification, which can be locally common in the TMF, is interpreted to have occurred via leaching and reprecipitating of sponge spicules. Moreover, the dolomite

calcitization is suggested to result from meteoric fluids as the rhombohedral pores are filled with equant crystals of calcite cement.

The porosity and permeability measurements of TMF indicate that reservoir quality is generally poor in both mud dominated and grain dominated facies, with porosity ranging from less than 2 % to a maximum of 19 %, and permeability in most cases below 1 mD. The reason for poor reservoir quality in the grain dominated facies is that extensive meteoric cementation has occluded the primary and secondary porosity. In contrast, in the mud dominated facies, reservoir quality is poor due to the original muddy texture of the sediment and the extensive meteoric cementation which has occluded primary and secondary porosity. Meteoric diagenesis can also have a positive effect on pore space evolution as it formed vuggy and moldic porosities by meteoric dissolution. This diagenetic alteration was more prominent in grain dominated facies than mud dominated facies. In addition, the contact angle measurements of different facies in the TMF revealed that the microfacies heterogeneity (in terms of surface rock chemistry, texture, and organic matter content) of the studied interval has a great impact on wettability and contact angle.

# ملخص الرسالة

**الاسم الكامل: محمود محمد سمير دسوقي نور اليماني**

**عنوان الرسالة: السحنات المجهريه و عمليات ما بعد النشأة لمتكون جبل الطويق، مركز المملكة العربية السعودية**

**التخصص: الجيولوجيا**

**تاريخ الدرجة العلمية: يناير 2017**

إن متكون جبل الطويق هو احد اهم المتكونات في تتابع العصر الجوراسي في المملكة العربية السعودية لأحتوائه على خزانين (فاضلي العلوي و حدريه) في حقلي الغوار و خريص و طبقة منشأ و خزان غير تقليدي في حقل جافوره. بمقارنة متكون جبل الطويق بباقية متكونات العصر الجوراسي سنجد عدد مقالات اقل و خاصة في مجال السحنات الصخرية المجهرية، بيئات الترسيب، عمليات ما بعد الترسيب و العوامل المسيطرة على الخواص البتروفيزيقائيه، و لذلك فان هذه الدراسه تهدف إلي دمج الدراسات الحقليه، البتروجرافيه، استخدام تقنيات تشتت الحيود السيني، وميض الحيود السيني والإستضاءة بالأشعة الكاثوديه و استخدام المجهر الماسح الألكتروني و ذلك لأجل التعرف على السحنات الصخرية المجهرية المختلفة، بيئات الترسيب، بناء نموذج ترسيب ثلاثي الابعاد، التعرف على بيئات و عمليات ما بعد الترسيب المختلفه و تحديد العوامل المسيطره على الخواص البتروفيزيقائيه لمتكون جبل الطويق.

تم التعرف على ثمان سحنات صخرية مجهرية و التي اوضحت ان متكون الطويق في منطقة شقراء قد ترسب في الجزء الداخلي من الرصيف الجيري المؤطر في ثلاث بيئات ترسيب و هم اللاغون العميق، اللاغون الضحل و الرصيف الصخري. علاوة على ذلك, اوضحت نتائج وميض الحيود السيني ان هناك مصدر لبعض الرواسب التفتتيه و التي قد يكون مصدرها من قناة مديجزري و/أو من هبوب الرياح من الدرع العربي.

إضافة إلى ذلك، اوضح تتابع السحنات الصخرية المجهرية ان هناك ميل للضحاله راسيا بالتدرج من اللاغون العميق للاغون الضحل و من ثم للرصيف الصخري. كما اوضحت الدراسة الدورويه ان الدورات متوسطة المقياس و صغيرة المقياس قد تكون من المرتبه الرابعة و الخامسة بنفس الترتيب. سبب هذه الدورويه قد يكون التغير في مستوى سطح البحر عن طريق دورات ميلانكوفيتش.

إن تاريخ عمليات ما بعد الترسيب لمتكون جبل الطويق يعتبر معقد لدرجه كبيره و ذلك لأحتوائه على: المكرته، الأنضغاط المكيانيكي، التحلل، اعاده تكوين الكرستالات، لاحم المياه العذبة، تكوين المتبخرات و الدولميت، التسليك، التشقق و من ثم اذابة المتبخرات و تحول الدولميت لكالسيت. التحاليل الجيوكيميائية باستخدام تقنيات تشتت الحيود السيني، وميض الحيود السيني اوضح وجود تأثير جم من عمليات النشأة المتأخرة المتعلقه ببيئة المياه العذبة على متكون جبل الطويق. علاوة على ذلك اوضح ان عدم وجود لاحم من اصل مياة بحريه أدي إلى وجود إنضغاط ميكانيكي بسيط. كما اوضحت استخدام تقنيات تشتت الحيود السيني، وميض الحيود السيني والإستضاءة بالأشعة الكاثوديه و استخدام المجهر الماسح الألكتروني ان مصدر المتبخرات و عملية الدلمته كان من موائع عالية الملوحه و على الجانب الاخر اتضح ان مصدر عمليت التسليك نابع من داخل متكون جبل الطويق و ذلك لأحتوائه على نسبه كبيره من الاحافير ذات تركيب كيميائي من السليكون. أما عملية تكلس الدولميت فأنها نشأت من موائع المياه العذبه التي اذابت المتبخرات و كونت موائع عالية التركيز من ايون الكالسيوم مما أدى إلى تكلس الدولميت.

اوضحت نتائج اخبارت المسامية و النفاذية لمتكون جبل الطويق انها تعتبر ضعيفه. و يعود هذا إلى قوة لاحم المياه العذبه التي تسببت في ملئ المسامات الاولية و الثانوية. على الجانب الاخر، ادت عمليات ما بعد الترسيب ذات بيئة المياه العذبة إلى تحسين خواص المساميه و النفاذيه بعض الشئ عن طريق اذابه بعد انواع المعادن الغير ثابتة تحت تلك الطروف مما كون مسامات فجويه. علاوة على ذلك اوضحت قياسات نقطة الالتقاء ان اختلاف السحنات له تأثر جم على اختلاف قياسات نقط الالتقاء بسبب اختلاف النسيج، المحتوي العضوي و طبيعة تركيز العناصر على سطح الصخر.

# CHAPTER 1

# Introduction

## 1.1. Carbonate Reservoirs

Carbonate rocks are sedimentary rocks that are fundamentally composed of carbonate minerals such as calcite, aragonite, and dolomite. The most common carbonate rocks are limestones, which are composed of calcite and/or aragonite, and dolostone, which is composed of dolomite. In 2007, Schlumberger's Market Analysis revealed that carbonate reservoirs held around 60 % of the World's oil and 40 % of the World's gas. In 2008, BP Statistical Review revealed that around 70 % of the proven conventional oil reserves of the Middle East are held in carbonate reservoirs. These analyses show the great importance of carbonate rocks as hydrocarbon reservoirs. Therefore, it is axiomatic that carbonate rocks should be for scientific research in areas of petroleum geosciences and engineering. Figure 1 shows the distribution of carbonate reservoirs vs. siliciclastic reservoirs all over the world. From this figure we can see how the carbonate reservoirs are dominant in the Arabian Gulf countries compared with siliciclastic reservoirs; and as a consequence, it is appropriate that more scientific research will focus on carbonate reservoirs than sandstone reservoirs.

In the last ten years, the interest in carbonate reservoirs has escalated. This interest was largely motivated by both the increasing demand on power and the importance of carbonate reservoirs in the oil industry. Analyses from Scopus using 'carbonate*'and 'reservoir*' or 'unconventional' as key words and limit-to subarea 'Earth' (accessed 2 November 2015) revealed that from 1967 to 2015, 8918 publications were published on subjects related to

carbonate reservoirs, and Saudi Arabia was ranked the sixth in the world in the number of publications by country/territory (Fig. 2). The same style of Scopus analyses on sandstone publications were done by using 'sandstone*'and 'reservoir*' or 'unconventional' as key words and limit-to subarea 'Earth' (accessed 2 November 2015). These analyses revealed that from 1912 to 2015, 8460 publications were done on subjects related to sandstone reservoirs, and Saudi Arabia was ranked the ninth in the world in the number of publications by country/territory (Fig. 3). These analyses show the significant scientific interest in carbonate reservoirs subjects' globally and that research in Saudi Arabia is central to that interest. Within the analyses from Scopus using 'carbonate*'and 'reservoir*' or 'unconventional' as key words and limit-to subarea 'Earth' (accessed 2 November 2015), 2077 publications were about diagenesis, 407 publications were about high resolution cycles, and 348 publications were about microfacies. This would reflect the importance of these subjects in carbonate reservoirs as these subjects represent approximately 32% from the whole bunch.

## 1.2.Motivation

The Tuwaiq Mountain Formation (TMF) contains two hydrocarbon reservoir intervals, the Upper Fadhili and Hadriya reservoirs as well as a main source rock interval for the Mesozoic reservoirs. This source rock interval is now targeted by Saudi Aramco as an unconventional reservoir and is being actively exploited in the Jafurah Basin (Mulhim et al., 2014). Therefore, the study of Tuwaiq Mountain Formation gives an opportunity to assess carbonate microfacies, cyclicity and diagenesis for both conventional and unconventional reservoirs in the same formation. This study will assist in enhancing our understanding of the reservoir architecture of this important succession by developing a

depositional model for the formation, in addition, cyclicity will assist in fluid flow modelling by linking the lateral and vertical rock fabrics within a high frequency stratigraphic framework (Lucia, 2007). A detailed understanding of the microfacies and stratigraphic architecture of carbonate reservoirs is not always possible using subsurface data alone; limitations in data availability and resolution inherent in subsurface derived datasets serve to encourage the use of surface outcrop analog. The outcrop analog can provide information about rock body dimension, size, lateral continuity, and orientation, which are unavailable from the subsurface (Abdullatif and Makkawi, 2004, 2010). In addition, outcrop studies provides a wide variety of scales ranging from nanometer to kilometer (Fig. 4). Consequently, outcrop studies can provide insights for improved geological modeling, understanding and predicting the behavior of reservoirs and aquifers.

## 1.3.Problem Statements and Objectives

The TMF has been studied in both surface and subsurface by many authors (ElAsa'ad, 1989; 1992; Hughes, 2004; 2008; and 2009; Hewaidy et al., 2016) but it is still not as well understood as other formations in the Jurassic of Saudi Arabia (e.g. Arab and Hanifa formations especially). The previous studies on microfacies and diagenesis (e.g. Okla, 1986; Dabbagh, 2006) utilized only microscopy and field observations, and did not employ an integrated approach that utilize various scales and analytical techniques (Fig. 4) of description including outcrop, hand samples, thin section, and on scanning electron microscopy scales. Also, most of the previous studies were focused in two localities either in studying the subsurface TMF interval in the Ghawar field (Hughes, 2004; 2008; and 2009) or in studying the outcrop of Riyadh-Mekkah road (Dabbagh, 2006; Hewaidy et al., 2016). No one has studied the TMF in the Shaqra' quadrangle. For this reason, the

outcomes from this research add to the literature by studying the microfacies, related diagenesis, and controls on porosity evolution of TMF in a new previously unpublished locality. In addition, this study is vital to understand the depositional setting and controls on the petroleum system development in the TMF as it encompasses two reservoir rock intervals, one source rock interval, and unconventional reservoir interval in the Jafura basin.

Therefore, the main objectives of this thesis are as follow:

- Recognition of various lithofacies and facies associations in the TMF and interpretation their palaeoenvironmental conditions along a strike oriented cross section in the basin.
- Conduct a detailed analysis of the microfacies for recognition of potential reservoir properties based on mineralogical and textural data. This detailed microfacies analysis leads to an establishment of a depositional model of the Tuwaiq Mountain Formation.
- Identification of the diagenetic patterns of the TMF and their effect on porosity and permeability
- Integration of depositional and diagenetic controls on the porosity evolution and resulting reservoir quality.

## 1.4.Methodology

The proposed work-flow is based on integrating field, laboratory work, and data interpretation. The following subsection summarizes the methodology used:

### 1.4.1. Field Work and Sampling

Two field trips to the Shaqra' quadrangle were carried out and here is the workflow:

- Three sections were measured and described (one section for each member).
- The field description answered the following points (bed thickness, bed boundaries, texture, macrofacies, sedimentary structures, macroporosity, stylolites, HCl affinity, macro fossils, and strata relationship.
- Samples were taken bed by bed to ensure that all details were captured. (10 samples from section T1 member (Baladiyah Member), which is 10.5 m height, 68 sample from section T2 member (Dadiyah Member), which is 50 m height, and 28 samples from section T3, which is 28 m height)
- Photographs were taken to easily tie between outcrop based description with hand samples and thin section description.
- Describe the stacking patterns and significant surfaces in each measured sections.
- Construction of stratigraphic measured logs for each member.

### 1.4.2. Laboratory Work

Different techniques were used to describe the samples in order to understand the various microfacies and diagenetic alterations. These techniques are discussed in the following points.

- One hundred and five polished thin sections were prepared from 105 samples. These thin sections underwent vacuum impregnation with blue epoxy resin, which enhances the study of porosity. Also, one half of each thin section was stained by Alizarin red-S to differentiate between dolomite and calcite.

- Petrographic analysis was done on these 105 thin sections using polarized light microscope [Olympus EX51] (Fig. 5). The study of the thin sections represents the core of the study as it represents the study of different components, fabrics, textures, sedimentary structures, porosity types and diagenetic features. Visual estimation of porosity and abundance of different pore types was conducted on representative thin section. Thin section porosity values were subtracted from plug measurement of porosity in order to calculate the microporosity. Selection of samples for subsequent analyses was based on the petrographic analysis.
- Measurement of porosity and permeability were conducted on 50 representative samples using Automated Porosimeter-Permeameter [AP-608] (Fig. 6). The porosity measurement were done on 1 inch diameter plugs which underwent end faces grinding. The samples were selected to cover the different facies in different stratigraphic positions throughout the succession of the TMF.
- Examination using X-ray Powder Diffraction (XRD) [Rigaku Miniflex II] (Fig. 7) was done on 15 powdered bulk samples. Certain samples were selected for XRD analysis based on the petrographic analysis of the thin section which showed the presence of: calcite, dolomite, microcrystalline quartz, chalcedony, and calcite replacing dolomite (dedolomite). Each of the powdered samples was placed in a sample holder with a 20 μm square capacity. The scan range was fixed from $2^{o}$ to $89.9^{o}$ to identify a wide range of minerals. The standard measurement software (Rigaku package) is synchronized with the personal computer (PC). The data were processed using PDXL2 integrated X-ray powder diffraction software to match the peaks with the minerals in the database of

the ICDD PDF software. The concentration of different minerals were calculated semi quantitatively.

- Examination utilizing Scanning Electron Microscopy with Energy-Dispersive X-ray Spectroscopy (SEM-EDS) [JEOL JSM-5900LV] (Fig. 8) was done on 27 gold coated chips to avoid sample charging (Goldstein and Yakowitz, 1975). The examination revealed the different crystal habits, microporosity, dolomite textures, and cements. The examined samples were selected to cover the different facies. SEM was performed in freshly broken surface of selected samples. SEM is an essential aspect in this study to address the small scale diagenetic features that cannot be observed under optical microscopy.
- Examination utilizing X-Ray fluorescence [JSX-3400RII] was done on 54 powdered bulk samples to get the elemental percentage of major and trace elements (Ca, Mg, Si, S, K, Fe, Ti, Sr, Mn, Al, Zr, P, and Ba). The examined 54 samples were selected to cover the different facies throughout the whole succession in different stratigraphic positions.
- Examination utilizing Micro Ct-Scan was done on 4 samples of different facies. This examination was done in order to see the 3D pore network the visualization of the 3D pore and identify the diagenetic and depositional controls on the development of the petrophysical properties of different facies.
- Four samples were examined under cathodoluminescence microscopy at Saudi Aramco [CITL Cold Cathodoluminescence 8200 mk3 unit operated at (10 to 14 kv and 180 to 240 μa beam current) attached to Nikon microscope with Leica camera] in order to (1) to distinguish different mineral species and (2) to visually estimate their abundance; (3)

to interpret different mineral paragenetic sequences and different mineral generations (characterized by different crystallization conditions so by different trace elements resulting in different luminescence); and (4)·to detect zoning in minerals because CL contrasts may be generated in some favorable cases by chemical contrasts of only a few ppm in activator elements such as $Mn^{2+}$ , REE, $Fe^{3+}$ , $Ti^{4+}$ , etc.

- Vinci Technologies IFT700 was used to measure contact angle. The following procedure was applied during contact angle measurements:

1. Rock plate was fixed on the holder using super glue.
2. The holder with fixed plate was placed inside the cell in a visible place to the camera.
3. The brine was pumped to reach the full level of the cell with caution to prevent forming bubbles.
4. The cell was heated and pressurized to 60 $^{o}$C and 128 Psi, respectively. It should be noted that this pressure is used just to allow the oil drop to move upward to the rock disc.
5. The system was left for 90 minutes to stabilize.
6. A drop of crude oil was introduced to the cell to settle on the disc
7. Camera system was connected to a computer with software which is responsible for capturing images every 5 second and analyzing the contact angle of the drop shape using Young-Laplace equation (Anastasaidi et al., 1987).

### 1.4.3. Data Interpretation and Integration

All the results from field work, sampling, and laboratory work were interpreted and integrated together to construct the microfacies framework and depositional model of the Tuwaiq Mountain Formation. Microfacies models of Wilson (1975) and Flügel (2010)

were used to assist in the interpretation of the microfacies types and to identify the depositional environments of different microfacies. A conceptual 3D depositional model was constructed by integrating the microfacies and depositional environment interpretations along with the vertical distribution of the microfacies in the studied outcrops. Porosity and diagenesis study used the methodology described in Moore (2001).

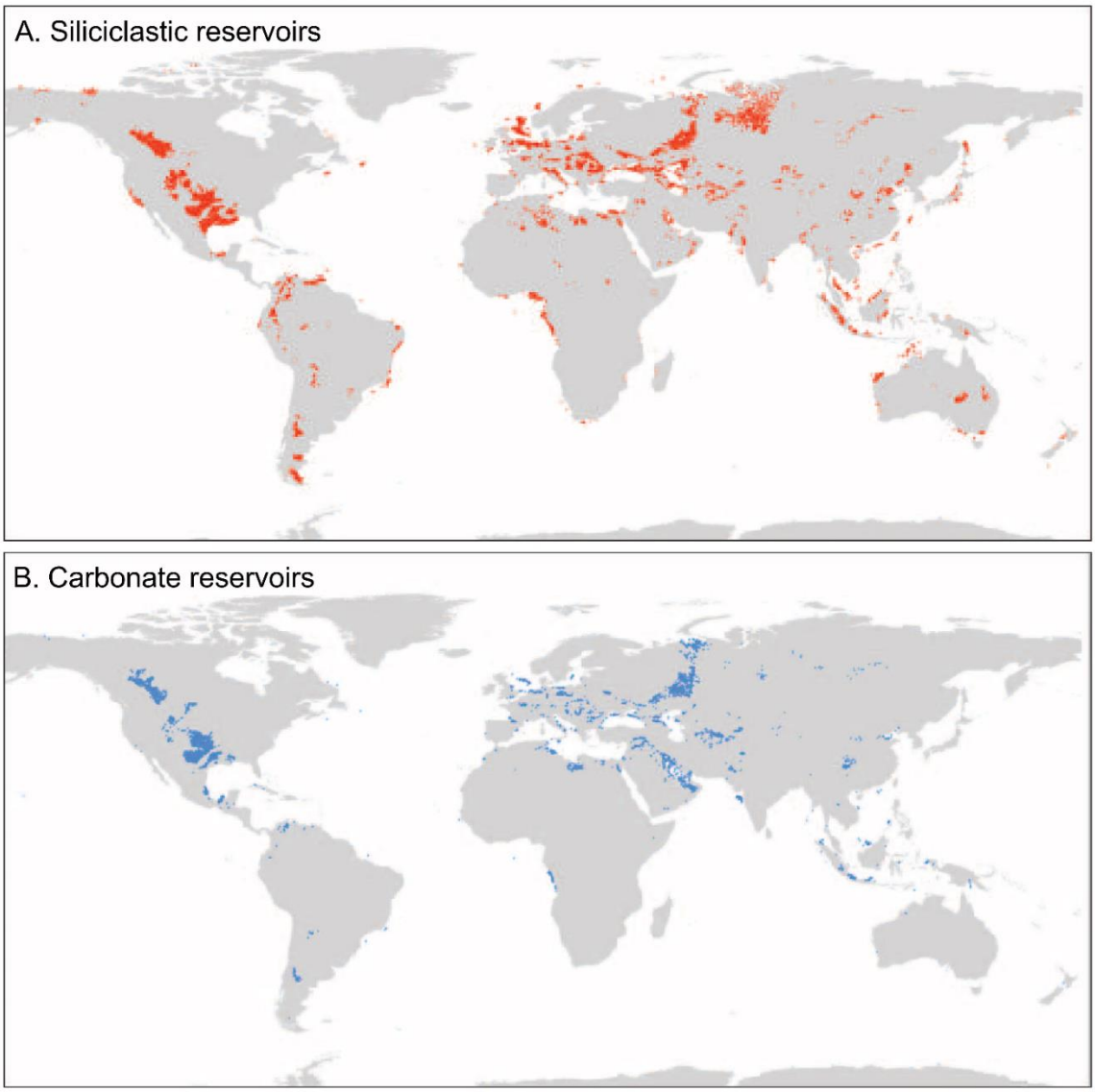


Figure 1 World maps showing distribution of (A) carbonate reservoirs and (B) siliciclastic reservoirs (Ehrenberg and Nadeau, 2005).

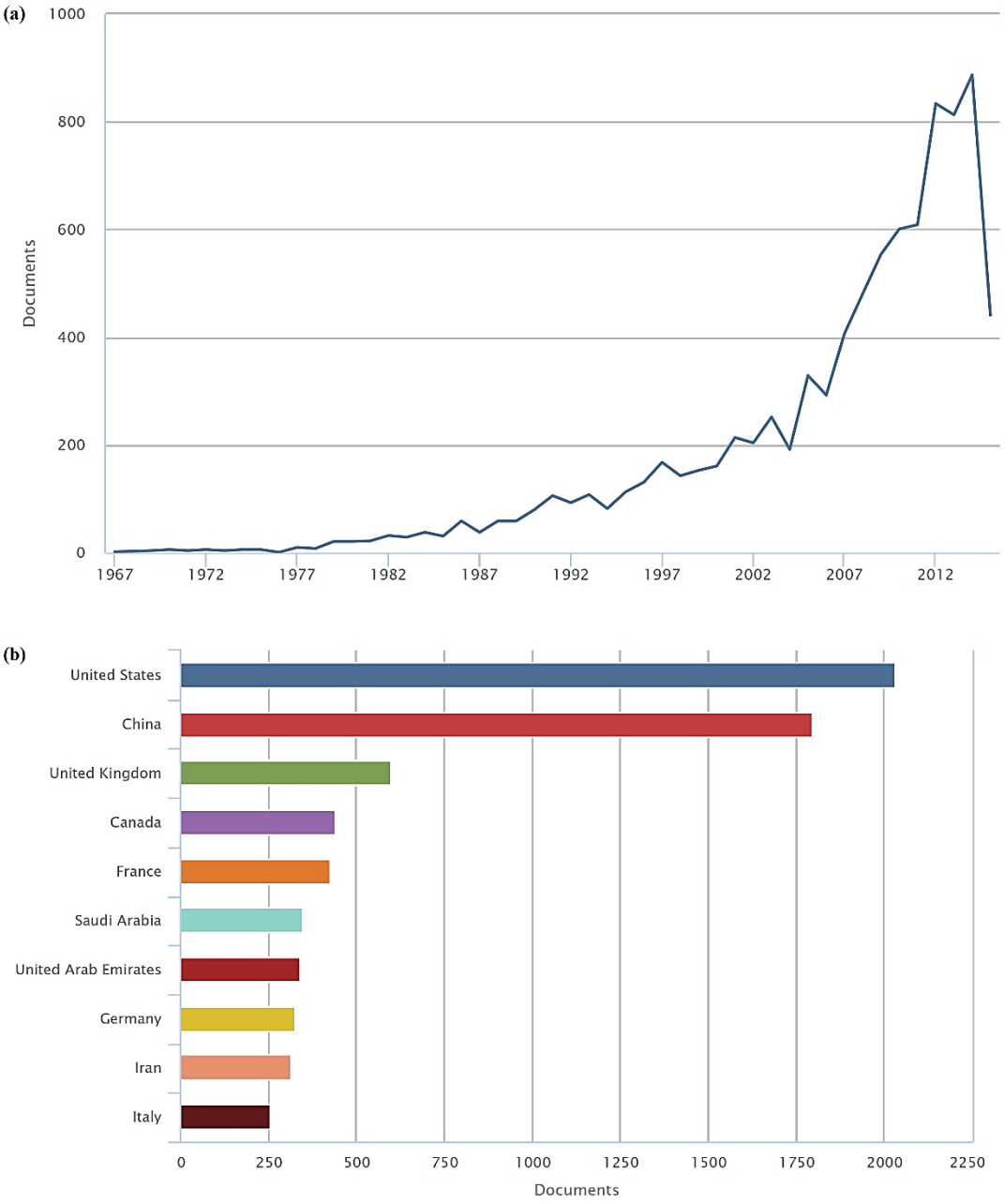


Figure 2 Statistical data on the number of research on carbonate reservoirs over the last 50 years extracted from the Scopus database using 'carbonate*'and 'reservoir*' or 'unconventional' as key words and limit-to subarea 'Earth' (accessed 2 November 2015). (a) The trend of publications from 1967 till 2015, (b) the number of publications by country/territory.

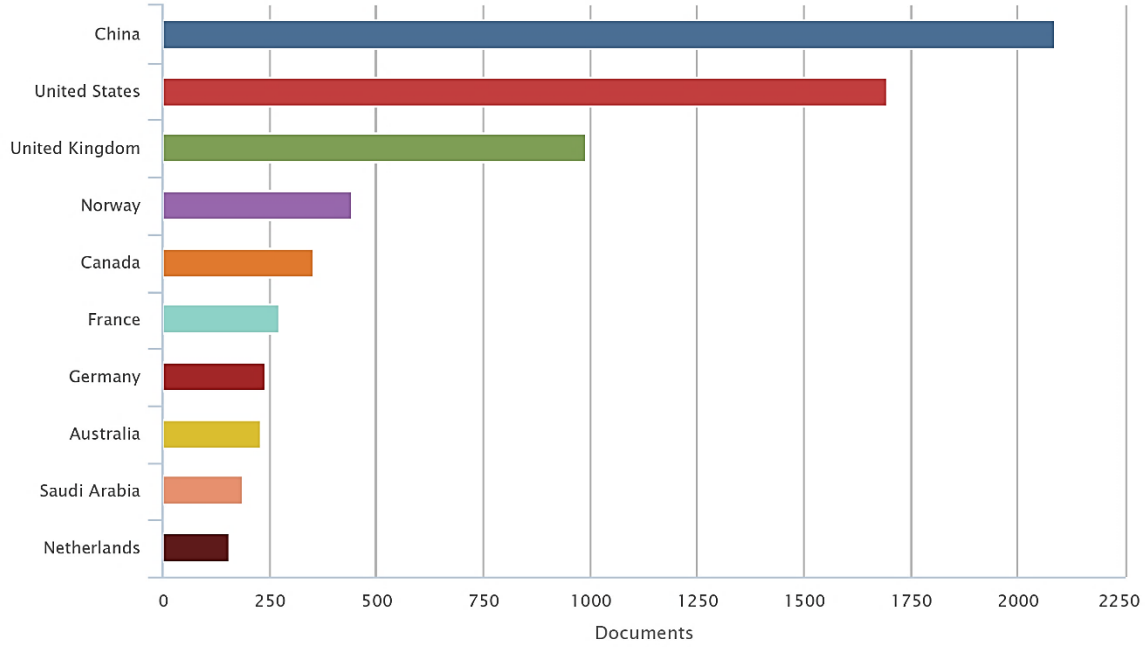


Figure 3 Statistical data on the number of publications by country/territory. The data was extracted from the Scopus database using ‘sandstone*’and ‘reservoir*’ or ‘unconventional’ as key words and limit-to subarea ‘Earth’ (accessed 2 November 2015).

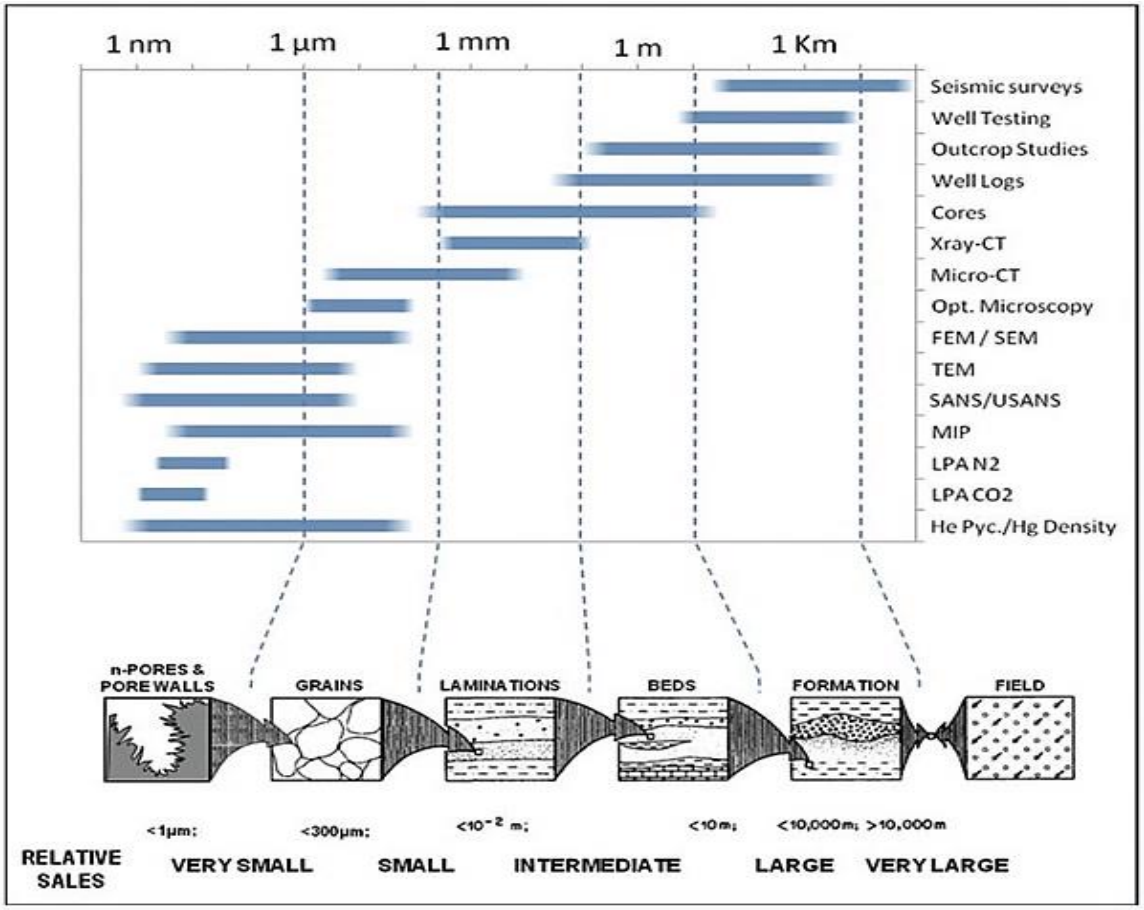


Figure 4 Ranges of different scales of Reservoir heterogeneity and the resolution limit of different methods or tools used for analysis (Krause et al. 1987, and Bustin et al. 2008).

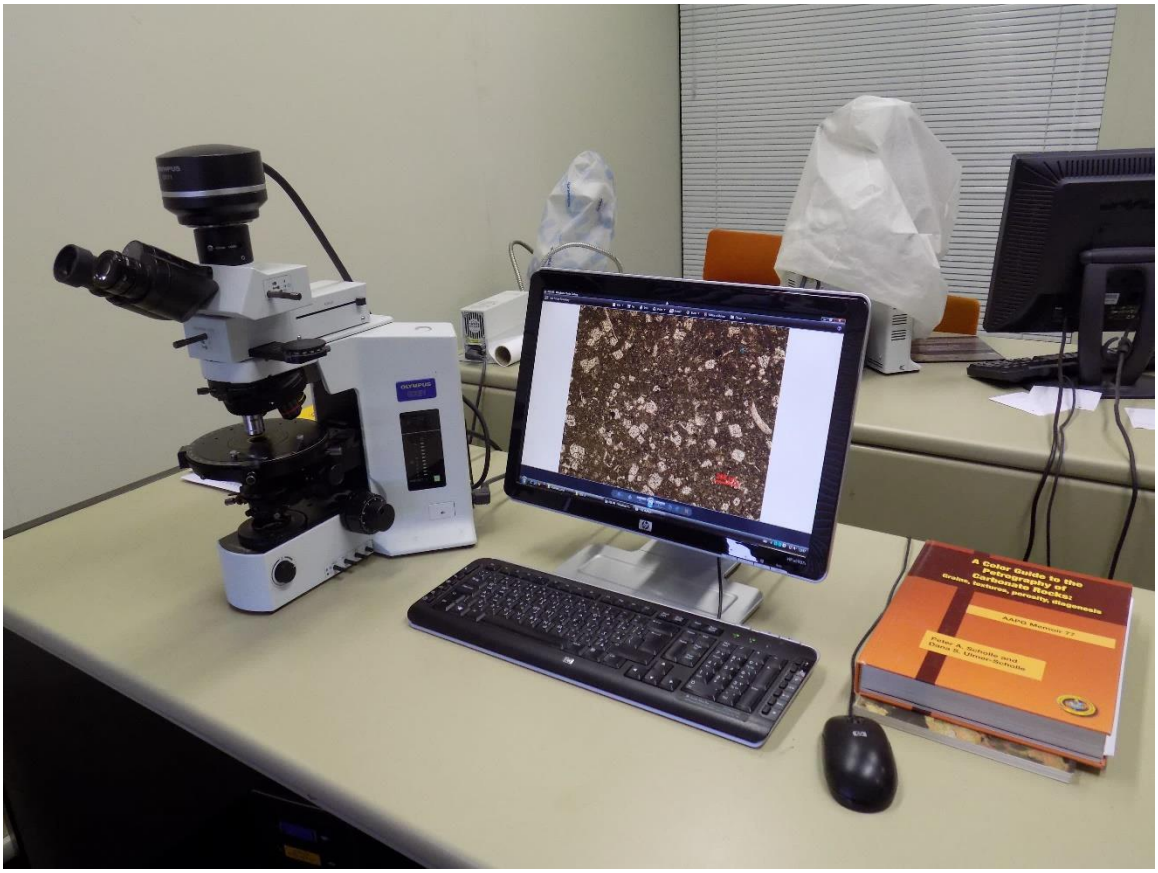


Figure 5 Polarized Microscope – Model: Olympus EX51 – used for the petrographic analysis of the thin sections.


Figure 6 Automated Porosimeter-Permeameter – Model: AP-608 – used for the measurements of porosity and permeability.


Figure 7 X-Ray Diffraction (XRD) – Model: Rigaku Miniflex II – this model was adjusted in scanning angle from 2º to 89.9º and the scanning time was 45 mins in order to identify the mineralogical composition of the powdered samples.

Figure 8 Scanning Electron Microscope - Energy Dispersive X-Ray Spectrometer (SEM-EDS) – Model: JEOL 5900 LV- Oxford X-MaxN – used to identify the small scale diagenetic features and microporosity that cannot be observed under optical microscopy.

# CHAPTER 2

# Literature Review

## 2.1. Jurassic Succession in Saudi Arabia

The Jurassic succession in Saudi Arabia represents the most prolific hydrocarbon producing succession in the world (Hughes, 2006). It is formed of seven formations which build up the Shaqra Group. These formations are from the bottom to the top; the Marrat, Dhruma, Tuwaiq Mountain, Hanifa, Jubaila, Arab, and Hith formations. The first lithostratigraphic studies of Shaqra Group was conducted by Powers (1968) and Powers et al. (1966) and followed by detailed work done by Vaslet et al. (1983, 1984, 1991), Manivit et al. (1985a, 1985b, 1986) in the detailed geologic mapping of Saudi Arabia. Enay (1987), Le Nindre et al. (1990), Al-Husseini (1997) and Sharland et al. (2001) summarized the regional lithostratigraphy and sequence stratigraphy of the Jurassic succession through Saudi Arabia.

The lower boundary of the Shaqra Group is the Minjur-Marrat unconformity which represents the Triassic-Jurassic boundary while the Marrat Formation is Toarcian in age. The Shaqra Group is unconformably overlain by the Sulaiy Formation (Fig. 9). The Marrat Formation (Toarcian age), it is mainly formed of interbedded marine sandstones, claystones and carbonate. The Dhruma Formation (Bajocian to Bathonian age) which unconformably overlays the Marrat Formation, is mainly carbonate in subsurface but in the outcrops it turns to carbonates and claystones in Central Arabia while in the northern and southern Saudi Arabia it turns to siliciclastics. The Tuwaiq Mountain Formation (Middle to Late Callovian age), which unconformably overlays the Dhruma Formation, is mainly

composed of lagoonal and stromatoporoid carbonates. The Hanifa Formation (Oxfordian age), which unconformably overlays the Tuwaiq Mountain Formation, consists of a lower and an upper unit. The lower unit represents deep marine carbonates, while the upper unit is composed of lagoonal stromatoporoid carbonate. The Hanifa Formation is disconformably overlain by the Jubaila Formation (Kimmeridgian) which is formed of a lower and an upper unit. The lower unit is formed of moderately deep marine carbonates. The upper unit is formed of shallow marine stromatoporoid associated assemblages. The Jubaila Formation is conformably overlain by the Arab Formation (Kimmeridgian age). The Arab Formation was formed by cyclic sedimentation which is reflected as four cycles of alternating carbonate and evaporites. The Hith Formation (Portlandian), which is mainly evaporite, overlies the Arab Formation conformably. It represents the evaporite portion of the youngest Arab cycle (Hughes, 2004; 2008; and 2009).

## 2.2. The Tectonostratigraphy of Late Middle Jurassic: Callovian to Oxfordian (164.4–154.1 Ma)

According to Ziegler (2001), this time span witnessed the deposition of the Upper Dhruma Formation and the Tuwaiq Mountain Formation in Saudi Arabia and their equivalents through the Arabian Plate, such as the Upper Araej in the United Arab Emirates. During most of this time span shallow marine carbonates were deposited across much of Saudi Arabia. The deposition happened in four intrashelf basins (Fig. 10) which are; Rub' Al Khali and Ras al Khaima basins, the Gotnia Basin, and the Arabian Basin. The Gotnia Basin and the Arabian Basin were created by rejunvenation of the N-trending Hercynian tectonic structures, while Rub' Al Khali and Ras al Khaima basins were controlled by Dibba fault zone (Ziegler, 2001). Most of the Arabian plate (Fig. 11) was dominated by

deposition of coral-algal and bioclastic limestone and sandstone deposits with clastic input supplied from the Arabian Shield. Shallow-marine carbonate shelf deposition predominated during this time span across much of the plate, although in the Gotnia Basin and the Ras al Khaima Basin, the facies graded into deep-marine carbonates and clastics. Areas near the Arabian Shield and Yemen were dominated by the shallow marine clastics and carbonates, with local development of marginal-marine/coastal/deltaic deposits. This time span witnessed deposition of some of the richest hydrocarbon source rocks in the Arabian Plate. These source rocks are mainly carbonates, which are; the Naokelekan Formation (Iraq), and the Tuwaiq Mountain and Hanifa formations (central Arabian plate) (Sharland et al., 2001).

## 2.3.Tuwaiq Mountain Formation

The Tuwaiq Mountain Formation crops out in east-central Saudi Arabia (Fig. 12), in the vicinity of ArRiyadh. According to Edgell (2006), the Tuwaiq Mountain "extends as a high escarpment from 70 km east of Buraydah at latitude 26º30′N, and runs south–east for 270–30 km SW of Ar Riyadh, where it is cut by the Central Arabian Graben or Nisah-Durma Graben, also called the Mugharah Graben. This mountainous escarpment has an elevation of 1,022 m, directly west of Ar Riyadh. It recommences immediately south of the Central Arabian Graben, and runs SSW for another 440 km, with elevations between 850 m and 1,060 m, until it is cut by Wadi ad Dawasir. South of this wadi, the escarpment reappears, trending N-S in Al 'Arid area, with elevations of 800–1,062 m, and extending into the south–western Rub'al Khali". The main escarpment of the Tuwaiq Mountain is composed of the cuesta of the Dhruma and Tuwaiq Mountain formations.

### 2.3.1. Lithostratigraphy

The Tuwaiq Mountain Formation was firstly introduced and defined by Steineke (1937, cited in Powers et al., 1966) as a member, and then it was raised to a formation by Bramkamp (1945, cited in Powers et al., 1966). Steineke et al. (1958) described the Tuwaiq Mountain Formation as a large plate of dense limestone that contains corals, while at the base it consists of chalky limestone with no corals. Powers et al. (1966) divided the Tuwaiq Mountain Formation into an upper and lower units. The upper unit is a massive limestone formed of calcarenitic limestone and calcarenite, while the lower unit has a thickness that ranges from 20-40 m and is formed of soft chalky limestone with some shale. The lower unit develops gradational from the Dhruma shale below to massive limestone at the top. Vaslet et al. (1983) divided the Tuwaiq Mountain Formation into three units T1, T2, and T3 which are informally named Baladiyah, Maysiyah, and Daddiyah members in the same order. These units were recognized also by Manivit et al., (1985). Enay et al., (1987) divided the Tuwaiq Mountain Formation in three units T1, T2, and T3 based on its fossil content. Ammonites are rare in T3 and T1, although T2 contains the ammonites Pachyerymnoceras. Alsharhan and Magara (1994) defined two lithofacies in the subsurface: the reservoir facies which are formed of skeletal lime packstones and grainstones, and the source facies which is formed of organic-rich lime mudstone.

Petrographic study of Jurassic Tuwaiq Mountain limestone was conducted by Dabbagh (2006). He reported that lime mudstones and wackestones constitute the bulk of the Tuwaiq Mountain while grainstone is less common and floatstone and boundstone are rare. Hughes (2009) redefined the Tuwaiq Mountain Formation to include five members by adding the Hisyan and Atash Members, which were previously considered to be part of the upper

Dhruma Formation, a redefinition that had been previously suggested by Le Nindre et al. (1987, 1990), Al-Husseini (1997), and Hughes (2004). Al Ibrahim (2014) studied the basinal interval of the Tuwaiq Mountain Formation from subsurface data located between Ghawar anticline and Qatar Arch. He identified two lithofacies in the basinal interval of the Tuwaiq Mountain Formation, wispy laminated skeletal wackstone to mudstones and cemented packstone/grainstone.

### 2.3.2. Age of the Tuwaiq Mountain Formation

The age of the Tuwaiq Mountain Formation is a debatable issue. Arkell (1952) and Imlay (1970) studied ammonites in the lower part of the Tuwaiq Mountain Formation and they found that the age of the lower part is Middle Callovian. Powers et al. (1966), however, assigned an Oxfordian age to the upper part of the Tuwaiq Mountain Formation on the basis of the age of two foraminifers, *Kurnubia wellingsi* (Henson) and *Steinekella steinekei Redmond.* Le Nindre et al. (1983) interpreted the age of the Tuwaiq Mountain Formation to be Middle to Upper Callovian by the distribution of fossils (ammonites) through T1, T2, and T3. In 1986, Enay et al. interpreted the age of the Tuwaiq Mountain Formation to be Upper Middle to Upper Callovian due to the presence of the ammonites *Pachyerymnoceras*, *Erymnoceras* and *Kurnubiella* cf. *hatirae* (Lewy). Enay et al. (1987) and Fischer et al. (2001) used the superposition of the Tuwaiq Mountain Formation on the Upper Dhruma "carinatum" ammonite zone to interpret that the Tuwaiq Mountain Formation is of Middle Callovian age. Whittaker et al. (1998) assigned the Tuwaiq Mountain Formation to be of mid-Callovian age by using foraminifera, *Pfenderina trochoidea* and *Kurnubia* species. Hughes (2009) reported that Varol (unpublished Saudi Aramco report, 2001) used calcareous nanofossils in dating the Tuwaiq Mountain

Formation to be of Callovian age. Enay et al. (2009) dated the Tuwaiq Mountain Formation to be of Early-Late Callovian age based on ammonite zonation.

### 2.3.3. Palaeontology

Okla (1987) performed a paleontological study on the Tuwaiq Mountain outcrops along the Ar-Riyadh-Mizahmia road. He divided the formation into a lower and an upper part with thicknesses of 103.3 m and 89.7 m, respectively. The lower part is a light colored biomicritic limestone, which is full of sponge spicules and molluscs, while the upper part is a light grey biomicritic limestone with abundant stromatoporoids, corals, and algal fragments. The upper part of Tuwaiq Mountain Formation is composed of four segments with thicknesses 44.8, 34.4, 4.5, and 6 m, respectively. The lower segment of the upper part is formed of well bedded biomicritic limestone with various forms of blue green algae Cayeuxia. These algae have calcareous tubes and some of them were broken into small fragments, which may indicate that they were transported is overall suggestive of shallow marine deposition. The upper three segments of the upper part of the Tuwaiq Mountain Formation are formed also of well bedded biomicritic limestone but with various forms of dasycladacean algae such as *Salpingoporella*, *Cylindroporella*, and *Polygonella incrustata*. Based on these findings, Okla (1987) interpreted that the lower part of the Tuwaiq Mountain Limestone was deposited in a low energy environment, while the upper part of the Tuwaiq Mountain Formation was deposited in a slightly higher energy environment. In addition, he suggested that the upper part of the Tuwiaq Mountain Formation is shoaling upward as dasycladacean algae represent depths of 10 m while Cayeuxia algae represent depths of 30 m.

ElAsa'ad (1989) performed a paleontological study on the Tuwaiq Mountain outcrop 200 km to the north of Ar-Riyadh. He found in the upper part of the formation the first coral bearing strata in Central Saudi Arabia. This coral bearing strata did not form a large barrier reef but instead occurred as a group of isolated corals, coral bioherms, and coral biostromes. He suggested that there was not a sufficient space to build up a big barrier reef due to the slow subsidence of sea floor. The coral heads range from 0.2-0.5 m in diameter and are scattered and found in life position through a limestone sheet of 20-40 m thickness, which extends for 1000 km along the Tuwaiq escarpment. The coral fauna of the Tuwaiq Mountain Formation consists of five species only, which are; *Meandraraea gazaensis Alloiteau* and *Farag, Oyalastraea caryophylloides Goldfuss, Trigerastraea collignoni* (Alloiteau), *Colimnococenia lamberti Alloiteau* and *Brachthelia* sp. He interpreted this low diversity of the coral fauna as a consequence of changes in the palaeobiogeography and palaeoenvironmental controls of this very shallow platform and the sensitivity of this fauna to these changes.

Ammonites from the upper part of the Tuwaiq Mountain Formation were studied by ElAsa'ad (1992) in Al Ma'ashbah, and results from this study assisted in dating the formation. He identified the following ammonite fauna in the lower part of T3: *Pachyceras (Pachyerymnoceras) jarri Douvillt;. Pachyceras (Pachyceras) lalandeanum (d'Orbigny), Pachycerus (Pchyceras) indicum Spath, Levaniiceras sinaiensis Lewy, Pelloceras (Peltoceras) cf. trifidum (Quenstedt) and Peltoceras (Pcltoccras) Pachygaster Gill, Thierry and Tintant*. This ammonite assemblage was used as an indicator of a late Callovian age for T3.

The palaeoenvironments and biostratigraphy of the middle to upper Jurassic carbonate reservoirs of Saudi Arabia and the Shaqra Group were studied by Hughes (2004, 2008, 2009) using micropalaeontology and especially the benthic foraminifera. The Tuwaiq Mountain Formation includes two reservoirs, the Upper Fadhili reservoir in T1 and Hadriya reservoir in T3. According to Hughes (2004, 2008), the biocomponents in the Upper Fadhili reservoir include benthic foraminifera, which include undifferentiated *nodosariids, Lenticulina spp., Bolivina spp., Trocholina elongata, Kurnubia palastiniensis, K. wellingsi, Nautiloculina oolithica, Valvulineria sp., Redmondoides lugeoni, Praekurnubia sp., Pfenderina trochoidea, Meyendorffina bathonica, and Trochamijiella gollesstanehi.* Branched and platy sponges are also present. The biocomponents of the upper Tuwaiq Mountain Formation include abundant representatives of the pelagic bivalve Bositra buchi within certain parts. This pelagic bivalve is associated with monaxon and tetraxon sponge spicules and dwarf or juvenile, costate brachiopods. This microfossil assemblage represents deep-marine intra-shelf basin palaeoenvironment with very low rate of carbonate production. In addition, there are also benthic foraminiferal assemblage which were deposited below wave-base, such as *Lenticulina, Nodosaria and Bolivina* and are indicative for deep-marine intra-shelf basin palaeoenvironment. Platy, domed and branched sclerosponges are also present. The biocomponents of deep lagoon palaeoenvironment show the biggest diversity as it include *Meyendorffina bathonica, Trochamijiella gollehstanehi, Redmondoides lugeoni, "Kurnubia" wellingsi, Praekurnubia* sp., "*Pfenderina" trochoidea, Valvulina* sp., *Trocholina elongata* and *Nautiloculina oolithica*. In addition, low diversity in the biotic content of the shallow lagoonal environment as it include; Nautiloculina oolithica, branched coral, large and

robust echinoid spines. Figure 13 shows a schematic diagram of the palaeoenviroments of the Tuwaiq Mountain Formation, as suggested by different biocomponents.

El Hedeny (2012) analyzed the trace fossils of the Tuwaiq Mountain and Hanifa formations. The trace fossil assemblage seen in the Tuwaiq Mountain Formation includes *Curvolithus multiplex, Thalassinoides suevicus, Th. horizontalis and Th. isp*. He interpreted this trace fossil assemblage to indicate that the depositional environment was a low energy shallow marine environment deposited below fair weather base but not above storm wave base. Figure 14 shows the distribution of the various trace fossils within the Tuwaiq Mountain Formation.

El-Sorogy et al. (2014) performed a paleontological study on marine benthic invertebrates of the Tuwaiq Mountain Formation in Khashm Al-Qaddiyah. He identified ten species of scleractinian corals, seven species of brachiopods, four species of bivalves, four species of gastropods and one species of cephalopods. From this fossils assemblage, he interpreted that the TMF represents a shoaling upward succession. He related the low diversity of the benthic fauna to several causes, which are (1) the high sedimentation rate resulted in turbidity and as a consequence no sufficient light penetration for corals to flourish, and (2) the muddy facies are inadequate for the filter feeders to flourish.

Youssef and El-Sorogy (2015) analyzed the benthic foraminifera, which are found in coral reefs of the Tuwaiq Mountain Formation. The foraminiferal assemblage shows a large palaeoenvironmental spectrum form open marine to deep marine. They interpreted this as either the assemblage has palaeoenvironmental tolerance or they are allochthonous.

### 2.3.4. Sequence Stratigraphy of the Jurassic Succession in Saudi Arabia

The first work in this area dates back to Vail et al., (1977) who provided the global eustatic-based sequence stratigraphic framework. In 1988, Haq et al. for the first time provide detailed global chronostratigraphy and sea level change cycles for the Mesozoic and Cenozoic era.

Le Nindre et al. (1990) were the first to study the transgressive-regressive sequences of the Mesozoic in Central Saudi Arabia, followed by Vaslet et al. (1991). A similar approach was followed by Al-Husseini (1997) who for the first time correlated the lateral distribution of Jurassic strata of Central Saudi Arabia to the formations of the western and southern Arabian Gulf region. He used biostratigraphic and stratigraphic studies as a basis of his work. His prominent correlation markers were the early Jurassic hiatus, Toarcian transgression, Aalenian hiatus, Bajocian-Bathonian transgression and the Callovian-Kimeridgian sequences. He put the upper Dhruma along with the Tuwaiq Mountain limestone in a single Callovian-Kimeridgian sequence.

The regional sequence stratigraphy of the Arabian plate was studied by Sharland et al. (2001), who divided the stratigraphic column of the Arabian plate into 11 megasequences and with 63 maximum flooding surfaces. The Tuwaiq Mountain Formation is located within TMS AP7, which is characterized by high eustatic sea level and contains some of the most prolific source rocks of the Arabian plate. In 2005, a regional chart was produced by Haq and Al-Qahtani in which they describe the regional cycle chart of sea level changes affecting the Arabian platform. In 2004, Hughes interpreted the upper Dhruma Member D7 and upper Tuwaiq Member T1 as transgressive-regressive cycle. Énay et al. (2009) interpreted the D6 and the lower part of the D7 as a transgressive system tract (TST), while

the remaining part of D7 and the Tuwaiq Mountain Formation are interpreted as a regressive system tract (RST). These system tracts are separated by a maximum flooding surface (MFS). Énay et al. (2009) neglected the Dhruma-Tuwaiq unconformity and MFS at the base of T3 (Fig. 15). Therefore, Al-Husseini (2009) interpreted the Tuwaiq Mountain Formation as Tuwaiq sequence.

### 2.3.5. Recent Work on Microfacies and Diagenesis of the Tuwaiq Mountain Formation

Recent work done by Hewaidy et al. (2016), Tawfik et al. (2016), and EL-Sorogy et al. (2016) has focused on microfacies and depositional environment, sequence stratigraphy, facies and diagenesis of the Tuwaiq Mountain Formation, respectively from many perspectives.

Hewaidy el al. (2016) conducted a pilot study on the microfacies and depositional environments of the Tuwaiq Mountain Formation (TMF). They studied three outcrops in Shaib El-Hisyan, Khashm Al-Giddayah and Dirab, near Riyadh City, Central Saudi Arabia. The cumulative thickness of the studied section is 257 m and the number of studied thin section was 36. This study is thought to be a pilot study to provide an overview of the TMF. They identified 12 lithofacies deposited in a ramp settings which somewhat contradicts with the literature consensus in which the whole Jurassic succession is thought to represent an epiric rimmed platform (Hughes, 2004; 2008; and 2009) with an intra-shelf basin.

EL-Sorogy et al. (2016) studied the reefal limestone interval in the upper most part of the TMF in the Khashm Al-Giddayah outcrop along Riyadh-Mekkah road. They identified 7 lithofacies in this succession and suggested that they were deposited in a variety of different settings, from shallow lagoon to reef flank. The diagenetic features of these facies were

identified, including cementation, recrystallization, dolomitization, and silicification. The study did not include the paragenetic sequence.

Tawfik et al. (2016), studied the TMF in the Khashm Al-Giddayah outcrop along the Riyadh-Mekkah road. They identified fifteen lithofacies ranging in depositional environment from lagoon to intra shelf basin. Also, they studied the sequence stratigraphy of that formation and they found a main trend of shallowing upward regressive sequences from deep marine facies association to shallow marine facies association occurs with non-erosional sequence boundaries.

## 2.4.Study Area

The study area is located within the Shaqra' quadrangle (Lat 25°and 26° N. and long 45°and 46°30) in Al-Majma'ah Governorate (Fig. 16) which is located to the northwest of Riyadh. The thickness of the Tuwaiq Mountain Formation ranges from 164 m at Khashm at Turab to 205 m at Khashm al Furuthi. Shaqra' quadrangle is a part of a large homocline with dipping strata to the northeast at angles 1-1.5 degrees. The western part of the Shaqra' quadrangle includes two grabens, which are; the Majma'ah graben and the Barrah graben (Vaslet et al., 1988).

The Majma'ah graben, named for Al Majma'ah in the northwestern corner of the quadrangle, contains rocks ranging from the Aruma Formation in the northern part to the Tuwaiq Mountain Limestone in the southern half of the structure. The graben is divided into eight structural segments that are offset against each other by oblique 'en echelon' faults and flexures. Downthrows vary from 80 m to over 200 m, but are nowhere consistent; in the Hurayq segment the throw increases from 50 m to 200 m over a distance of 500 m

from north to south. These segments are; The Hattabah segment, the Madrub, the Furuthi, the Mishqar, the Dahinah, the Jurayfah, the Hurayyiq, and the Qasab (Vaslet et al., 1988).

## 2.5. Contact Angle

Wettability describes the physical behavior of the rock-fluid interaction and according to Craig (1971), the wettability is defined as the ability of one fluid to be spread or adhered on a rock surface in the existence of another immiscible fluid. Another definition of wettability is addressed by Tiab and Donaldson (1996) as the relative adhesion of two fluids to the surface of solid object. Four different types of wettability states of reservoir rocks; oil wet, water wet, intermediate wet and fractional wettability (Fig. 17). Addressing the wettability of the reservoir rocks is very crucial in the production of hydrocarbon, developments of hydrocarbon fields, primary recovery, secondary recovery, tertiary recovery, and the shape of the relative permeability curves (Agbalaka et al., 2008; Dandekar, 2013; Xuetao et al., 2017).

There are different ways to address the phenomena of wettability of reservoir rocks (Anderson, 1986a,b; Tiab and Donaldson, 1996; Li and Horne, 2003) including quantitative methods (contact angle, Amott wettability index (AWJ), USBM (U.S. Bureau of Mines) wettability index, and Li and Horne method) and qualitative methods (imbibition rate, flotation, microscopic examination, capillary pressure curves, reservoir logs, permeability/saturation relationship, nuclear magnetic resonance, and dye adsorption). Although no single accepted method exists, the most used method is the contact angle method.

Several factors are affecting the wettability of reservoir rocks and therefore the contact angle, such as:

1. The effects of mineralogical composition of the rock:

Many authors (Abdallah et al., 1986; Vijapurapu et al., 2002; Ziauddin, 2007; Agbalaka et al., 2008; Dandekar, 2013; Xuetao et al., 2017) discussed the different effects of the mineralogical composition of the rock surface on the wettability of the rock. Most of the reservoirs all over the world are composed mainly either of siliciclastic or carbonate rocks. The composition of carbonate rocks are less heterogeneous compared to siliciclastic rocks as carbonate rocks are composed mainly of calcite and or dolomite while siliciclastic rocks are composed of quartz, feldspars and clay minerals. Due to the greater heterogeneity of siliciclastic rocks, the siliciclastic wettability is more complex than the carbonate rocks. The rocks are classified into two categories based on the measurements of the contact angle. The first group is the water wet group which includes quartz, silicates, glass, carbonate, and aluminosilicate. The second group is the oil wet group which includes hydrocarbon organic solids and the metal sulfides in minerals. Taking about the wettability of reservoir rocks, most of the minerals in the composition of the reservoir rocks are water wet but the wettability degree is different from one minerals to another one. For instance, the most hydrophilic minerals are the clay minerals and the degree of wettability decreases as the follow from quartz to carbonates to feldspars. All these reflect that there are different wettability degrees for different minerals and the reservoir rocks are heterogeneous both in mineral composition and sediment sources which is reflected in complexity and heterogeneity in the wettability degree both vertically and laterally and also from microscopic scale to macroscopic scale.

2. The effects of crude oil composition

The effect of crude oil composition on the wettability of the reservoir rocks comes out from the different substances in the composition of the crude oil. The main components of crude oil in reservoirs are; the nonpolar components which are the hydrocarbons in the crude oil, the polar components which include compounds of $O_2$, S, $N_2$ and the active components of the crude oil. The nonpolar components of the crude oil include different hydrocarbons with different carbon atom number and different degrees of nonpolarity. Table 1 shows how the contact angle is directly proportional to the carbon atom number. In addition to the nonpolar components, there are polar components which can change the degree of wettability of reservoir rock and may result in wettability reversal. Experiments done on quartz surfaces with different oil composition showed changes in the contact angle as a result of different polar components (Fig. 18). For instance, asphalt is a polar substance and it could change the rock wettability into oil wet. Johansen and Dunning (1958) did a set of experiment on oil/water/glass systems using asphalted and deasphalted crude oil. They found that the asphalted crude oil changed the wettability of the system from water wet to oil wet. Yu and Buckley (1997) and Al-Maamari and Buckley (2003) performed similar study and the results showed matching with the findings of Johansen and Dunning (1958).

3. The effects of brine composition

Not only is the composition of the crude oil affecting the wettability of the reservoir but also the brine composition. Vijapurapu and Rao (2003) did a set of experiments using oil–water–rock (dolomite surface) system with different concentrations of brine to see the impact of brine concentration on rock wettability. Their findings showed that by diluting

the brine concentration the wettability of the system changed from oil wet to intermediate wet. Tang and Morrow (1996) studied also the effect of the concentration change of the brine on wettability. They did a set of displacement experiments using Berra sandstone and different concentration of oil-brine systems in order to see the effect of brine concentration on wettability and so the oil recovery. Their findings can be summarized in a point that the oil recovery increased by reducing the concentration of both connate and invading brines.

4. The effects of surface active compounds

Many authors (e.g. Nelson et al., 1984; Standnes and Austad, 2000; Hirasaki and Zhang, 2004: Zhang et al., 2006; Xie et al., 2005; Wu et al., 2008) discussed the effect of the surfactants on rock wettability. The effects of surfactants are very significant that a small amount of active agent can lead to wettability reversal. The main idea is that the active agents are adsorbed on the surface of the rock which results in reduction of the number of adsorption and on the other hand increasing the dissolved electrolytes and these active agents reduce the oil–water interfacial tension which helps in improvement of the efficiency of oil displacement and oil recovery.

5. The effects of temperature and pressure

The temperature and pressure of reservoirs generally do not have a direct impact on the wettability of the rock but they have an impact on the fluid characteristics in case of changing pressure and temperature which in turn affect the wettability of the rock. For instance, the change in pressure and temperature of the reservoir rock can lead to changes in the composition of the crude oil which in turn may affect the precipitation of asphalts from the crude oil and the effects of asphalts on wettability were discussed previously in point 4. The point of the effect of temperature and pressure on the wettability is a debatable

issue as Wang and Gupta (1995) did not find a correlation between changes in pressure and temperature on contact angle of quartz or calcite. Phillips and Riddiford (1956), Poston et al. (1970) and Lo and Mungan (1973) investigated the effect of temperature on the contact angles and they found different average temperature coefficient for the contact angle which are; 0.29°/°C, 0.27°/°C and 0.20°/°C, respectively. Jadhunandan and Morrow (1995) performed a study on aging temperature of two different systems of oil–brine–rock. They used temperature range of 20°C–80°C. The study showed that aging temperature directly affected the wettability.

6. The effects of the depth of the reservoir structure

The position of the reservoir rocks relative to the oil-water contact can play an important role on the variation of reservoir rock wettability. Jerauld and Rathmell (1997), studied the change of wettability of the Prudhoe Bay reservoir as a function of the reservoir structure's depth. They found that the wettability is more toward oil wet by moving up into the oil column from the oil water contact. Therefore, they documented that the wettability can be different from place to another within the same field as a factor of the depth of the reservoir structure.

7. The effect of surface roughness of mineral

Treiber et al. (1972) indicated that a smooth, homogenous surface is necessary to apply the sessile droplet method to produce direct-angle measurement of surface wettability. They mentioned that polished quartz and calcite plates are commonly used for this purpose.

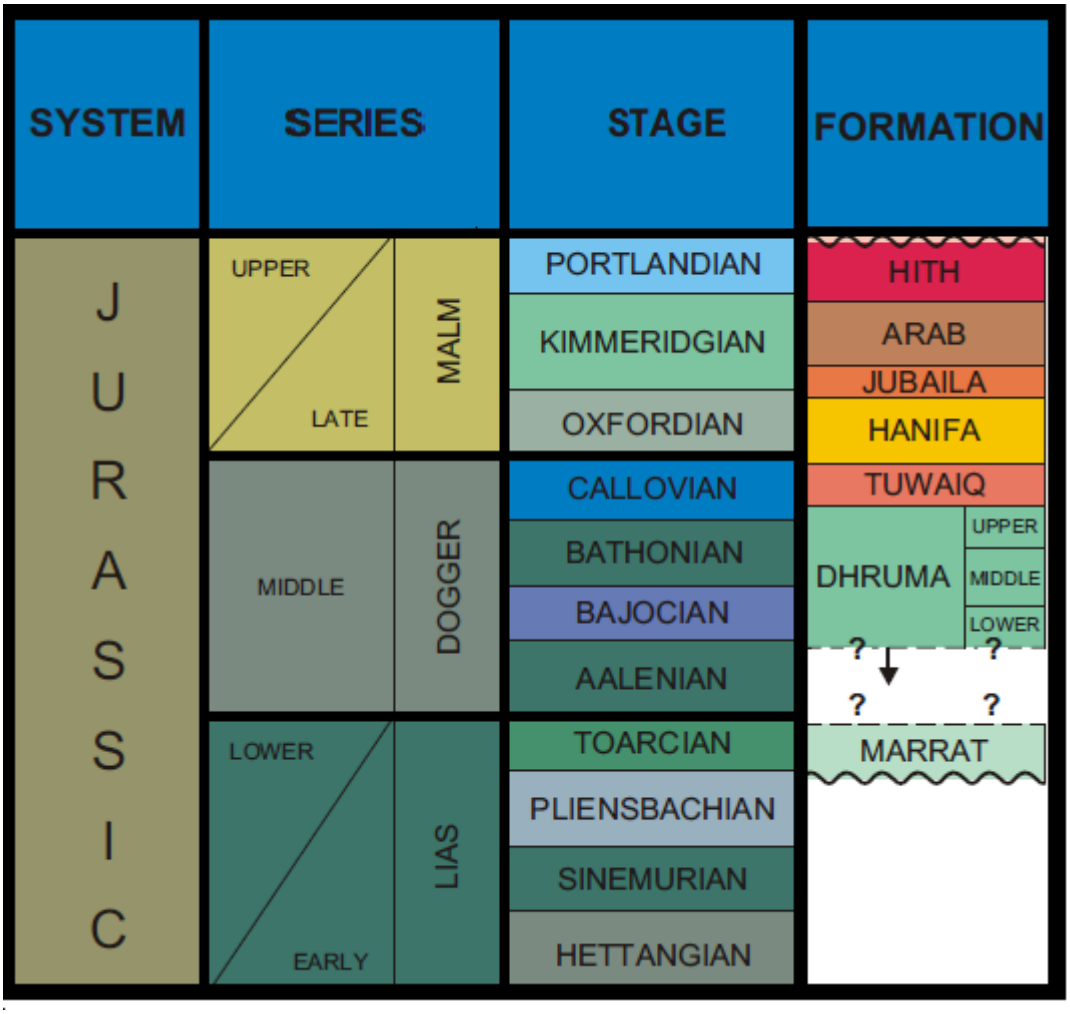


Figure 9 Generalized stratigraphic column of the Jurassic succession of Saudi Arabia (Halawani, 2012).

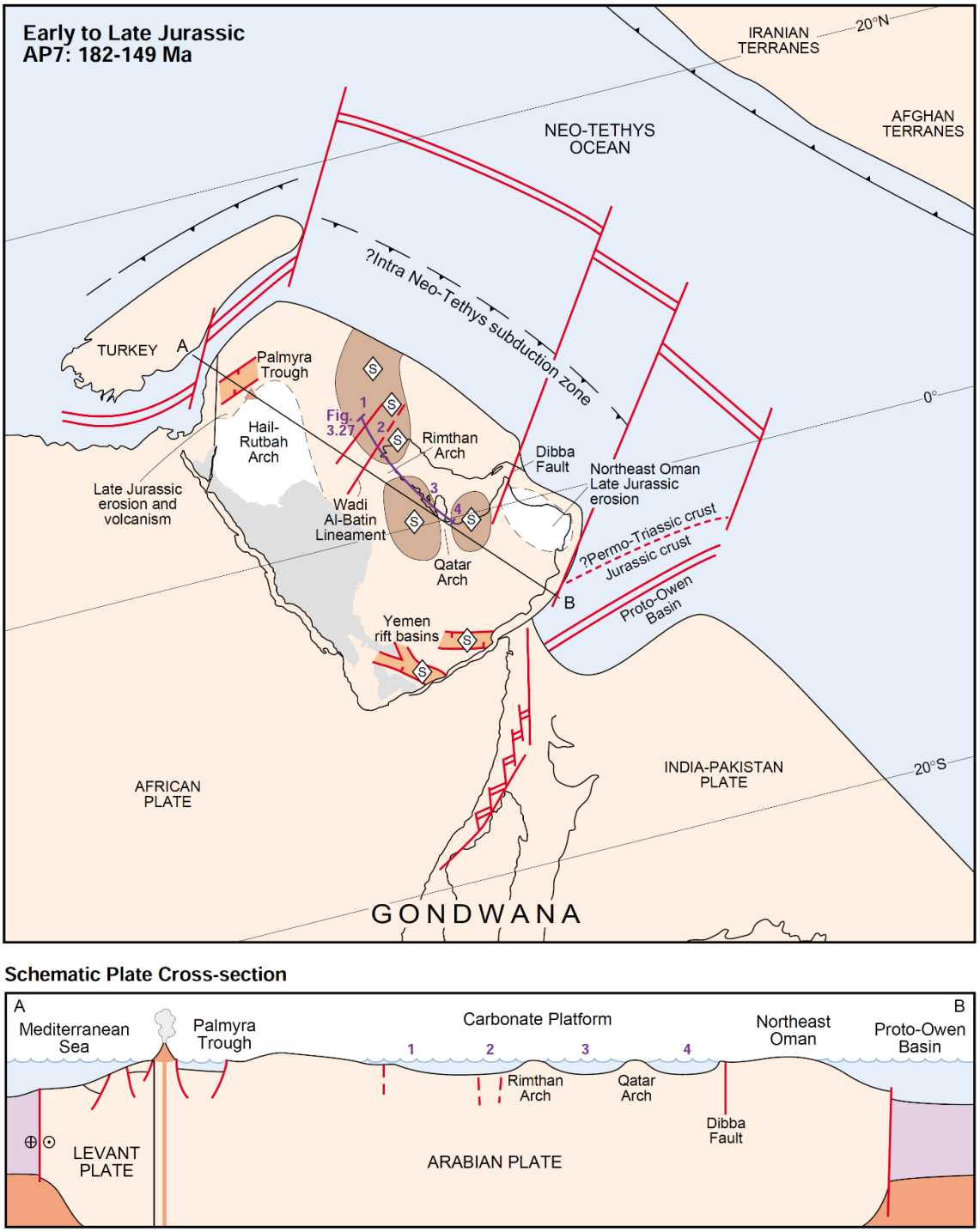


Figure 10 Paleogeographic map and cross section through the Arabian Plate showing the location of the four intrashelf basins Rub' Al Khali and Ras al Khaima basins, the Gotnia Basin, and Arabian Basin. 1-4 represent the location of four main source rocks were deposited during that time (Sharland, 2001).

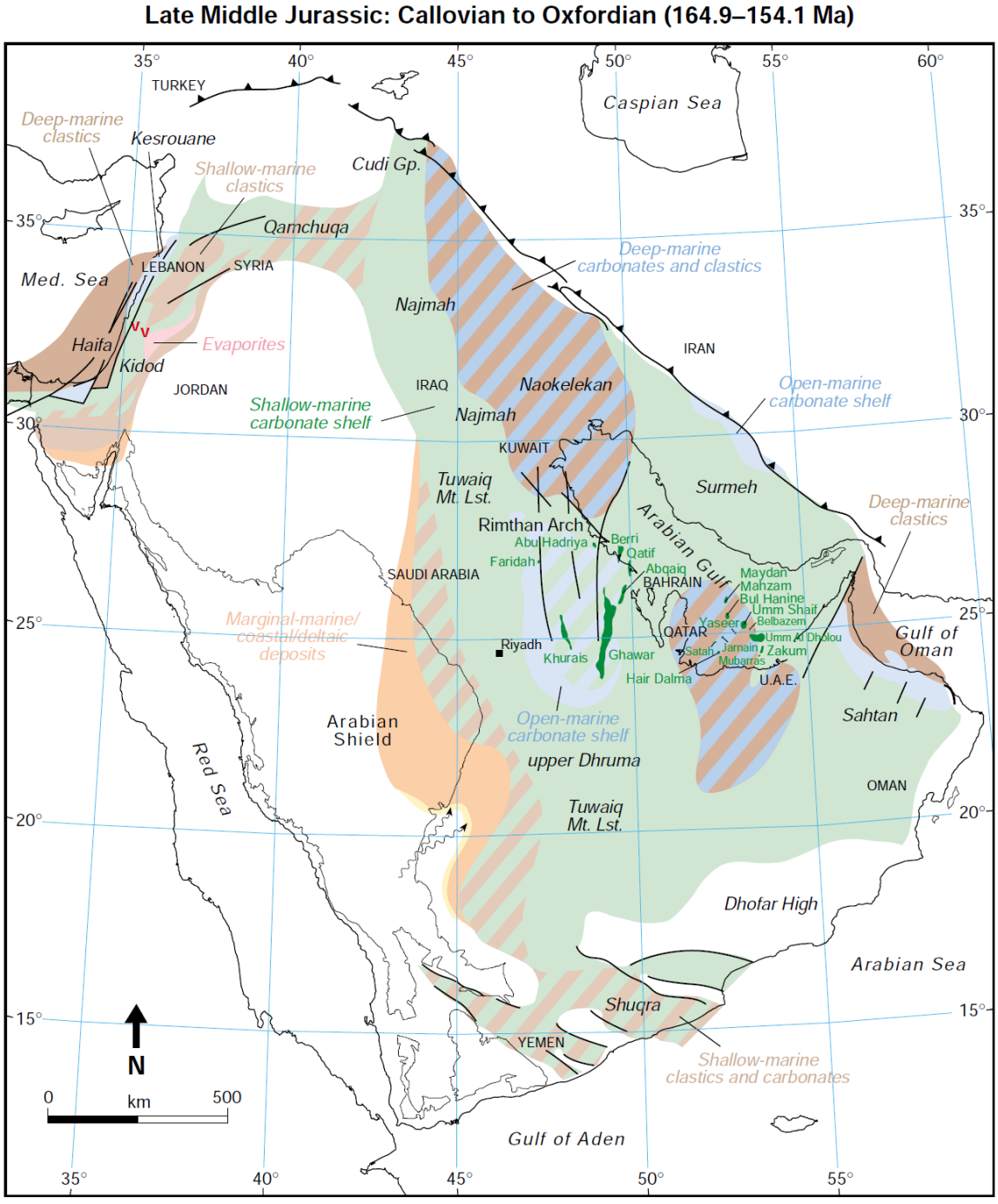


Figure 11 Paleofacies map of the Late Middle Jurassic of the Arabian Plate (Ziegler, 2001)

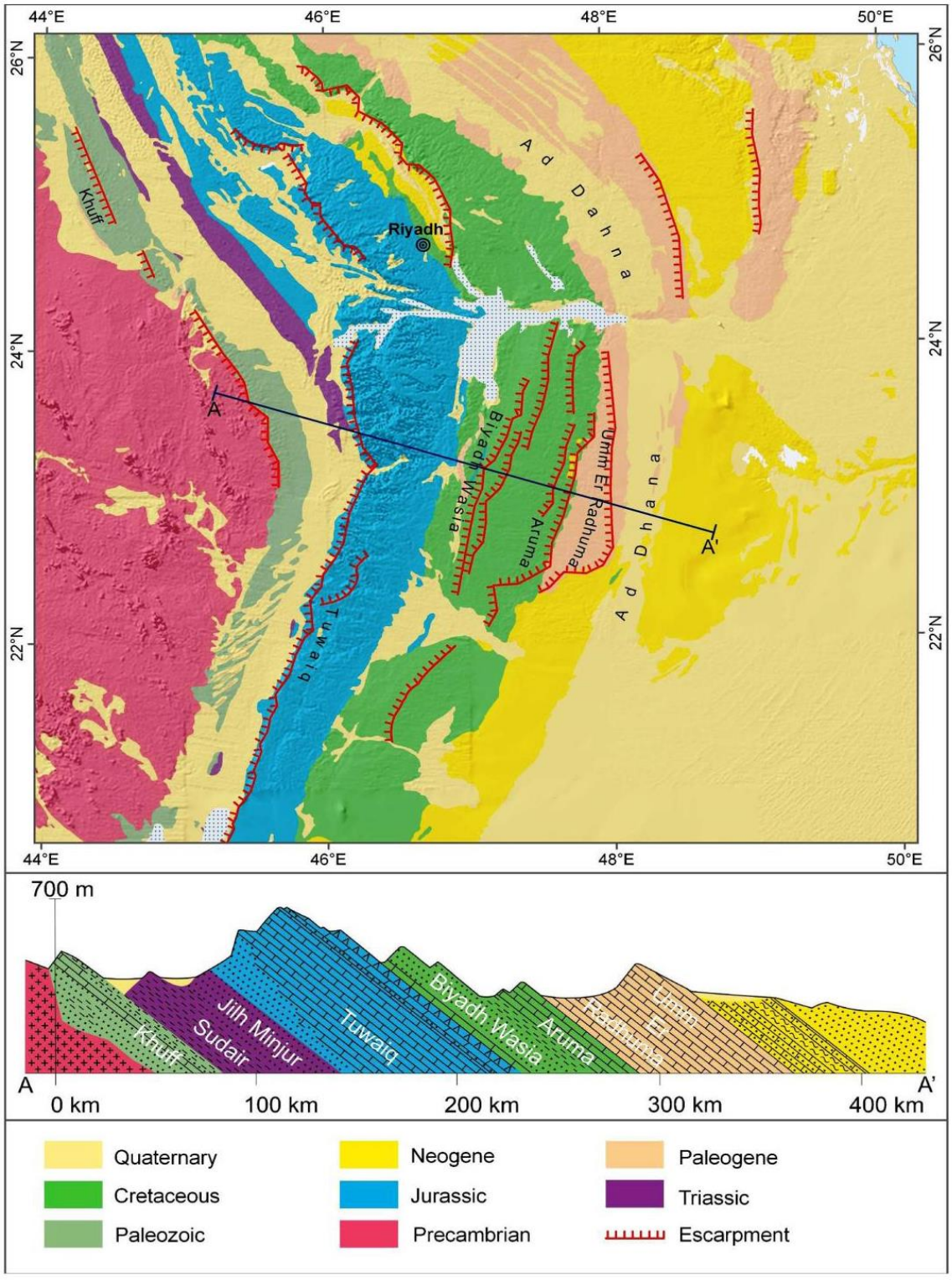


Figure 12 Geologic map and cross section showing the escarpments in the central part of Saudi Arabia (Rausch et al., 2014)

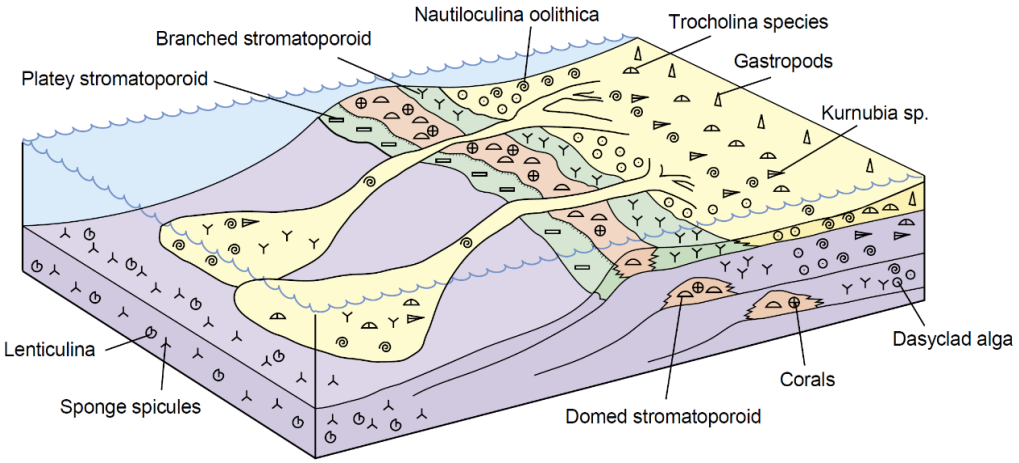


Figure 13 Schematic diagram of the middle to late Jurassic palaeoenviroments and their different biocomponents (Hughes, 2004).

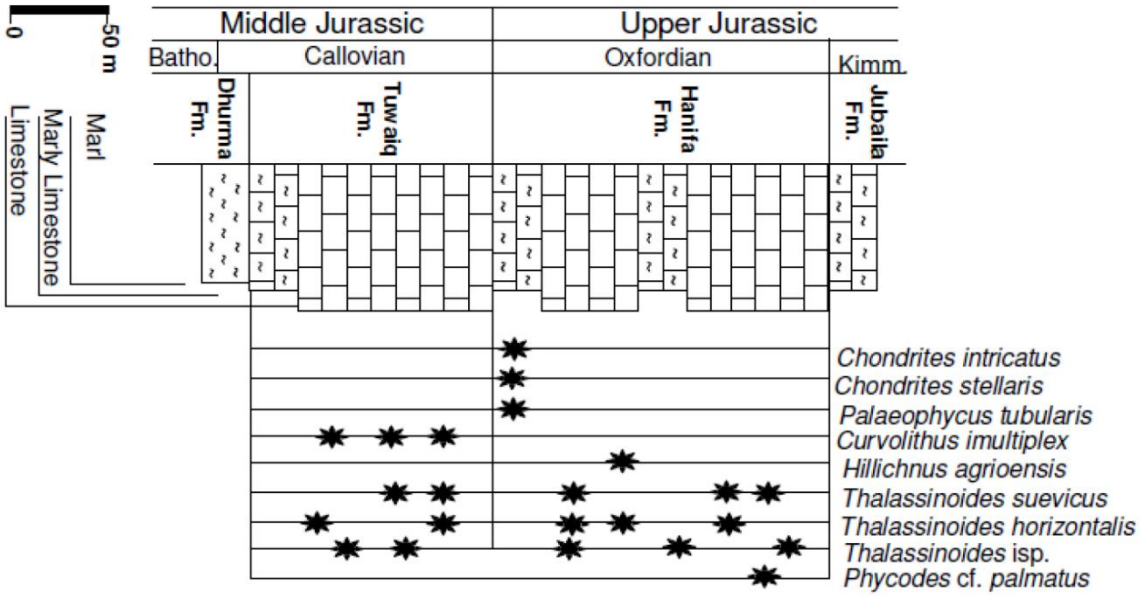


Figure 14 The distribution of trace fossils within the Tuwaiq Mountain Formation (ElHedeny, 2012).

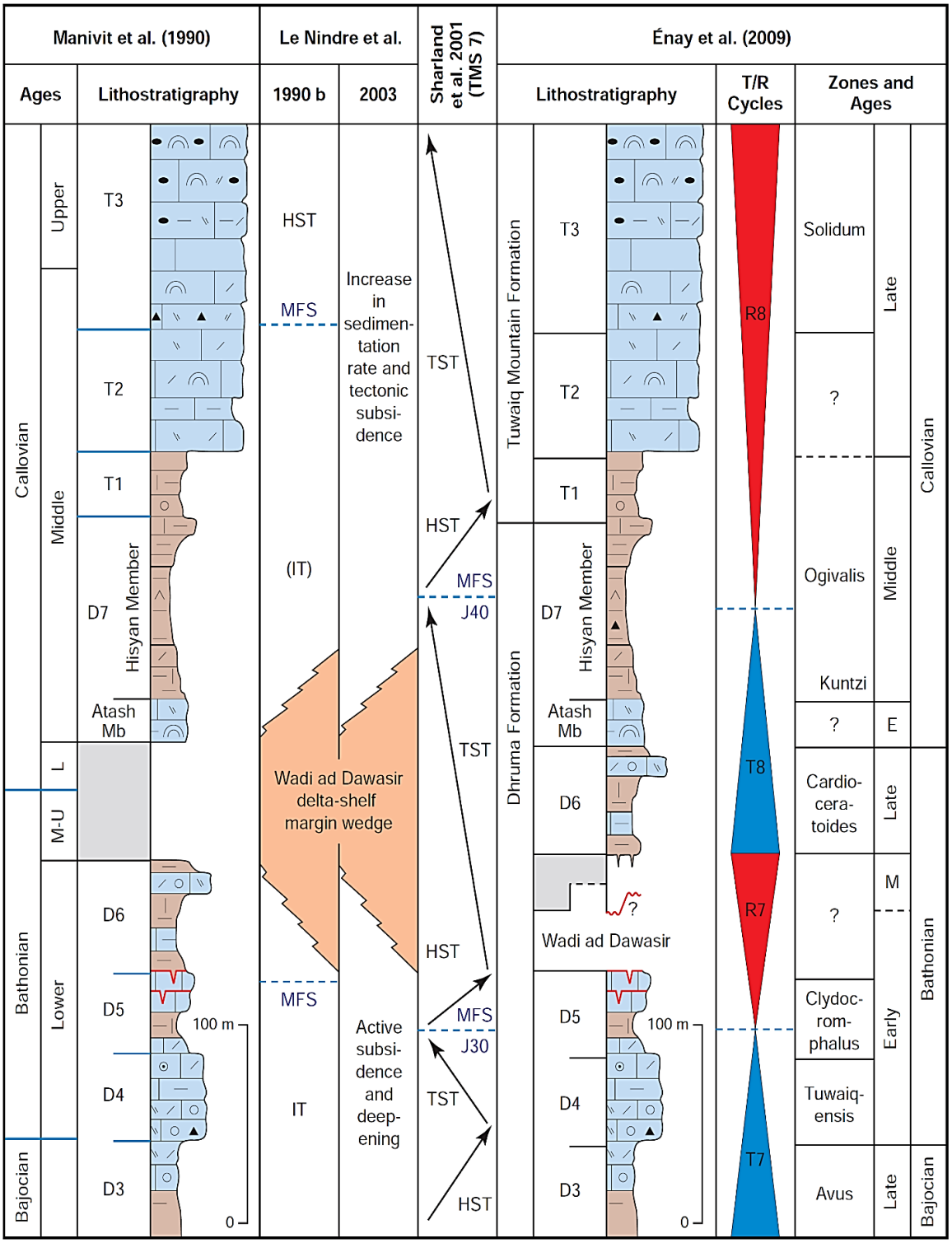


Figure 15 The sequence stratigraphy of the Tuwaiq Mountain Formation (Al-Husseini, 2009).

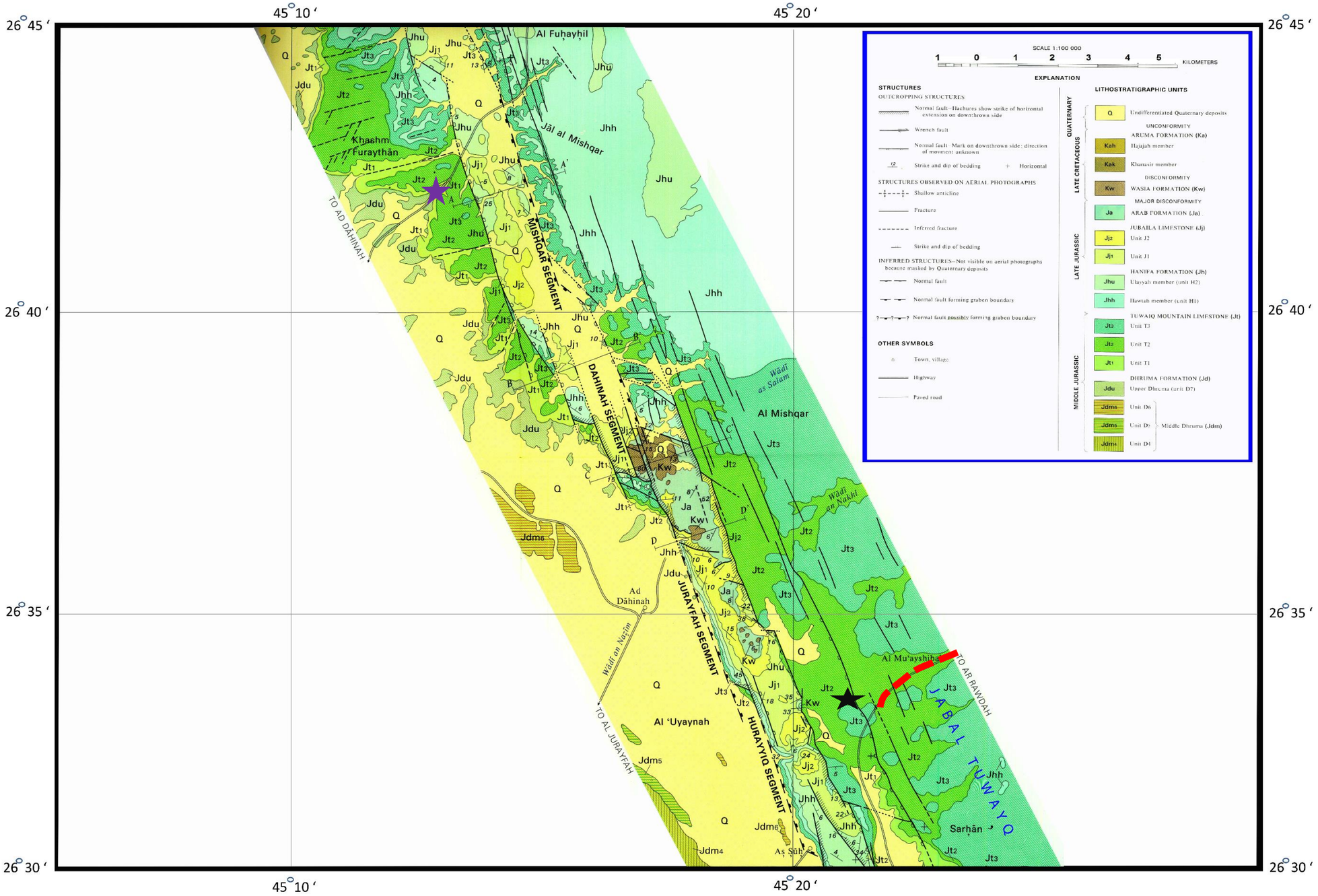


Figure 16 Geological map of the Majma’ah graben system modified after Vaslet et al. (1988). The location of the studied sections are represented by star symbols and dashed line. The purple star represents the studied section of T1, the red dashed line represents the studied section of T2 and the black star represents the studied section of T3

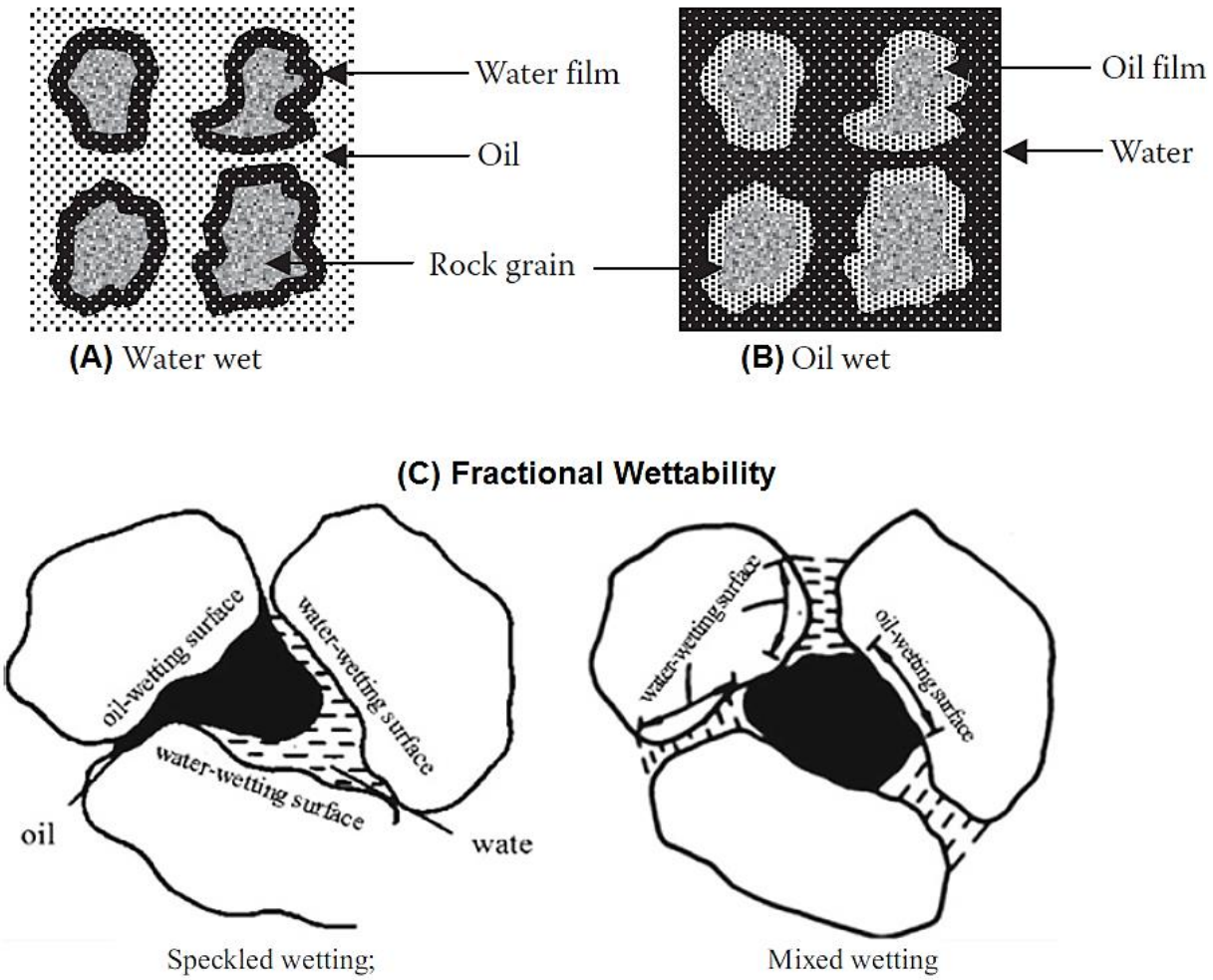


Figure 17 Schematic diagram of oil wet, water wet, speckled wetting and mixing wetting (Xuetao et al., 2017).

| Hydrocarbon | Pentane ($C_5H_{12}$) | Hexane ($C_6H_{14}$) | Octane ($C_8H_{I8}$) | Twelve alkyl ($C_{12}H_{26}$) |
|---|---|---|---|---|
| Advanced angle(°) | 0 | 8 | 26 | 42 |

Table 1 The different Advancing angle of different hydrocarbons (Xuetao et al., 2017).

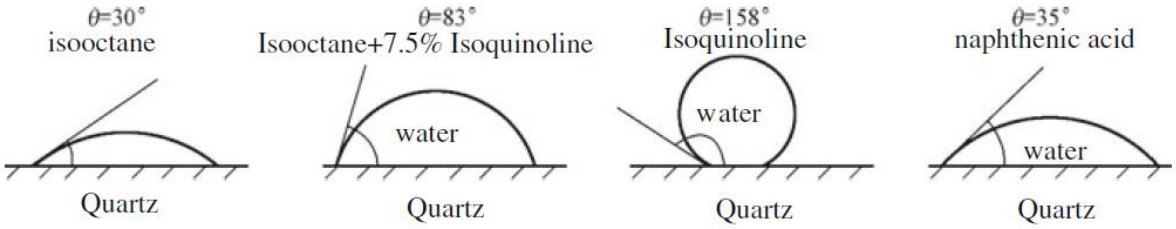


Figure 18 Contact angles of different systems of oil and water quartz surface (Xuetao et al., 2017).

# CHAPTER 3

# Microfacies and Depositional Model: Results and Discussion

## 3.1.Microfacies and Field Observations

### 3.1.1. Field Observations

This study examined outcrops in localities (Figs. 16, 19, 21, and 24) in the Shaqra' quadrangle (Lat 25°and 26° N. and long 45°and 46°30) in Al-Majma'ah Governorate, which is located 200 km northwest of Riyadh. The three members of the TMF (T1, T2 and T3) were described, logged and sampled on a bed-by-bed basis to capture the changes in texture, lithofacies and reservoir quality. Field photos were captured for every bed, in order to tie the thin section interpretation with field observations.

The outcrop of the T1 member, which is located in Ad Dahna (Fig. 16) has a thickness of 10.5 m and contains three different lithofacies. Two of the lithofacies are coral derived facies (rudstones and wackstones with dispersed coral fragments) which show a resistive pattern in the field and it resembles most of the outcrop thickness. These lithofacies alternate with the third lithofacies (Fig. 19), which is mud supported facies (skeletal mud-wack-stone) with weathered pattern in the outcrop (Fig. 20).

The outcrop of the T2 member is exposed along a roadcut in the Al Majma'ah area (Fig. 16), and has two distinctive units (Figs. 21 to 23). The lower unit, which has a thickness of 38 m, is composed of reef derived facies (rudstones and wackstone with dispersed coral fragments) alternating with mud supported facies. It is characterized by thick to massive

bedding with bed thickness ranging from 30 cm to 170 cm, and by mud supported textures with coral and stromatoporoid fragments. No sedimentary structures are observed in the lower unit although some bioturbation and nodular bedding occur in some beds. The upper unit, which has a thickness of 12 m, is composed of grain supported peloidal facies alternating with wackestone facies and very few to no reef derived facies. It is characterized by thick to massive bedding with bed thickness around 40 to 80 cm. No sedimentary structures are observed in the upper unit except burrowing and bioturbation.

The outcrop of T3 is located near the outcrop of T2 in the Al-Majma'ah area (Fig. 16), and has a thickness of 28 m (Figs. 24 and 25). Field observations indicated that it is mainly composed of reef derived facies (rudstones and wackstone with dispersed coral fragments) which has resistive pattern in the outcrop, and alternates with mud supported facies with weathered pattern (Fig. 33). No sedimentary structures or trace fossils were observed. The upper most part of the outcrop is composed of grain supported facies where patch reefs and two chert beds are encountered (Figs. 35.b and c). The outcrop of T3 has places where there are in situ accumulations of corals and stromatoporoids that shows evidence of depositional mounding. Theses depositional mounds are interpreted as a patch reef and they have ellipsoidal to irregular in shape and may be up to 6 m across and 1–3 m in height.


(a)
1 m

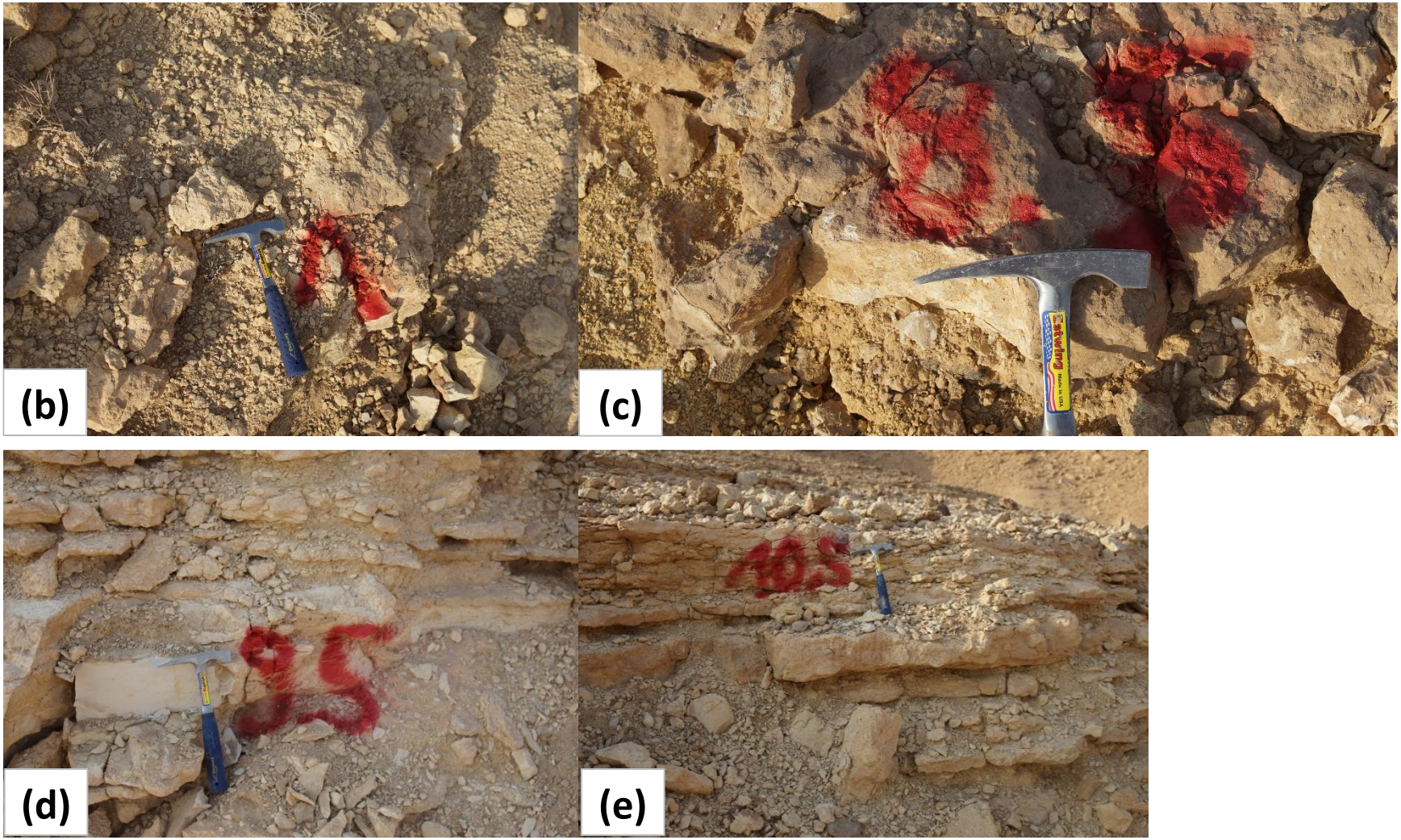


Figure 19 Field photos of the outcrop of Member T1 at Ad Dahna showing: (a) the alternation between resistive and weathered beds. (b and d) Field photos of mud supported facies. (c and e) coral derived facies of rudstone (c) and wackstone (e) texture with dispersed coral fragments.

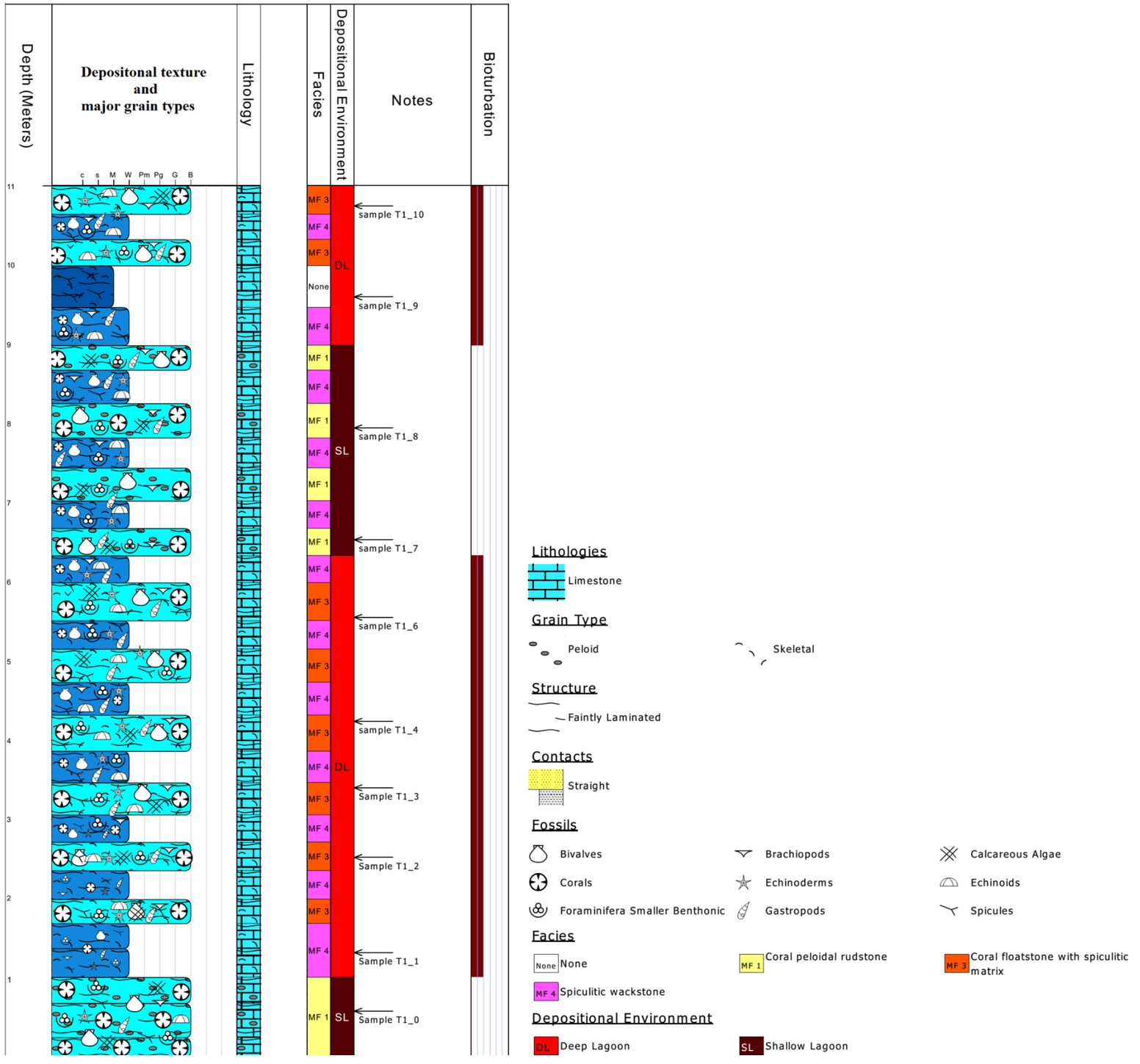


Figure 20 Measured section of the T1 member at locality 3 in Ad Dahnah area showing the vertical distribution of microfacies, fossils, lamination, bioturbation, depositional environment of different facies and samples locations.

Figure 21 Panoramic Photo of Al Mu’ayshibah area showing the outcrop of member T2 (note the car as a scale).

(a)

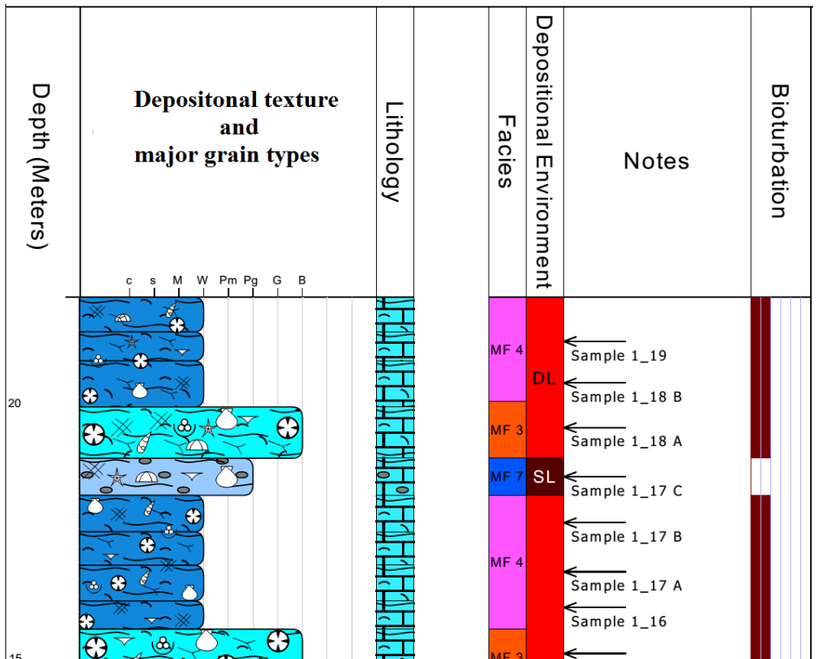


Lithologies

Limestone

Grain Type

Peloid

Skeletal

Structure

Faintly Laminated

Contacts

Straight

Fossils

Bivalves

Brachiopods

Calcareous Algae

Corals

Echinoderms

Echinoids

Foraminifera Smaller Benthonic

Gastropods

Spicules

Facies

None None

MF 3 Coral floatstone with spiculitic matrix

MF 4 Spiculitic wackstone

MF 7 Peloidal packstone

Depositional Environment

DL Deep Lagoon

SL Shallow Lagoon

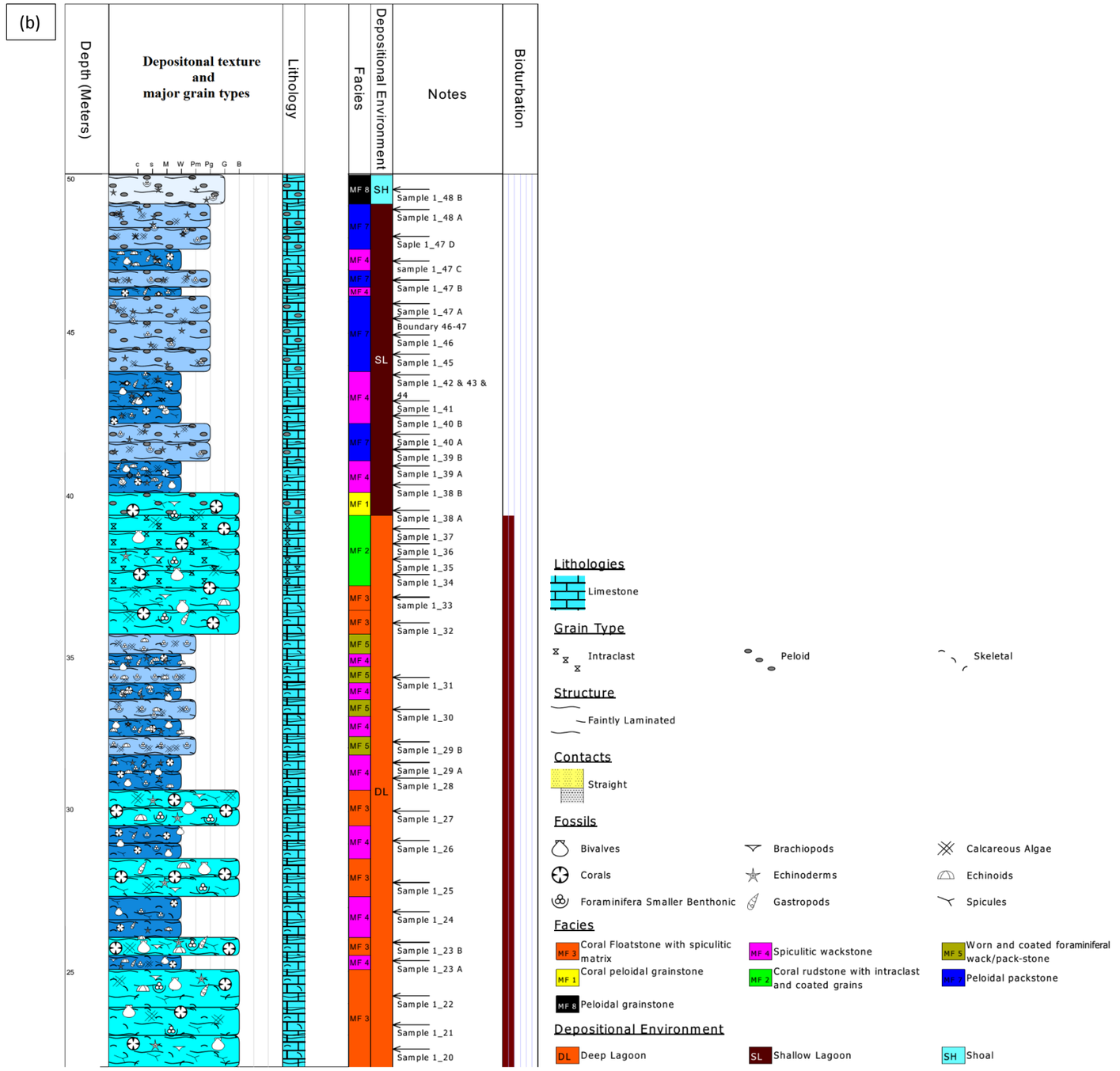


Figure 22 Measured section of the T2 member at locality 1 in Al Mu'ayshibah area. (a) Measured section of T2 member part 1 from 0 to 22 m. (b) Measured section of T2 member part 2 from 22 to 50. Both (a) and (b) showing the vertical distribution of microfacies, fossils, lamination, bioturbation, depositional environment of different facies and samples locations.

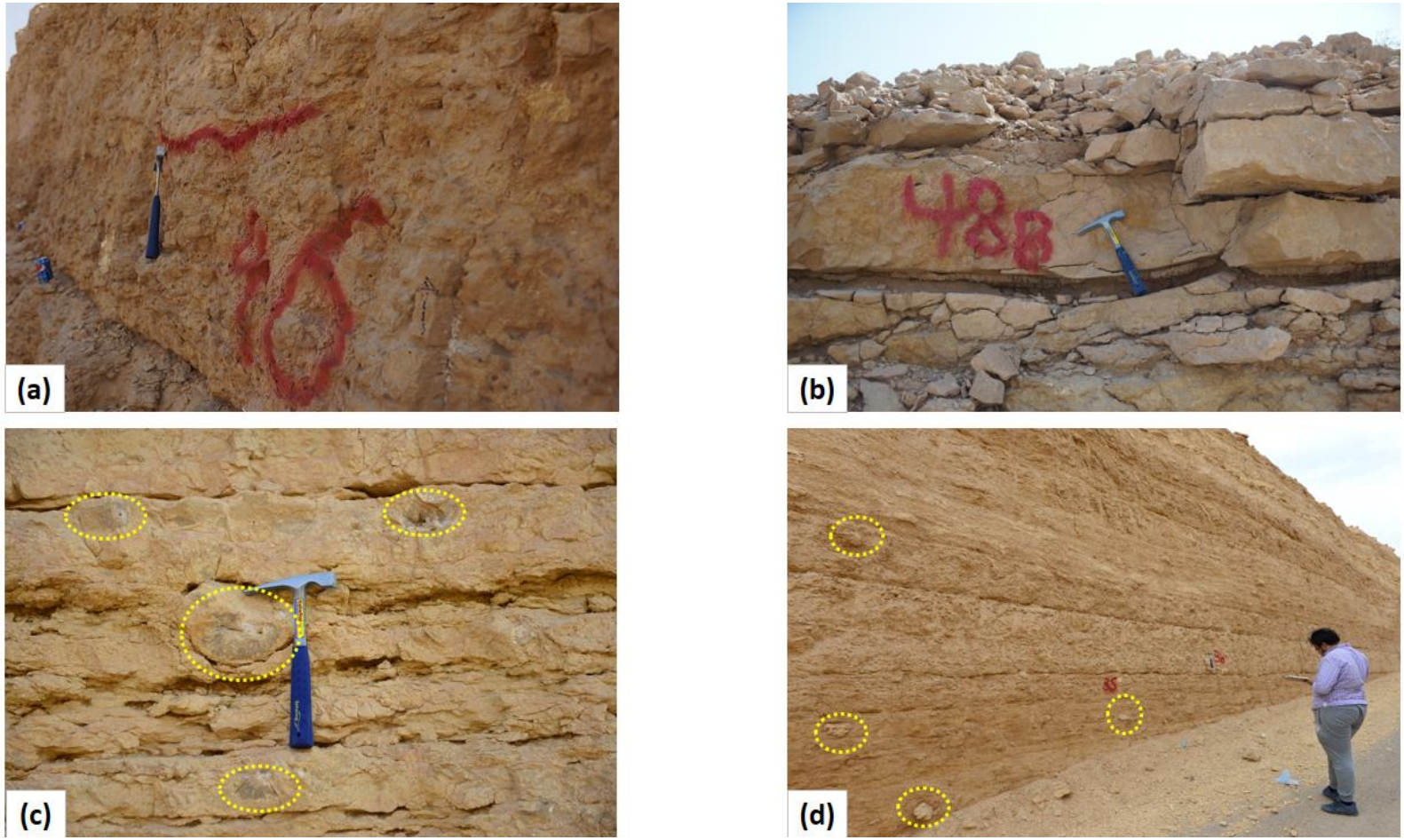

Figure 23 Field photos of Member T2 in Al Mu'ayshibah area showing: (a and b) the beds of upper unit of T2 which are characterized by an absence of coral fragments, bioturbation and burrowed beds and thick to massive bedding. (c and d) the lower unit of T2 which is characterized by abundance of coral fragments scattered within muddy burrowed and bioturbated groundmass (Note the dashed yellow circles around the coral fragments).


Figure 24 Field photo showing the outcrop of the T3 member. The red color numbers written on the outcrop (e.g. 1.6 m) are the locations where samples were taken. (Note scale 1m).


Figure 25 Measured section of the T3 member at locality 2 in the Al Mu'ayshibah area showing the vertical distribution of microfacies, fossils, lamination, bioturbation, depositional environment of different facies and samples locations.

### 3.1.2. Microfacies Description

In this section the carbonate microfacies and facies associations are described by integrating field observations (bed thickness, bed boundary, macrofacies, sedimentary structure, macroporosity, presence or absence of stylolite, HCl affinity, macro fossils, strata relationship) with thin section descriptions (skeletal, and non-skeletal components, texture, fabrics, porosity types, diagenetic alteration, sorting, and grain size). Based on the microfacies description and their stratigraphic position in the outcrop, a depositional model is constructed. The Dunham classification (1962) as modified by Embry and Klovan (1971) is used in the description of the different depositional texture. The depositional environment of each facies is identified using Wilson's facies belt (1975) and microfacies are interpreted according to Flügel (2010). Eight microfacies were recognized in the Tuwaiq Mountain Formation and these microfacies have been grouped into three lithofacies associations. A summery for all microfacies characteristics is summarized in Table 1.

#### 3.1.2.1. MF 1: Coral peloidal rudstone

In the outcrop, this facies has a bed thickness that ranges from 15 cm to 80 cm with a thick to massive bedding style. The beds contain corals fragments scattered within grain supported groundmass. In the polished slabs (Fig. 26.a), this facies shows grainstone texture with big coral fragments (up to 3 cm length) and brachiopod fragments (1 cm length). Locally, silicified bioclasts occur mainly a leached moldic pores in coral were observed. Macrospores are rare, and are found as vugs that are filled by calcite cement and form geodes (Fig. 26.a).

In the thin sections, the texture of this facies is grain supported with large coral fragments that may exceed the 4 mm in size. In some cases, the corals are completely or totally dissolved and filled with sparry calcite cement, and locally, lime mud (micrite) fills portions of the primary intraparticle porosity in coral fragments (Fig. 26.b). The other skeletal and non-skeletal grain components include monaxon and triaxon sponge spicules, peloids, brachiopod and bivalve fragments, lime mud (micrite), gastropods, and foraminiferas (Fig. 26). These peloids have a size ranging from 0.1-0.2 mm (Fig. 26.c). Calcareous algae is present but rare. The benthic foraminiferal assemblage include *Nautiloculina* sp., *Kurnubia* sp., and *Everticyclammina* cf. *virguliana* sp.. The calcitic brachiopod fragments are partially silicified

**Environmental Interpretation**

The grain dominated texture and the small amount of lime mud observed in this facies is suggestive of deposition in moderate to high energy environment, while the foraminiferal assemblage of this facies (*Nautiloculina* sp., *Kurnubia* sp., and *Everticyclammina* cf. *virguliana* sp.) is indicative of deposition in shallow marine settings that might be deep or shallow lagoon (Hughes, 2004; 2008; and 2009). With such a grain dominated texture, it is more likely that this facies was deposited in a shallow lagoon settings above the fair weather wave base (FWWB) but influenced by frequent storm events. Further support to this interpretation comes from the fact that the foraminiferal assemblage appears to be in place and not transported to deep water settings because of the absence of any deep water planktonic forams such as *Nodosaria* sp. and *Lenticulina* sp. which were described by Hughes (2004; 2008; and 2009). A similar facies with similar components was interpreted

by Beresi et al. (2017) to be deposited in restricted lagoon around patch reefs above FWWB under influence of storm.

#### 3.1.2.2. MF 2: Coral Rudstone with intraclasts and coated grains

In outcrop, this facies has a bed thickness ranging from 50 cm to 74 cm and shows thick bedding with no obvious sedimentary structures. Dispersed coral fragments are found throughout this facies (Fig. 27.b). This facies has a grain supported texture (rudstone) with presence of lime mud. In polished slabs, large overturned and rotated coral fragments occur in a muddy packstone matrix (Fig. 27.a).

In thin section, coral fragments are abundant and are either totally dissolved fragments and filled with sparry calcite cement or contain lime mud filling and partially preserving the internal structure (Fig. 27.c). The other skeletal grain components of this facies include benthonic foraminiferas, gastropods, brachiopods, echinoderm fragments, bivalves, sponge spicules and calcareous algae (Fig. 27). The benthic foraminiferal assemblage of this facies includes *Kurnubia* sp., *Andersenolina alpina* sp., *Redmondoides* sp. and *Nautiloculina* sp. and no deep water planktonic foraminiferas (Fig. 27.d). Some of the skeletal grains (e.g. brachiopods and gastropods) have a micrite envelope (Fig. 27.e). The non-skeletal grain components include peloids and rare monaxon and triaxon sponge spicules. In several samples, two types of intraclasts occur, those intraclasts composed mainly of mud with some dispersed undifferentiated bioclasts, and intraclast composed mainly of similar faunal assemblage to that of this microfacies (same benthic foraminiferas encountered in the groundmass; Fig. 27.d).

**Environmental Interpretation**

The foraminiferal assemblage observed in this facies includes; *Kurnubia* sp., *Andersenolina alpina* sp., *Redmondoides* sp. and *Nautiloculina* sp. This assemblage is indicative of a shallow marine environment that is possibly of deep or shallow lagoon settings (Hughes, 2004; 2008; and 2009). The lime mud content of this facies is suggestive of moderate to low energy environment. Therefore, it is more likely that this facies was deposited in the deep lagoon environment just below FWWB under influence of storm. Three lines of evidence support this interpretation. First, the foraminiferal assemblage is suggested to be in place and not be transported to deep water settings because of the absence of any deep water planktonic foraminiferas such as *Nodosaria* sp. and *Lenticulina* sp. which were described by Hughes (2004; 2008; and 2009). Second, similar facies with similar components was interpreted by Beresi et al. (2017) to be deposited in restricted lagoon around patch reefs above FWWB. Third, the presence of intraclasts in that facies is indicative of shallow marine settings (Flügel, 2010).

#### 3.1.2.3. MF 3: Coral Floatstone with spiculitic matrix

In outcrop, the bed thickness of this facies ranges from 50 to 120 cm and it has a mud supported texture (wackstone) with scattered coral fragments (Fig. 23.b). The mud dominated texture is also reflected in some cases in the bedding style as some beds show nodular bedding. Burrowing and bioturbation are observed in both outcrops and polished slabs (Fig. 29.e). In the slabs, large coral fragments with length ranging from 2 cm to more than 10 cm occur in a mud dominated matrix. These coral fragments appears in three different ways either totally dissolved or filled with sparry calcite cement (Fig. 28.a), partially silicified (Fig. 28.d), or with the internal structure filled with lime mud (Fig. 29.a).

This facies has a mud dominated texture of peloidal lime mud (micrite) with abundant monoaxial and triaxial sponge spicules (Fig. 28.c). Within the peloidal lime mud, large coral fragments of different sizes ranging in from 2 to 5 mm, are scattered (Fig. 28.b and d). Some of them occur as molds filled with sparry calcite cement, while others are partially silicified or filled with micrite. The foraminiferal assemblage of this facies includes different species (*Andersenolina cherchiae* , *Kurnubia* sp. , *Nautiloculina* sp., and *Redmondoides* sp.) but Kurnubia sp. and Nautiloculina sp. are the most dominant ones (Fig. 28.d). The other skeletal components include bivalves (Fig. 24.b), echinoderm fragments and spines (Fig. 28.e), brachiopods, and rare micrite filled gastropods (Fig. 28.e). Peloids are also present but are not a major contributor. There are two types of bivalves; large fragments (Fig. 28.c) and fragments of thin walled bivalve; *Bositra buchi* sp. (Fig. 29.d). Calcareous algae (*Salpingoporella annulata*) are also found but are rare (Fig. 29.b). Fragments of silicified stromatoporoids with sizes up to 5-7 cm occur locally. In some samples the coral fragments showed borings which is filled with micrite (Fig. 29.c). Echinoderm fragments and spines ranging in size from 500 μm to 2 mm occur, as well as brachiopod fragments that exceed 1 cm in size.

**Environmental Interpretation**

The muddy texture of this facies is an indicator of a low energy depositional environment. In addition, the foraminiferal assemblage (*Andersenolina cherchiae, Kurnubia* sp.*, Nautiloculina* sp.*, and Redmondoides* sp.*)* is indicative of a shallow marine environment that is possibly of deep or shallow lagoon settings (Hughes, 2004; 2008; and 2009). Based on the foraminiferal assemblage and the muddy texture, it is more likely that this facies was deposited in a deep lagoon settings below FWWB. Three lines of evidence support

this interpreted depositional environment. First, the foraminiferal assemblage is suggested to be in place and yields no evidence of transport into a deep water settings due to the absence of any deep water planktonic forams such as *Nodosaria* sp. and *Lenticulina* sp. as described by Hughes (2004; 2008; and 2009). Second, The characteristics of this facies is similar to SMF 8, which is based on Flügel (2010) and Wilson (1975) might be deposited either in facies zone (FZ) 2 or FZ 7 but Flügel (2010) suggested that the presence of calcareous algae is indicative to FZ 7, which is open marine platform interior. Third, similar facies were reported by Machel and Hunter (1994) in the Devonian, by Beresi et al. (2017) in coral patch reef systems of an Oxfordian shallow-marine carbonate platform in Argentina, and by Afghah (2016) in Upper Cretaceous–Lower Paleocene strata in south Zagros basin.

#### 3.1.2.4. MF 4: Spiculitic wackstone

In outcrop and hand samples, this facies ranges in thickness from 50 cm to 100 cm and, similar to MF 3 in terms of mud supported texture, shows abundant coral fragments, nodular bedding style, and the presence of burrowing and bioturbation, although the abundance and the size of corals fragments are less than in MF 3 (Fig. 23.b).

In thin section, this facies has a mud dominated texture (wackstone) and abundant monaxon and traixial sponge spicules (Fig. 30.b) but locally becomes a packstone where there are cluster of sponge spicules within the lime mud. The benthic foraminiferal assemblage of this facies includes different species (*Textulariopsis* sp., *Kurnubia* sp., *Nautiloculina* sp., *Redmondoides* sp.) (Fig. 30.d). Different types of skeletal fragments are found in this microfacies (Figs. 30 and 31) including brachiopods, bivalves, small coral fragments, and echinoderm fragments and spines. Large fragments of brachiopods can reach 5 mm length

(Fig. 30.e). This facies also includes large fragments of bivalves and fragments of thin walled bivalve (*Bositra buchi* sp.; Fig. 31.b). Dasycladacean calcareous algae (*Salpingoporella annulata*) (Fig. 31.c) and gastropods occur rarely in the thin sections. In this facies, intensive burrowing is observed both in slabs (Figs. 30.a and 31.a) and thin section (Fig. 31.d and e). These burrows are filled with sparry calcite cement (Fig. 31.e) where peloids, foraminiferas, and fragments of brachiopod, echinoid, and bivalve grains are cemented by sparry equant calcite. In some cases the burrows are filled with lime mud (micrite) and a similar faunal assemblage to that of this microfacies (Fig. 31.d).

**Environmental Interpretation**

The muddy texture of this facies is an indicator of a low energy depositional environment, and the foraminiferal assemblage (*Textulariopsis* sp. , *Kurnubia* sp. , *Nautiloculina* sp. , *Redmondoides* sp.) is indicative of a shallow marine environment that is possibly of deep or shallow lagoon settings (Hughes, 2004; 2008; and 2009). Based on the foraminiferal assemblage and the muddy texture, it is more likely that this facies is deposited in deep lagoon settings below FWWB. There are three lines of evidence supporting the interpreted depositional environment. First, the foraminiferal assemblage is suggested to be in place and not transported to deep water settings because of the absence of any deep water planktonic foraminiferas such as *Nodosaria* sp. and *Lenticulina* sp. as described by Hughes (2004; 2008; and 2009). Second, The characteristics of this facies is similar to SMF 9, which is based on Flügel (2010) and Wilson (1975) might be deposited either in facies zone (FZ) 2 or FZ 7 but Flügel (2010) suggested that the presence of calcareous algae is indicative to FZ 7, which is open marine platform interior. Third, similar facies was reported by Beresi et al. (2017) in a coral patch reef system of the Oxfordian

shallow-marine carbonate platform in Argentina, and by Afghah (2016) in Upper Cretaceous–Lower Paleocene strata in the south Zagros basin and by Mirza et al. (2016) in the Garagu Formation of the Gara Mountain in Iraq.

#### 3.1.2.5. MF 5: worn and coated foraminiferal wack/pack-stone

In outcrop, beds of this facies have an average thickness of 50-70 cm and coral fragments locally occur (around 15 cm) within a foraminiferal wack/pack-stone matrix (Fig. 33). In polished slabs, they display a variable depositional texture but generally range from wackstone to packstone. Some small coral fragments (2-3 cm) occur dispersed within the samples (Fig. 32.a).

In the thin section, this facies has a mud supported texture in most samples which is dominated by worn and coated foraminifera scattered within lime mud. Locally, grain supported textures occur, but the mud content is always high. The foraminiferal assemblage of this facies includes (*Andersenolina elongata* sp., *Andersenolina alpina* sp., *Andersenolina cherchiae* sp., *Kurnubia* sp., *Globovulvulina* sp., *Nautiloculina* sp.) but *Andersenolina alpina* sp. and *Andersenolina cherchiae* sp. are the most abundant (Fig. 32.b). Other skeletal components include sponge spicules, brachiopod fragments, echinoderms, gastropods, calcareous algae and small coral fragments up to 5 mm in length (Fig. 32.b, c and d). This facies contains mud clasts (rip up clasts) with size ranges between 2-4 mm and it is mainly composed of mud with some dispersed calcitized dolomite crystals.

**Environmental Interpretation**

The muddy texture of this facies is an indicator of low energy depositional environment, while foraminiferal assemblage (*Andersenolina elongata* sp. , *Andersenolina alpina* sp. ,

*Andersenolina cherchiae* sp. , *Kurnubia* sp. , *Globovulvulina* sp. , *Nautiloculina* sp.) is indicative of a shallow marine environment that is possibly of deep or shallow lagoon settings (Hughes, 2004; 2008; and 2009). Based on the foraminiferal assemblage and the muddy texture, it is more likely that this facies is deposited in deep lagoonal settings below the FWWB. There are four lines of evidence support this interpreted depositional environment. First, the mud clasts "rip up clasts" are indicative of shallow marine environments (supratidal, intertidal, and subtidal) (Flügel, 2010). Second, the foraminiferal assemblage is suggested to be in place and not to be transported to deep water settings because of the absence of any deep water planktonic foraminiferas such as *Nodosaria* sp. and *Lenticulina* sp. as described by Hughes (2004; 2008; and 2009). Third, this facies has similar characteristics as SMF 10 which is based on Flügel (2010) and Wilson (1975) can be deposited either in FZ 7 or FZ 2 but based on the previously discussed points about faunal assemblage, calcareous algae, and mud clasts, it is interpreted to be deposited in FZ 7 (open marine platform interior). Fourth, similar facies was reported by Al-Dabbas (2012) in the Mauddud Formation (age Albian–Early Cenomanian) in Iraq. Therefore, the depositional environment is interpreted as deep lagoon below the fair weather wave base (FWWB).

#### 3.1.2.6. MF 6: Fine-grained peloidal grainstone

In the outcrop, the beds of this facies have an average thickness of 50-70 cm with thick bedding style. Small patch reefs are found within the succession of this facies in the upper most part of T3 (Fig. 35. a, b and c). In the polished slab it shows very fine grained texture with rare open fractures (Fig. 34.a).

This facies has a grain supported texture with no mud content and it is composed mainly of small muddy peloids that range in size from 80-100 µm to 250 µm (Fig. 34.b). It contains fragments of corals which can exceed 1 centimeter in length (Fig. 34.b). Also, it contains echinoderm fragments and spines which have a wide range of sizes from less than 200 µm to 1 mm. The peloids and echinoderm fragments represent the major components of this facies, although other skeletal grains occur (Fig. 34.b and c). The foraminiferal assemblage of this facies includes *Nautiloculina* sp., *Redmondoides* sp., and *Riyadhella* sp., although the most common species here is Nautiloculina sp. (Fig. 34.e and 35.d). Rare bivalve and brachiopod fragments with size less than 0.5 mm occur throughout this facies (Fig. 34.d). Dasycladacean green algae occur locally (Fig. 34.b).

In the upper part of TMF, the stromatoporoids and corals accumulations formed mounds. This mounding forms patch reefs with length ranges up to 6 m and height up to 4 m. The patch reefs are composed of colonized platy and domal corals with stromatoporoids (Burgundia and Shuqraia) and the substrate is composed of fine grained peloidal grainstone. The sediments filling the space between the patch reefs is mainly of wack/pack-stone texture containing fragments of corals and stromatoporoids.

**Environmental Interpretation**

The grainy and mud free texture of this facies is indicative of a high energy environment, while the foraminiferal assemblage of this facies including *Nautiloculina* sp., *Redmondoides* sp., and *Riyadhella* sp. is suggestive of deposition in a deep or a shallow lagoon settings (Hughes, 2004; 2008; and 2009). The absence of any mud content is interpreted to suggest that this facies was likely deposited in shallow lagoon environment above FWWB. This interpretation is supported by the fact that this facies has characteristics similar to SMF 16 which is indicated to be deposited in FZ 8 with moderate energy of shallow lagoon environment (Flügel, 2010 and Wilson, 1975), as well as by the presence of patch reefs that are thought to be associated with that facies which is indicative of lagoonal environment, as described by (El-Asa'ad, 1991; Leinfelder, 2005).

#### 3.1.2.7. MF 7: Peloidal Packstone

In outcrop, the beds are thick-bedded with thicknesses ranging from 40 cm to 60 cm. Burrowing activity is apparent both the thin section and hand samples (Figs. 37.a, 37.e and 38). The polished slabs show the grainy mud poor texture of this facies and the presence of large brachiopod fragments (Fig. 36.a).

In thin section, this facies has a grain supported mud poor texture which is composed mainly of peloids and micritized grains (Fig. 36.b). The peloids have a size range from 100 µm to more than 250 µm. No coral fragments have been observed in this facies although other skeletal grains are common including bivalves, echinoid fragments and spines, and brachiopods. Large brachiopod fragments occur locally and have sizes that can exceed 1 cm. Mud clasts ("rip up clasts") are found throughout this facies (Fig. 36.e). The mud content does not exceed 5-7 %. The foraminiferal assemblage of that facies includes; *Nautiloculina* sp., *Redmondoides* sp., *Riyadhella* sp., and *Kurnubia* sp., but the most

common type is *Riyadhella* sp. (Fig. 36.d). Ooids occur locally, and range in size from 0.2 mm to 1 mm (Fig. 37.c). Calcareous algae are also present but are not common (Fig. 37.d).

**Environmental Interpretation**

This facies has a grain supported mud poor texture which reflects deposition in a moderate to high energy environment. The foraminiferal assemblage of that facies includes; *Nautiloculina* sp., *Redmondoides* sp., *Riyadhella* sp., and *Kurnubia* sp., which is indicative of deposition in a shallow marine environment that is possibly of a deep or shallow lagoonal settings (Hughes, 2004; 2008; and 2009). Based on the foraminiferal assemblage and the grainy texture, it is more likely that this facies was deposited in shallow lagoon settings above FWWB. This facies is more likely to represent a shoal transitional part in shallow lagoon depositional environment which means that this facies is more adjacent to shoal than MF 6. There are two lines of evidence supporting the interpreted depositional environment. First, the foraminiferal assemblage is suggested to be in place and not to be transported into deep water settings because of the absence of any deep water planktonic foraminiferas such as *Nodosaria* sp. and *Lenticulina* sp. as described by Hughes (2004; 2008; and 2009). Second, this facies has characteristics similar to SMF 16 which is indicated to be deposited in FZ 8 with moderate energy of shallow lagoon environment (Flügel, 2010 and Wilson, 1975).

#### 3.1.2.8. MF 8: Peloidal Grainstone

In outcrop, the beds are thick-bedded with thickness around 70 cm (Fig. 39.b), while the polished slabs show the grainy mud free texture of this facies (Fig. 39.a). In thin section, this facies has a grain supported texture which is composed mainly of peloids (Fig. 39.c), that range in size from 100 µm to 500 µm. No coral fragments or mud were observed.

Echinoid fragments and spines, bivalves, and coated brachiopod fragments are the dominant skeletal fragments observed in this facies (Fig. 39.c and d). Large mud clasts with size ranges from 1 mm is to 3 mm were found dispersed throughout this facies (Fig. 39.e). Extensive micritization affected the components of this facies, and to some extent obliterated the structure of the foraminiferal assemblage in this facies. The foraminiferal assemblage includes *Nautiloculina* sp., *Redmondoides* sp., *Pfenderina salernitana* sp., and *Andersenolina alpine* sp. (Fig. 39.c and d).

**Environmental Interpretation**

This facies has a grain supported mud free texture which might suggest deposition in high energy shallow marine environment. The foraminiferal assemblage present in this facies is indicative of deposition in a shallow marine environment either deep or shallow lagoon settings (Hughes, 2004; 2008; and 2009). Based on the foraminiferal assemblage and the grainy mud free texture, it is suggested that this facies was deposited in shoal settings above the FWWB. There are four point that strengthen the interpreted depositional environment. First, the foraminiferal assemblage is suggested to be in place and not transported into deep water settings because of the absence of any deep water planktonic foraminiferas such as *Nodosaria* sp. and *Lenticulina* sp. as described by Hughes (2004; 2008; and 2009). Second, the mud clasts are also indicative of shallow marine settings (Flügel, 2010). Third, the absence of lime mud is suggestive for high energy environment. Fourth, similar facies were reported by Mehrabi et al. (2014) in the Cretaceous Ilam Formation in Iran, and by Koeshidayatullah et al. (2016) in the Jauf Formation in Saudi Arabia.

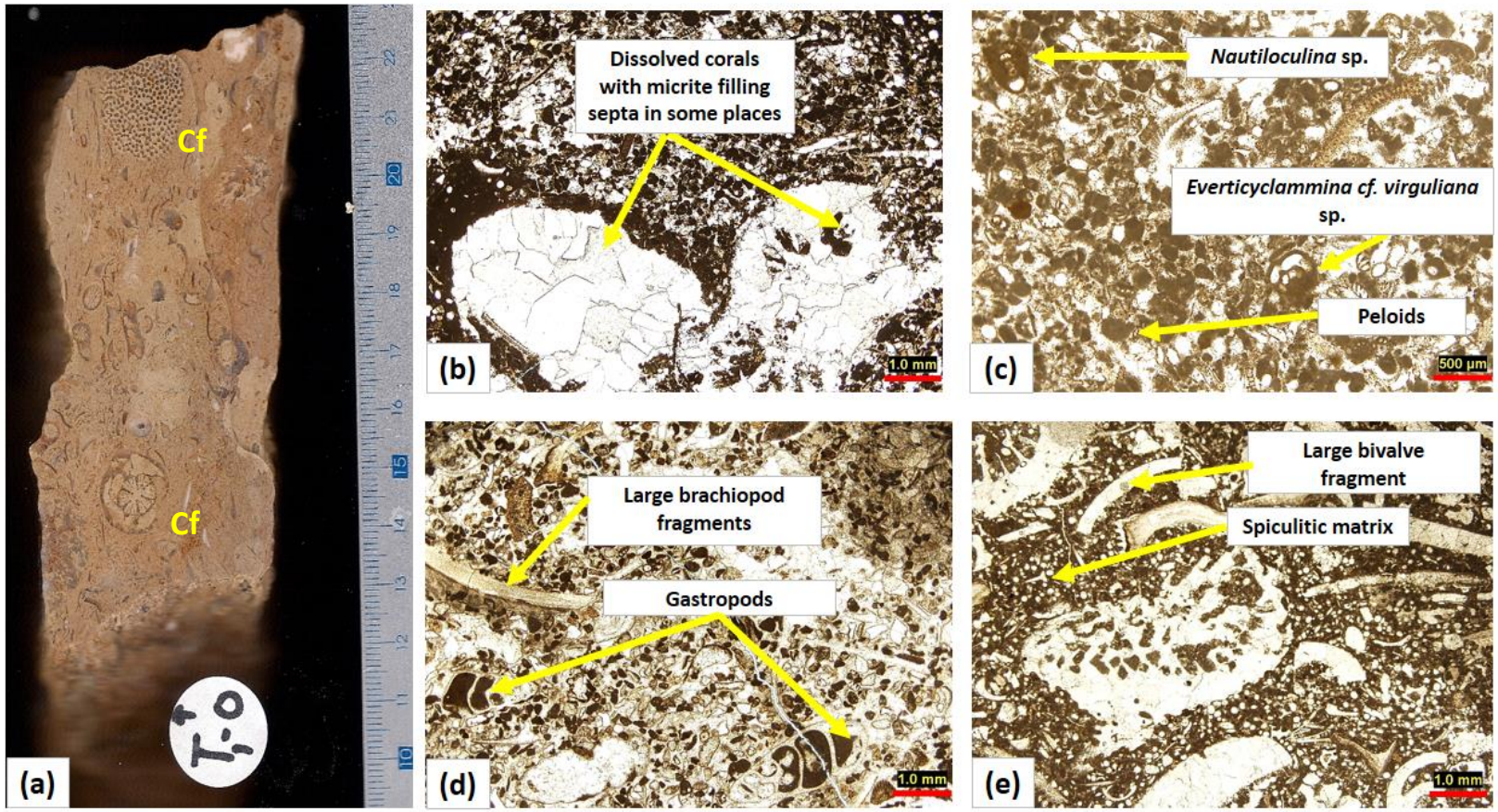


Figure 26 Scanned slab (a) and thin section photomicrographs (b-e) of MF 1 coral peloidal rudstone showing: (a) large coral fragments (Cf) scattered within a peloidal packstone matrix. (b) Dissolved corals with micrite filling space between septa in some places. (c) Benthic foraminiferal assemblage and peloids. (d) Brachiopod fragment and gastropods. (e) Spiculitic matrix, coral fragments, and large bivalve fragments.

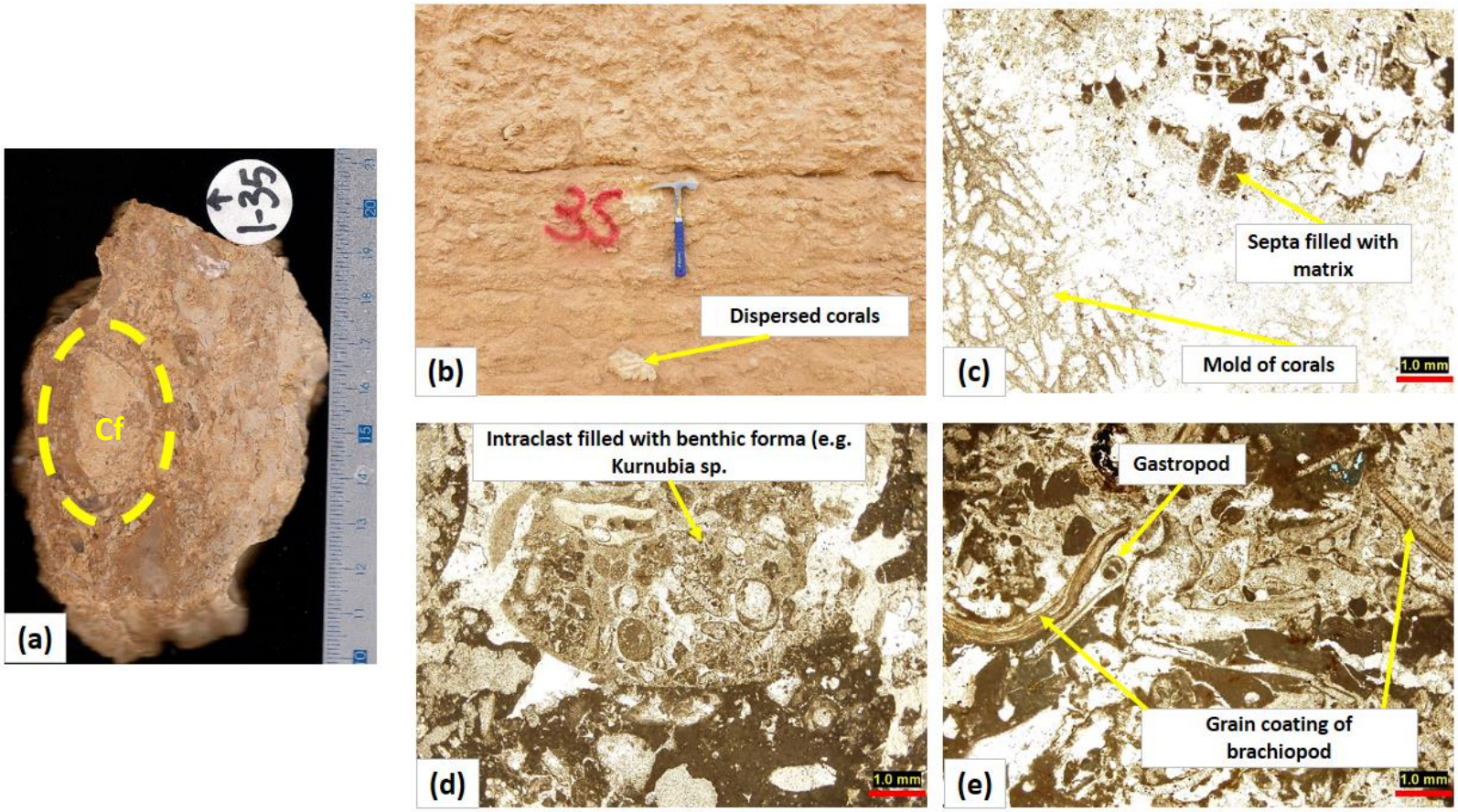


Figure 27 Scanned slab photo (a), field photo (b), and thin section photomicrographs (c-e) of MS 2 coral rudstone showing: (a) a rotated coral fragment (Cf) within a packstone texture (note arrow and scale). (b) Thick bedding and the presence of fragmented dispersed corals. (c) Mold of coral filled with sparry calcite micrite. (d) The presence of intraclasts containing similar foraminiferas assemblages to that seen in the matrix (e.g. *Kurnubia*, sp.). (e) Coated brachiopod and gastropod fragments.

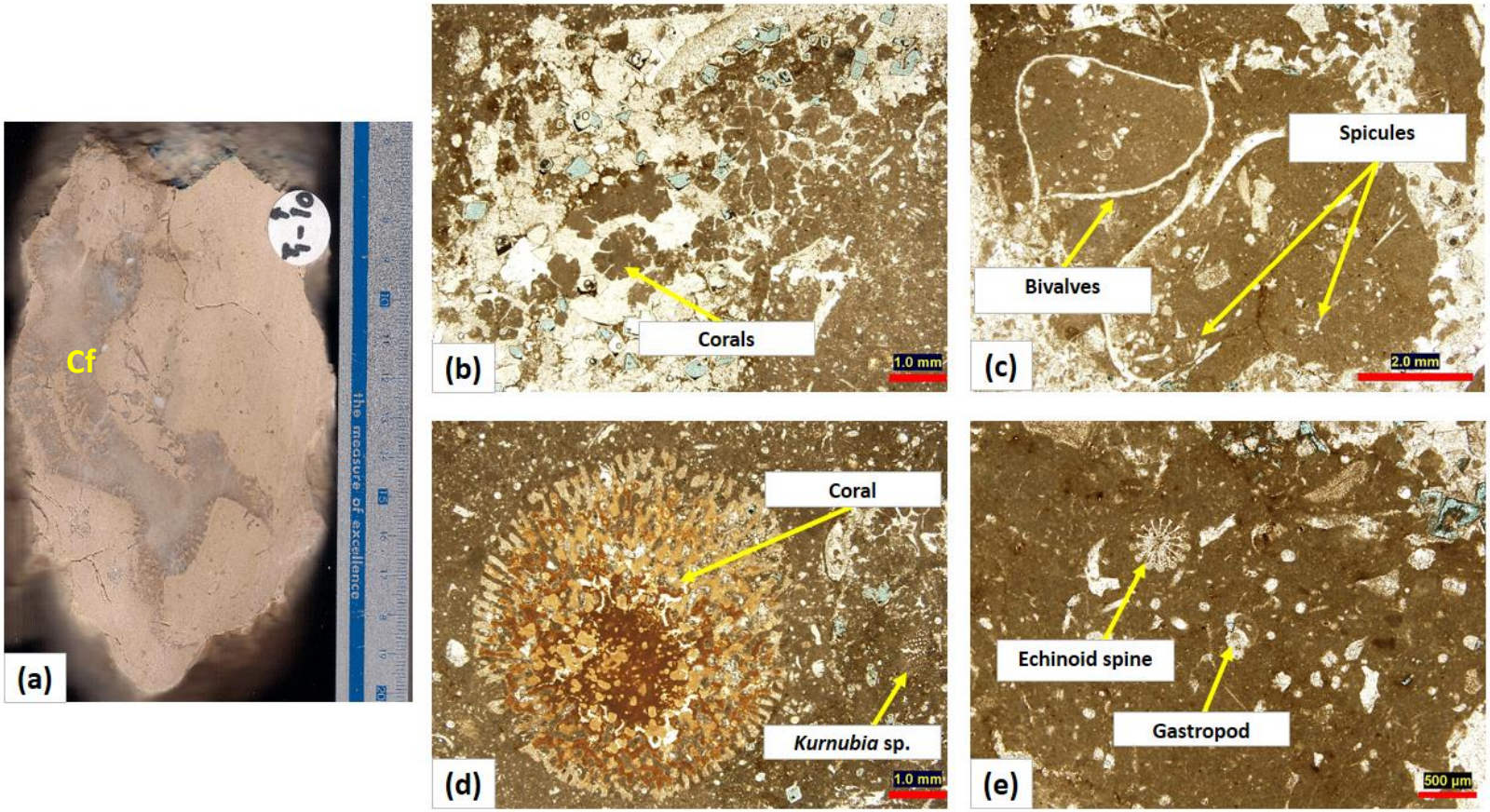


Figure 28 Scanned slab (a) and thin section photomicrographs (b-e) of MF 3 coral floatstone with spiculitic matrix showing: (a) A large coral fragment (Cf) within mud dominated groundmass. (b) Coral molds with individual corallites are filled with micrite. (c) Spiculitic matrix with the presence of large fragments of bivalves. (d) Silicified coral and *Kurnubia* sp. (e) Echinoid spine and gastropod partially filled with micrite.

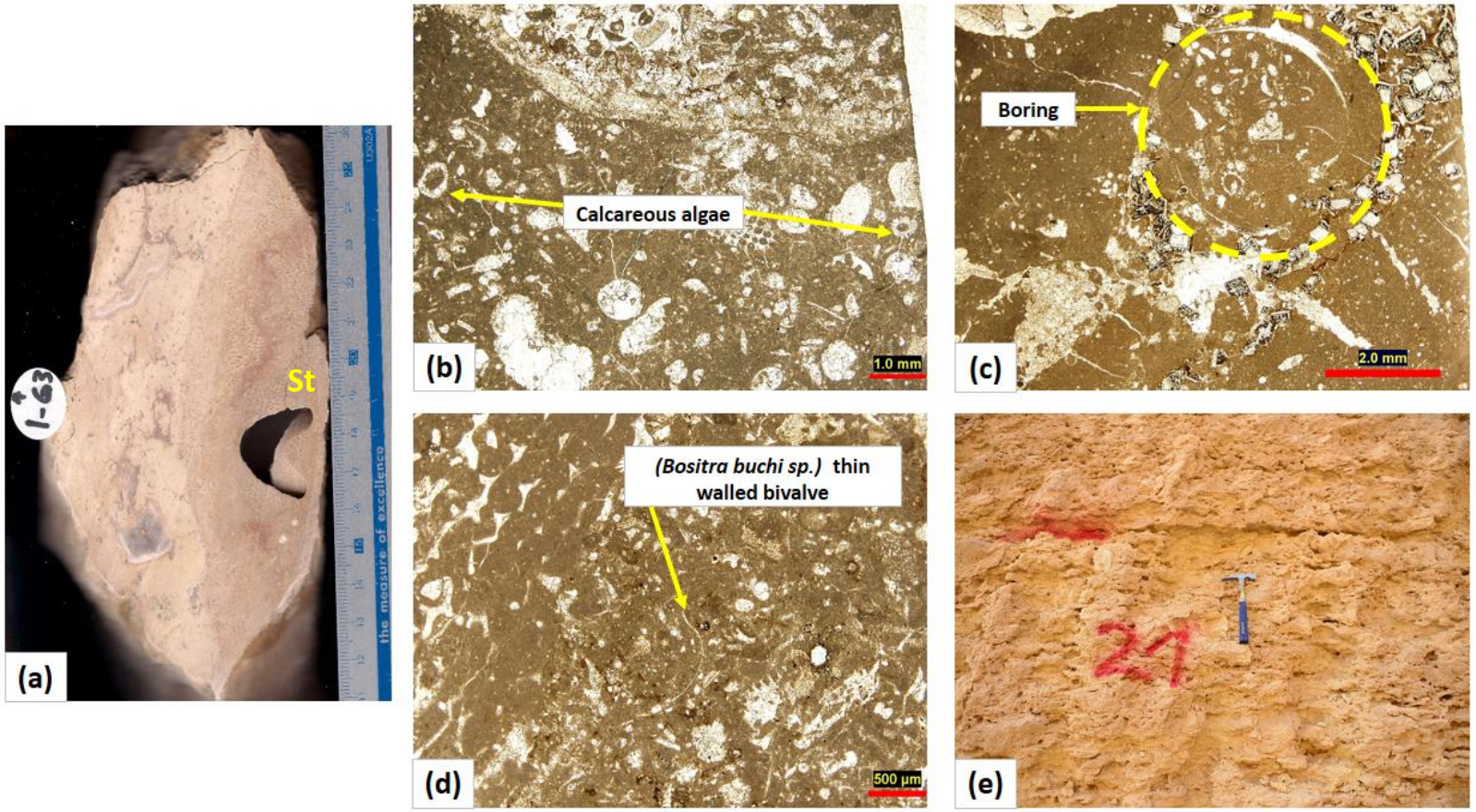


Figure 29 Scanned slab (a), thin section photomicrographs (b-d), and field photo (e) of MF 3 coral floatstone with spiculitic matrix showing: (a) large coral and stromatoporoid (St) fragments scattered within mud supported texture. (b) The presence of calcareous algae (*Salpingoporella annulata*). (c) Biological boring activity within corals. (d) The thin walled bivalve (*Bositra buchi* sp.). (e) Burrowing and bioturbation.

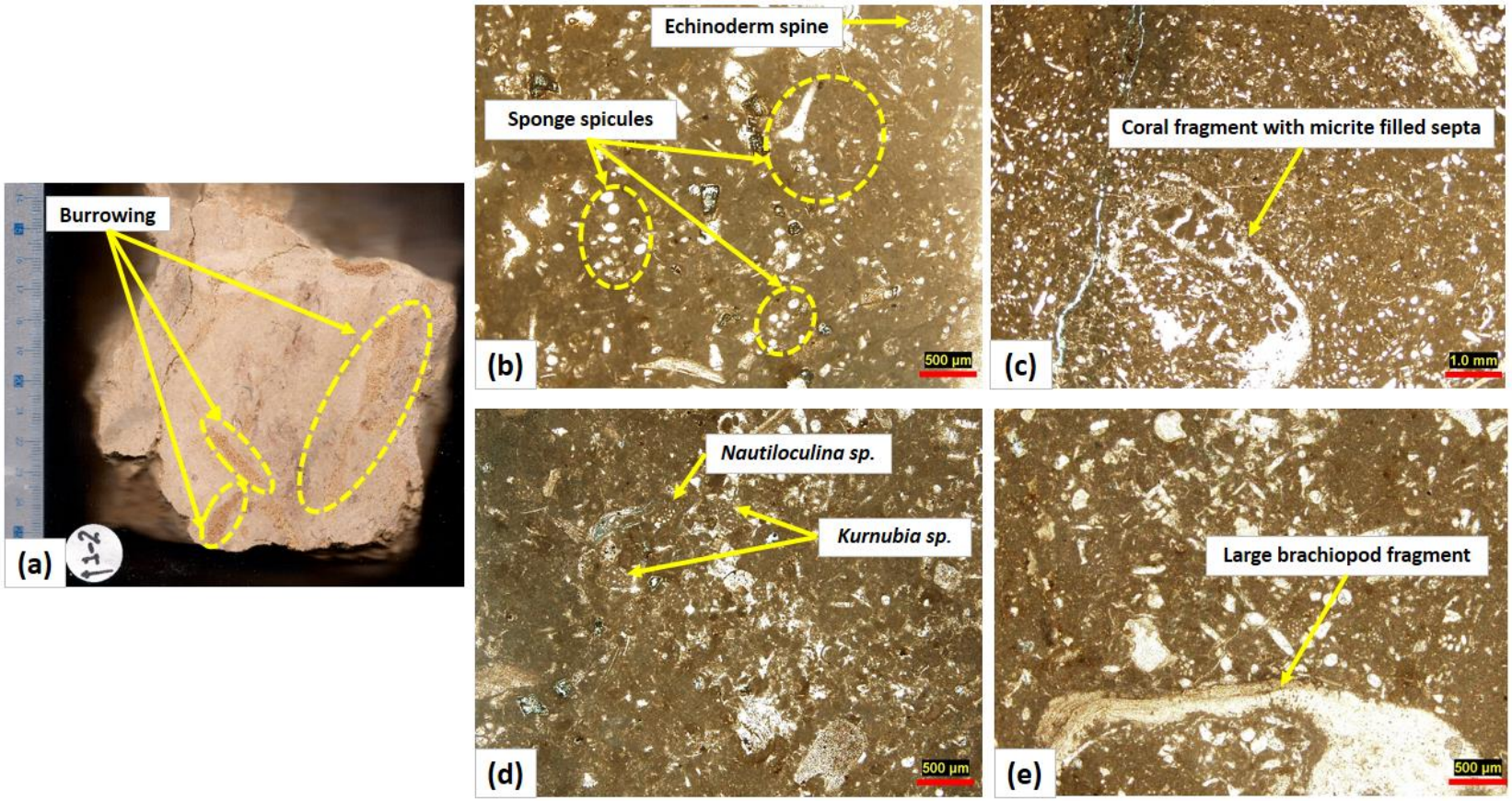


Figure 30 Scanned slab (a) and thin section photomicrographs (b-e) of MF 4 spiculitic wackstone showing: (a) Common burrow traces. (b) Echinoderm spine and clusters of dominant sponge spicules. (c) Coral fragment within spiculitic matrix. (d) The foraminiferal assemblage including: *Kurnubia* sp. and *Nautiloculina* sp.. (e) A large brachiopod fragment.

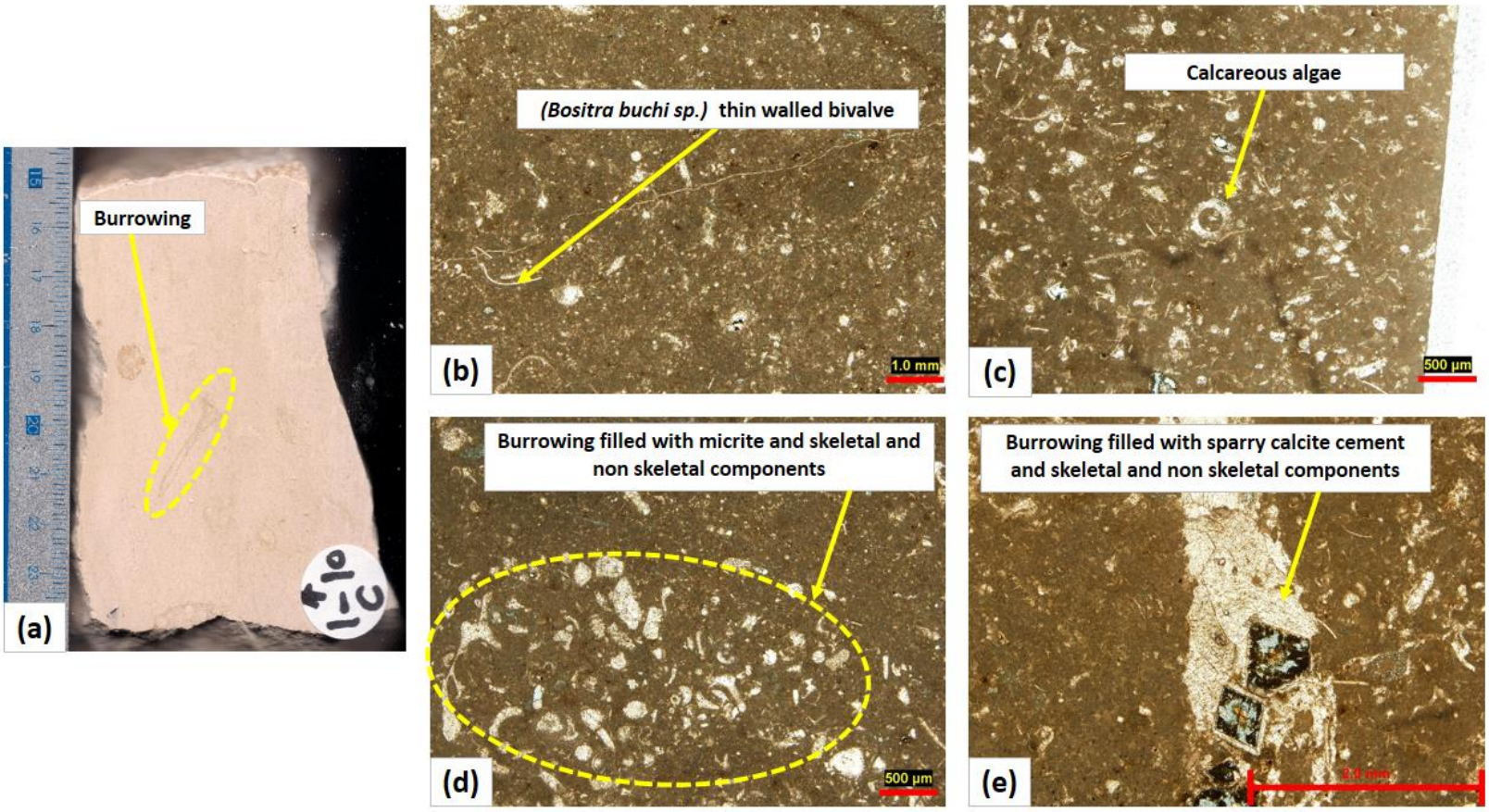


Figure 31 Scanned slab (a) and thin section photomicrographs (b-e) of MF 4 spiculitic wackstone showing: (a) A burrowing trace. (b) The rare occurrence of thin walled bivalve. (c) The rare occurrence of calcareous algae (*Salpingoporella annulata*). (d) A burrowing filled with micrite and skeletal and non-skeletal components. (e) A burrowing filled with sparry calcite cement and skeletal and non-skeletal components and dolomite.

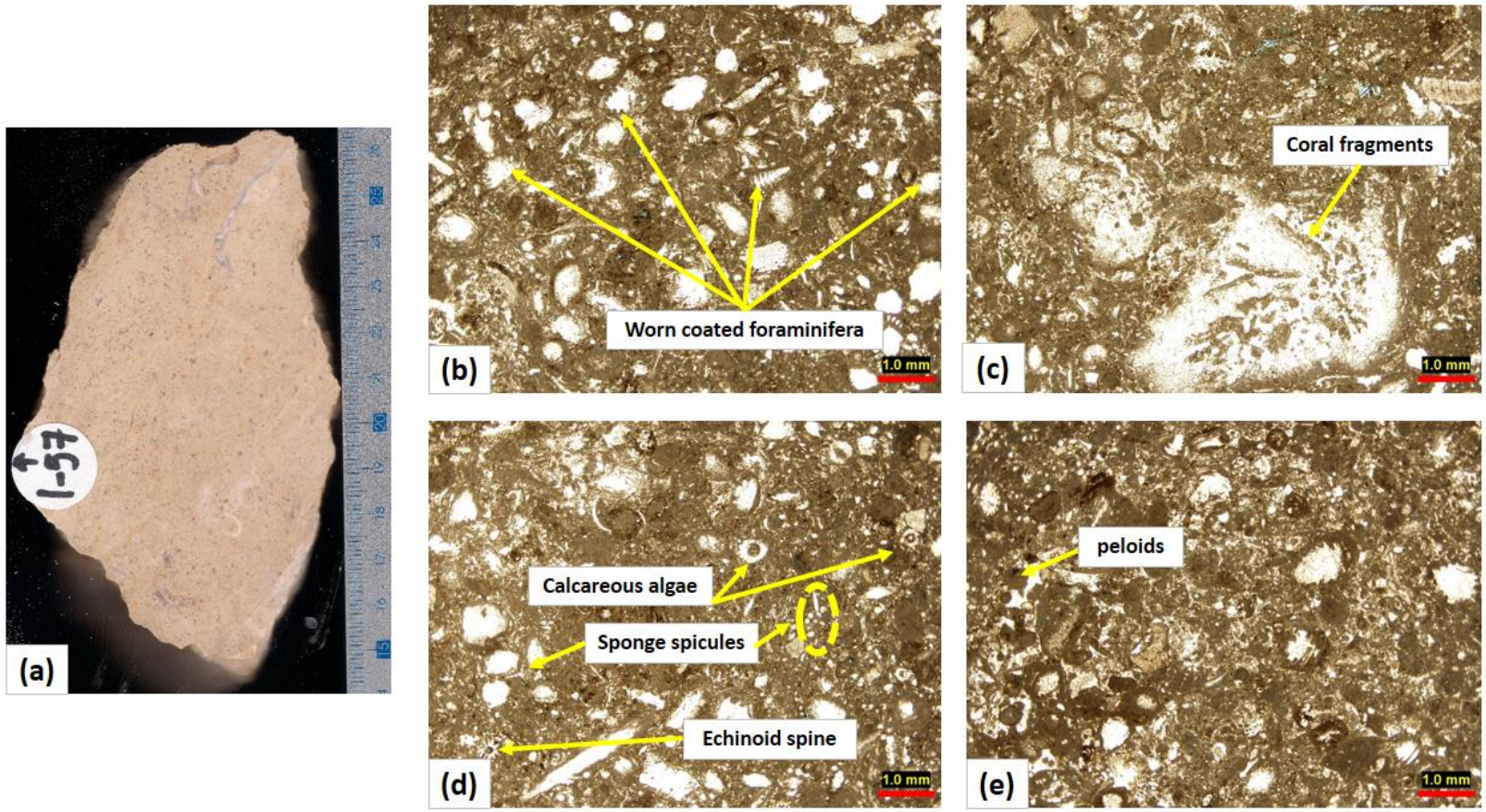


Figure 32 Scanned slab (a) and thin section photomicrographs (b-e) of MF 5 worn and coated foraminiferal wack/pack-stone showing: (a) worn and coated foraminiferal packstone with the presence of dispersed coral fragments. (b) The dominance of worn and coated foraminiferas. (c) Locally occuring coral fragment. (d) The presence of calcareous algae (*Salpingoporella annulata*), echinoderm spine, and sponge spicules. (e) The presence of peloids and coated foraminiferas.

Figure 33 Field photo showing a large coral fragment in worn and coated foraminiferal packestone interval at T3 at elevation 57 m from the base of the measured section of T2 in Ma'ayshbah.

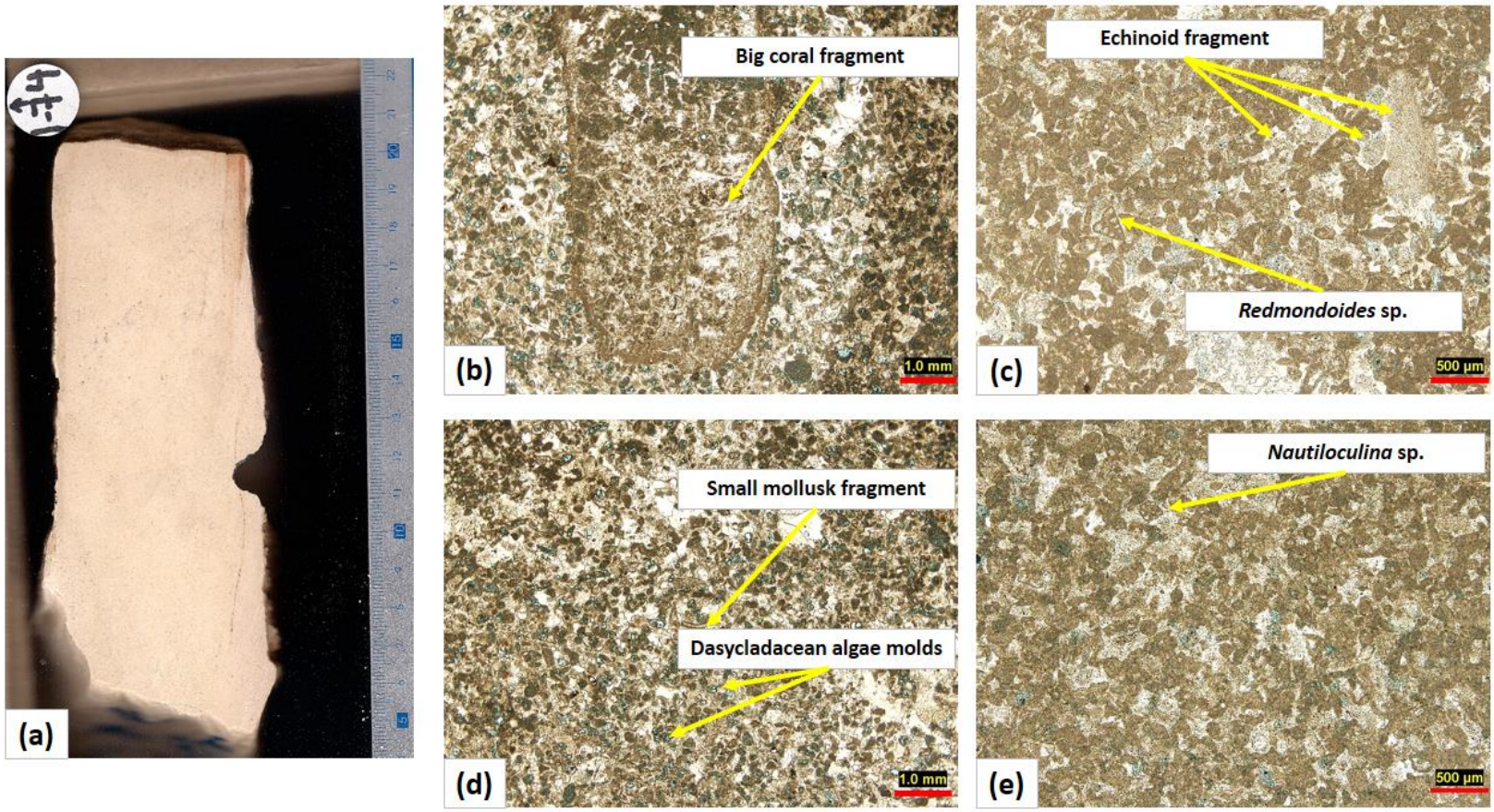


Figure 34 Scanned slab (a) and thin section photomicrographs (b-e) of MF 6 fine grained peloidal grainstone showing: (a) The very fine texture of this facies. (b) Large coral fragment. (c) The presence of echinoderm fragments of different sizes and the foraminifera *Redmondoides* sp. (d) A small mollusk fragment and moldic porosity formed by leaching of a dasycladacean algae. (e) The most common foraminiferal species in this facies; *Nautiloculina* sp.

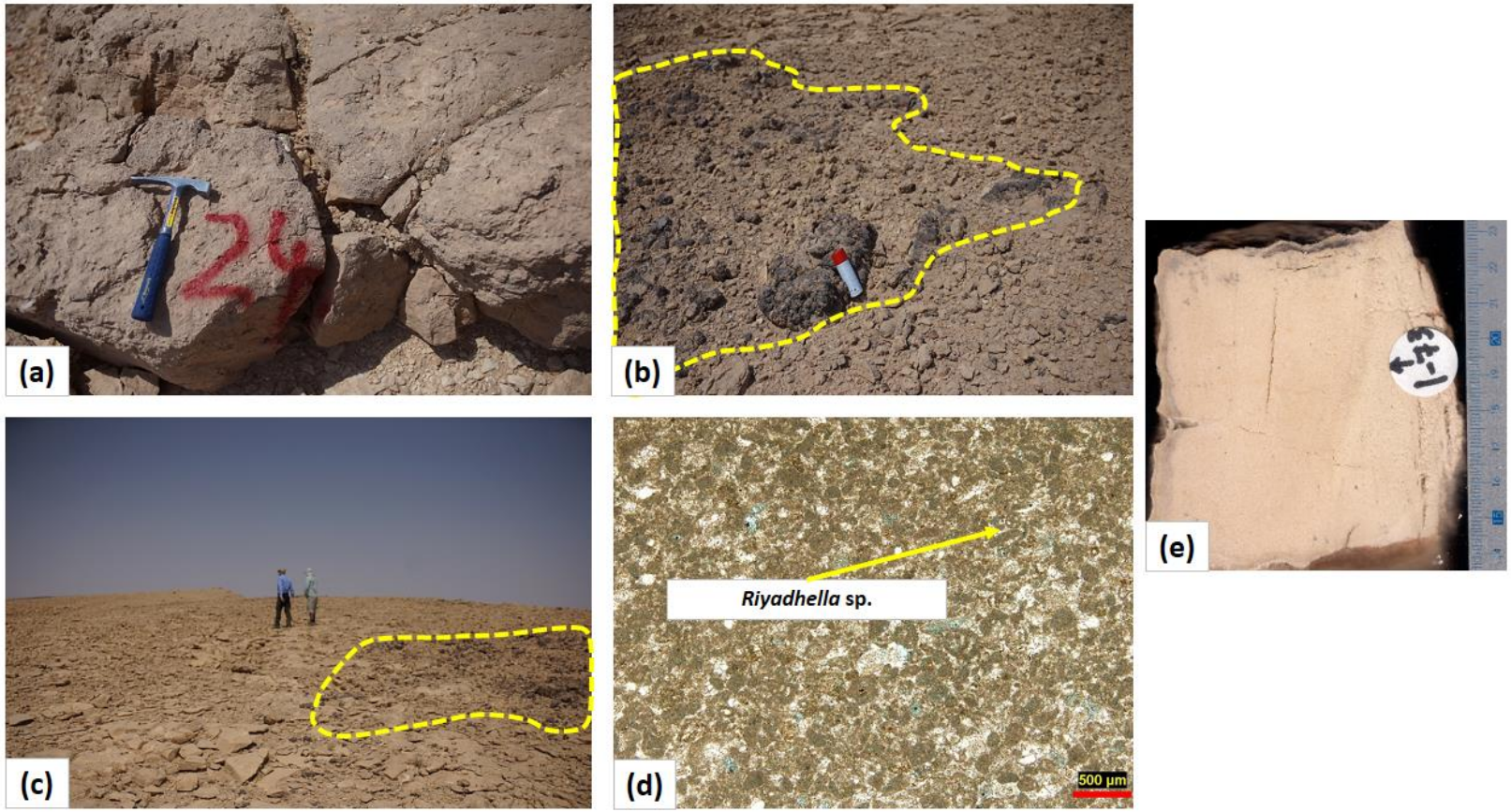


Figure 35 Field photos (a-c), thin section photomicrograph (d) and scanned slab (e) of MF6 fine grained peloidal grainstone showing: (a) The poorly stratified beds of this facies. (b) The top of T3 showing top view of a patch reef found within this facies. (c) The top of T3 showing the top view of a patch reef found also within this facies. (d) The most common foraminifera Riyadhella sp. (e) The very fine grained texture.

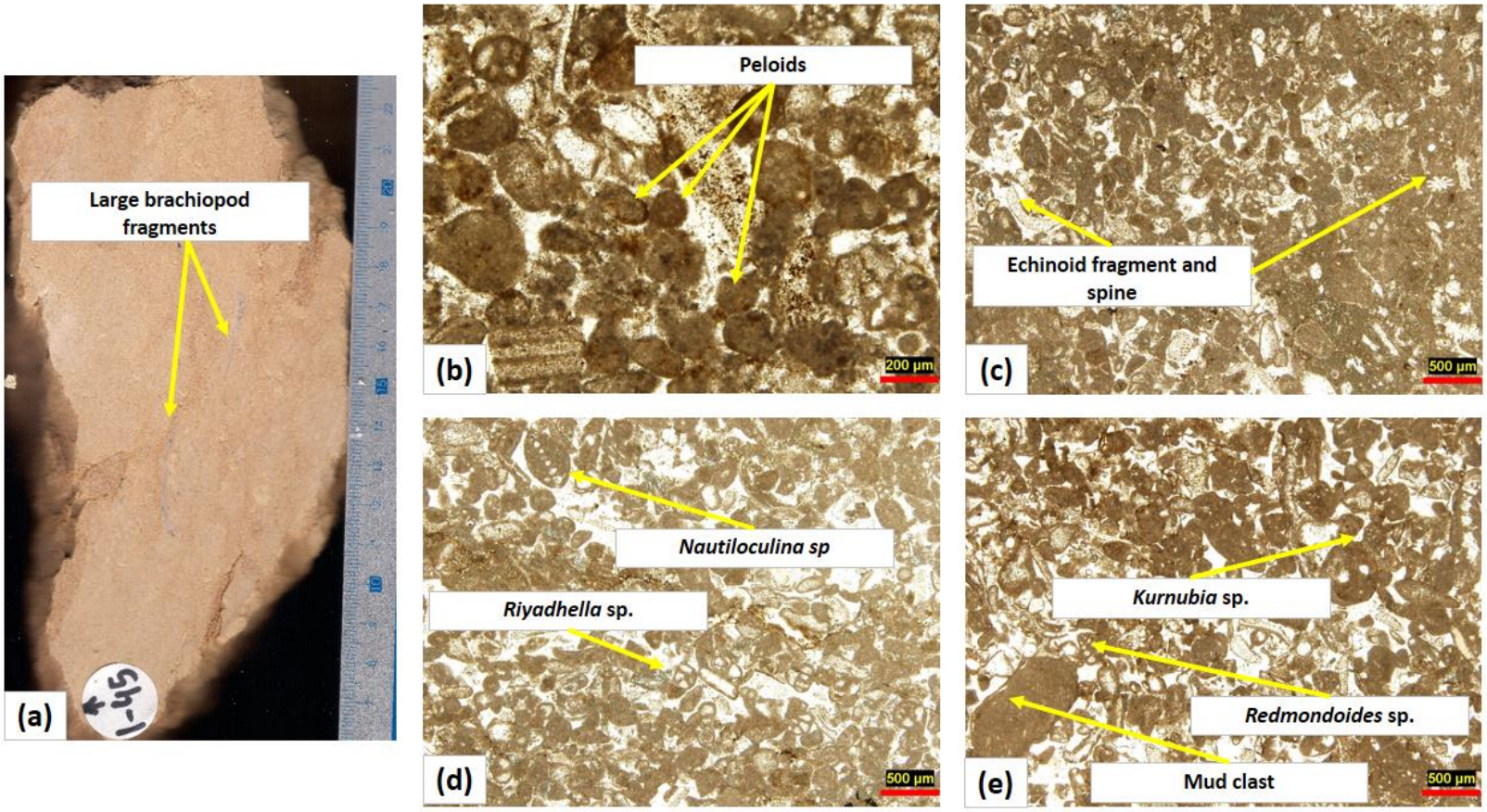


Figure 36 Scanned slab (a) and thin section photomicrographs (b-e) of MF 7 peloidal packstone showing: (a) the grainy texture and the presence of large brachiopod fragments. (b) The different sizes of peloids. (c) The abundant echinoderm fragments and spines. (d and e) The foraminiferal assemblage and the mud clasts.

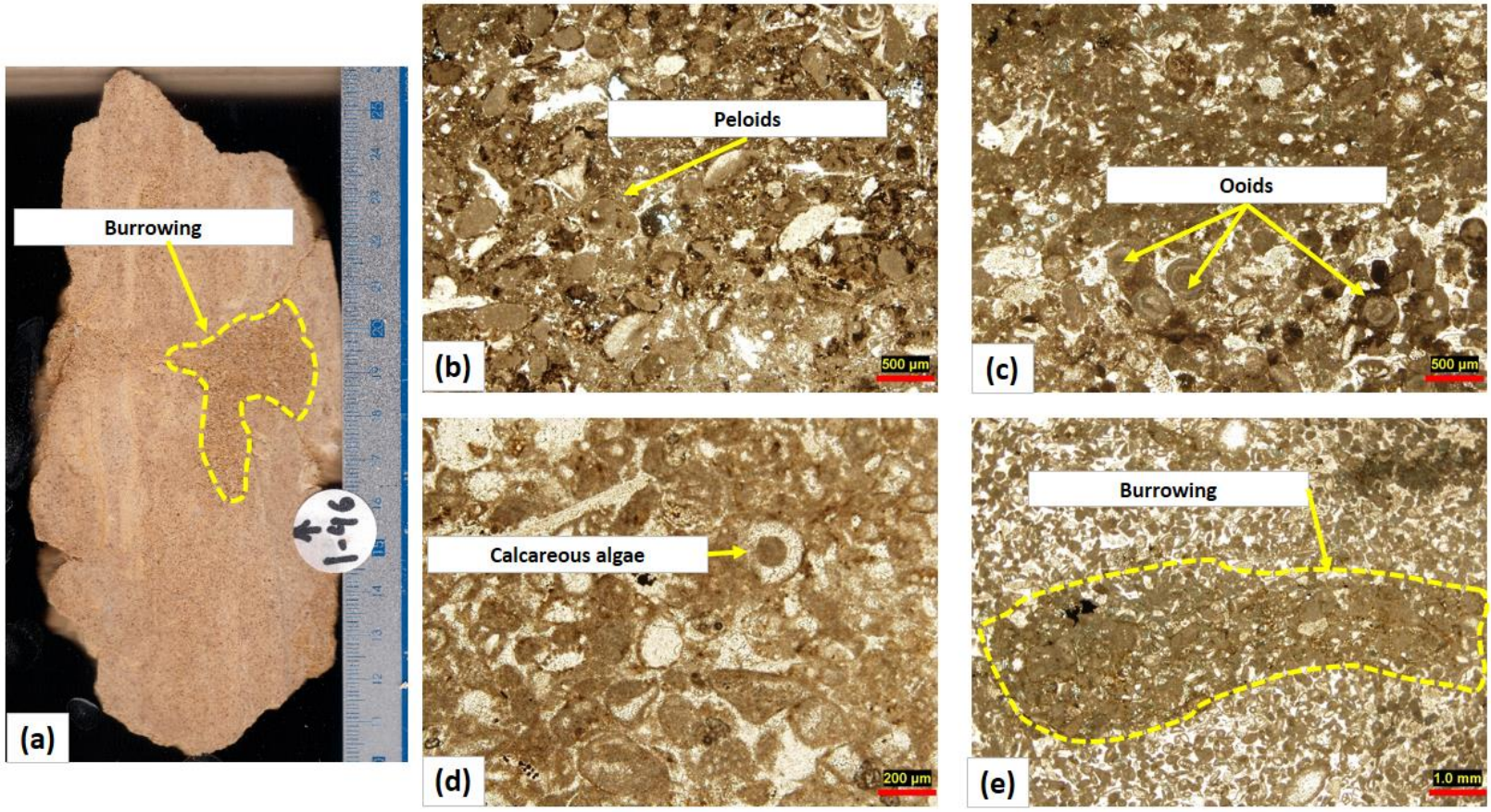


Figure 37 Scanned slab (a) and thin section photomicrographs (b-e) of MF 7 peloidal packstone showing: (a) A trace of a burrowing activity. (b) Peloids within muddy matrix. (c) The presence of ooids. (d) The presence of calcareous algae (*Salpingoporella annulata*). (e) The presence of burrowing.


Figure 38 Field photo showing the burrowing activity in bed 1_47 (note the hammer is the scale and arrows are pointing at the burrow traces).

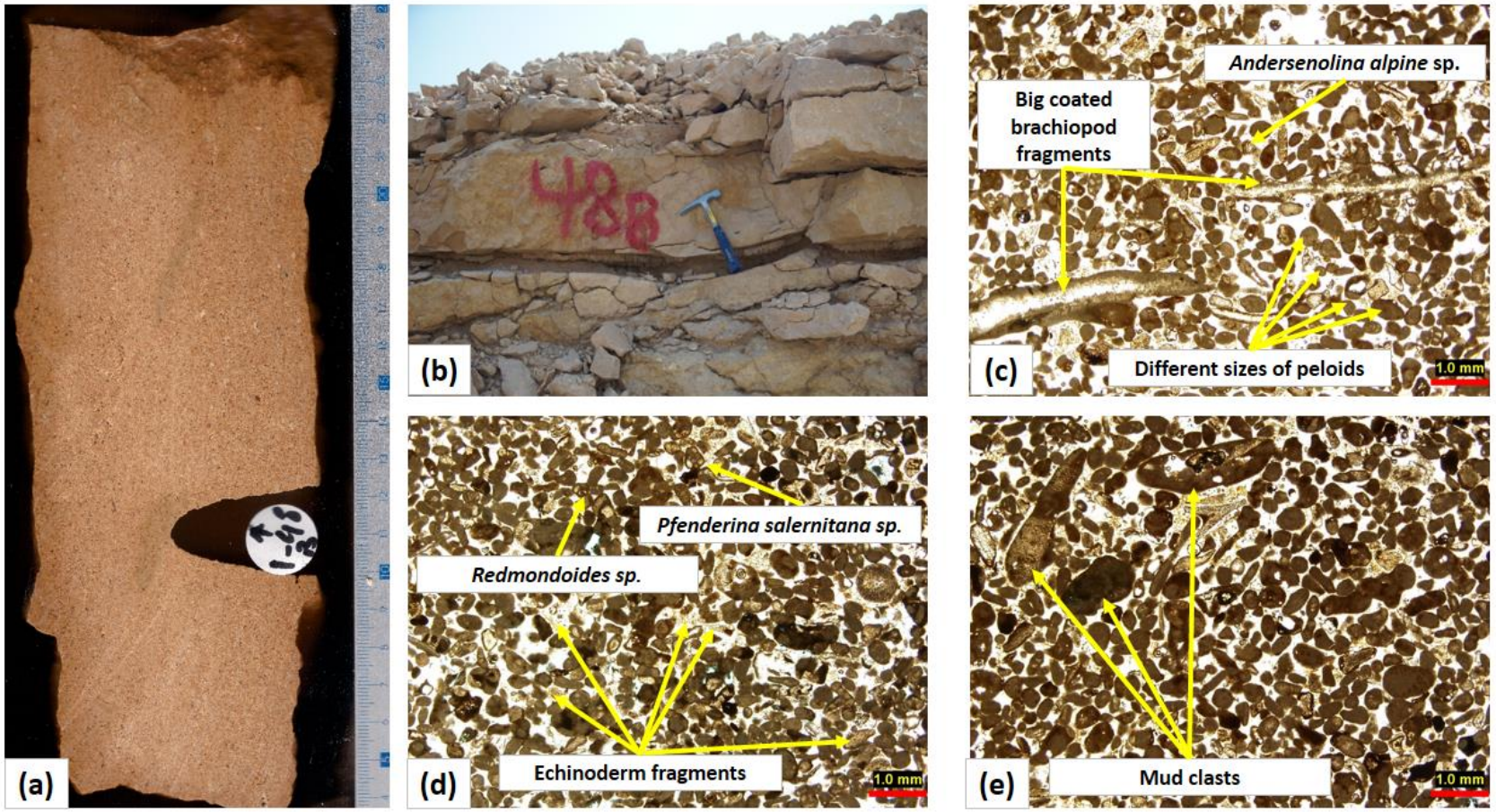


Figure 39 Scanned slab (a), field photo (b), and thin section photomicrographs (c-e) of MF 8 peloidal grainstone showing: (a) The grainy texture. (b) Thick structurless bedding. (c and d) The different sizes of peloids, the coated brachiopod fragments, foraminifera *Andersenolina alpine* sp., echinoderm fragments and foraminiferas *Redmondoides* sp. and *Pfenderina salernitana* sp. (e) The presence of mud clasts.

| Microfacies, microfacies code and depositional texture | Facies Association | Description | Main porosity types | Macroscopic features in outcrop and slab and facies distribution in the outcrop | Grain size and sorting | Hydrodynamic energy | Depositional environment * |
|---|---|---|---|---|---|---|---|
| MF 1: Coral peloidal rudstone<br><br>Depositional texture Rudstone | FA 2 (Shallow lagoon facies association) | Composed mainly of large coral fragments scattered within a groundmass composed of skeletal and non-skeletal components. Skeletal components includes; small benthic foraminiferas (*Nautiloculina* sp., *Kurnubia* sp., and *Everticyclammina* cf. *virguliana* sp.), brachiopods, bivalves, echinoderms, gastropods and sponge spicules. Non skeletal components include peloids. | Moldic porosity of dolomite dissolution | In the outcrop, beds were well bedded with scattered corals fragments. | Calcirudite, moderately sorted | Moderate to high energy | Shallow lagoon FZ 8 above fair weather wave base (FWWB) under influence of storm |
| MF 2: Coral Rudstone with intraclast and coated grains<br><br>Depositional texture Rudstone | FA 1 (Deep lagoon facies association) | Composed of coral fragments mainly with other skeletal and non-skeletal components including benthic foraminiferas (*Kurnubia* sp., *Andersenolina alpina* sp., and *Nautiloculina* sp.), brachiopods and echinoderms, gastropods, sponge spicules, intraclasts, and peloids. Percentage of mud is low compared to MF 3, 4, and 5. Some of the skeletal fragments showed grain coating. | Moldic porosity, interparticle porosity, microporosity in the matrix | Thick to massive bedding with scattered coral fragments dispersed, corals were often overturned and the coral fragments are scattered in packstone texture | Siltite to rudite, poorly sorted | Moderate energy | Just below fair weather wave base (FWWB) in the deep lagoon (FZ 7) under influence of storm |
| MF 3: Coral floatstone with spiculitic matrix<br><br>Depositional texture Wackstone | FA1 | Composed of abundant sponge spicules and large coral fragments scattered within mud dominated texture that contains peloids (peloidal lime mud). Skeletal fragments include brachiopod, bivalves, and echinoderms, and calcareous algae. Thin walled bivalves (*Bositra buchi* sp.) is present. The assemblage of small benthic foraminiferas includes; *Andersenolina cherchiae*, *Kurnubia* sp., *Nautiloculina* sp. | Moldic porosity, interparticle porosity, microporosity in the matrix | Massive bedding with scattered coral fragments. It was highly bioturbated and burrowed in some beds. | Siltite to rudite, poorly sorted | Low energy | Below FWWB in deep lagoon (FZ 7). This facies represent a coral debirs facies in quite deep lagoon settings but shallower than MF 4. |
| MF 4: Spiculitic wackestone<br><br>Depositional texture Wackstone | FA 1 | Mud dominated facies composed mainly of a spiculitic matrix with other skeletal and non-skeletal components. The skeletal components include fragments of brachiopods, bivalves, echinoderms, calcareous algae, and thin walled bivalve (*Bositra buchi* sp.). Small coral fragments occur in this facies with size and percentage less than MF 3. Non skeletal components primarily include peloids. | Moldic porosity, interparticle porosity, microporosity in the matrix. In some cases vuggy porosity present. | Burrowing activity and in some cases the filling material either to be sparry calcite cement or coarser material than the matrix which consists of skeletal fragments and matrix | Siltite mainly but with large brachiopod and coral fragments becomes rudite. Mainly moderately sorted but in some cases badly sorted | Low energy | Below FWWB in deep lagoon (FZ 7). This facies has a finer and muddier texture than MF 3 so it is suggested that this facies is deposited in quite deep lagoon settings but deeper than MF 3 |
| MF 5: worn and coated foraminiferal wack/packe-stone<br><br>Depositional texture Wack/Pack-stone | FA 1 | Grain supported texture composed mainly of worn and coated foraminiferas dispersed with spciulitic matrix. The benthic foraminiferal assemblage includes (*Andersenolina elongata* sp., *Andersenolina alpina* sp., *Andersenolina cherchiae* sp., *Kurnubia* sp., *Globovulvulina* sp., *Nautiloculina* sp.) but Andersenolina alpina sp. and Andersenolina cherchiae sp. are the most abundant. The other skeletal components are sponge spicules, brachiopods, echinoderms, gastropods, and small coral fragments up to 5 mm length. Some intraclasts are found in the thin sections. | moldic porosity, microporosity in matrix | Coral fragments were found scattered and within mud supported texture. Burrow activity was also observed | Mainly arenite with siltite matrix and with the presence of large fragments of corals it tends to be rudite. poorly sorted | Low energy | Below FWWB in deep lagoon (FZ 7). The cleaner and grainer texture of this facies suggest that it was deposited in quite deep lagoon settings but shallower than MF 3 and 4 |

| | | | | | | | |
|---|---|---|---|---|---|---|---|
| MF 6: Fine grained peloidal grainstone<br><br>Depositional texture Grainstone | FA 2 | Composed mainly of tiny rounded clasts of muddy peloids: contains echinoderm fragments and spines, benthic foraminiferas, bivalves, brachiopods, and Dasycladacean algae. The foraminiferal assemblage of this facies includes; *Nautiloculina* sp., *Redmondoides* sp., and *Riyadhella* sp. but the main species here is *Nautiloculina* sp. | Moldic and vuggy porosity | Thick bedding with local patch reefs | Mainly arenite, well to moderately sorted | Moderate to high energy | Restricted platform interior (shallow lagoon FZ 8). This facies represents the patch reef substrate |
| MF 7: Peloidal Packstone<br><br>Depositional texture Packstone | FA 2 | Composed mainly of peloids and micritized grains. No single fragment of coral has been observed. Skeletal fragments includes; bivalves, echinoid fragments and spines, foraminiferal assemblage, calcareous algae and brachiopods. Foraminiferal assemblage of that facies includes; *Nautiloculina* sp., *Redmondoides* sp., *Riyadhella* sp., and *Kurnubia* sp. locally occurrence of ooids | Moldic, interparticle, microporosity in matrix. In some cases vuggy porosity present. | Thick to massive bedding with local burrowing | Arenite, moderately sorted | Moderate to High energy | Restricted platform interior (shallow lagoon FZ 8). This facies represents the shoal transition. |
| MF 8: Peloidal Grainstone<br><br>Depositional texture Grainstone | FA 3 (Shoal facies association) | Composed mainly of peloids. No coral fragment or mud were observed at all. Echinoid fragments, spines, bivalves, foraminiferas, and coated brachiopod fragments are the skeletal fragments. The foraminiferal assemblage in this facies includes; *Nautiloculina* sp., *Redmondoides* sp., *Pfenderina salernitana* sp., and *Andersenolina alpine* sp. Large mud clasts with size ranges from 1 mm is to 3 mm were found | Moldic, vuggy porosity | Thick bedding with local burrowing | Mainly arenite but with large brachiopod fragments it becomes rudite. Well sorted | High energy | shoal complex above FWWB |

Table 2 summarizing the main features, components, description, facies association, porosity types, grain size, sorting, and depositional environment and its energy. * based on Wilson (1975) and Flügel (2010).

## 3.2.Depositional Model

In this section, the microfacies descriptions (bedding patterns, components and sediment textures) and the environmental interpretation are integrated together along with the recurrence in lithofacies successions (Walther's law) within the outcrop to create 3D conceptual depositional model of the TMF (Fig. 40). This model illustrates three depositional environment within carbonate platform interior setting and summarizes the interpretation of the eight microfacies. These depositional environments are; deep lagoon (MF 2, 3, 4, and 5), shallow lagoon (MF 1, 6, and 7) with patch reef, and shoal (MF 8).

### 3.2.1. Shoal Environment

The shoal environment is characterized by high energy and has no coral fragments or mud content as seen in MF 8. This environment is characterized by the presence of peloids, brachiopod, echinoderm fragments, mud clasts, and benthic foraminifera. The foraminiferal assemblage of this sub-environment includes *Nautiloculina* sp., *Redmondoides* sp., *Pfenderina salernitana* sp., and *Andersenolina alpine* sp. The presence of mud clasts is also indicative of shallow marine environment as these clasts usually can't be transported to longer distance (Flügel, 2010).

### 3.2.2. Shallow Lagoon Environment

The shallow lagoon environment (as seen in MF 1, 6 and 7) is characterized by moderate to high energy as it is located in the restricted part of the platform interior FZ 8 above FWWB. In this environment, the facies is characterized by grain supported texture dominated by peloids as the wave action winnowed the mud. Little mud is encountered in the peloidal packstone (pelmicrite) as it is deposited in protected shallow-marine environments with moderate water circulation (FZ 8; Wilson, 1975; Flügel, 2010). The

faunal content includes coral fragments, echinoderm fragments and spines, calcareous algae, small benthonic foraminiferas, brachiopod fragments, and no thin walled bivalves and sponge spicules. Another important component in this depositional environment is mud clasts "rip up clasts". These rounded mud clasts are indicative of shallow marine environment as they cannot be transported for long distance (Flügel, 2010).

In the upper most part of T3, coral dominated patch reefs are found associated with MF 6 but no coral fragment are seen in the peloidal packstone MF 7 which is suggested to be due to the increase of salinity in moving from a restricted shallow lagoon to a shoal depositional settings within the platform interior. This increase in salinity is suggested to result in a decrease in the size of patch reefs until it reaches a point where they cannot develop in such conditions (as suggested by the transition from MF 6 to MF 7). In contrast, moving from deep to shallow lagoon environment provides conditions more suitable for patch reef development and may result in an increase in their size for reasons: First, the substrate becomes more cemented and harder and so provides a better location for reef initiation. Second, the energy of the environment increases, which reduces the amount of mud in the water and thus is more conducive for coral growth. This interpretation is strengthened by the work done by Leinfelder et al, (2005) on the stromatoporoids in Jurassic reefs and carbonate platforms.

### 3.2.3. Deep Lagoon Environment

The deep lagoon environment (as seen in MF 3, 4 and 5) is characterized by low energy as located in the open marine zone FZ 7 below FWWB. In this environment, muddy facies dominate and are characterized by thick to massive bedding with no sedimentary structures visible except for the nodular bedding styles of the muddy beds of MF 3 and 4. Also, some

of the beds are burrowed and bioturbated. The groundmass of the deep lagoon facies is characterized by peloidal lime mud (peloidal matrix), while the faunal content includes sponge spicules, thin walled bivalves, coral fragments, shallow marine benthonic foraminiferas, echinoderm fragments and spines, brachiopod fragments, gastropods, and calcareous algae.

### 3.2.4. The Evidence Supporting Depositional Model

In the study area, the stromatoporoid bank aren't exposed and this might suggest two possible settings either platform interior or fore reef to intra shelf basin. The most likely setting is the platform interior. This interpretation is supported by three supporting lines of evidence. First, the foraminiferal assemblage (*Nautiloculina* sp., *Redmondoides* sp., *Pfenderina salernitana* sp., and *Andersenolina alpine* sp., *Riyadhella* sp., *Andersenolina elongata* sp., *Andersenolina cherchiae* sp., *Kurnubia* sp., and *Globovulvulina* sp.,) present in the studied sections are indicative of shallow marine water ranging from deep lagoon to intertidal based on the suggested palaeoenvironmental model for Middle to Late Jurassic biocomponents by Hughes (2004; 2008; and 2009). This assemblage is suggested to be in place and not to have been transported into a deep water setting because of the absence of any deep water planktonic foraminiferas such as *Nodosaria* sp. and *Lenticulina* sp. as described by Hughes (2004; 2008; and 2009). Second, the presence of grain dominated peloidal facies with mud clasts; such mud clasts are indicative of a shallow marine environment (Flügel, 2010) and the peloidal grain/pack-stone facies are indicative of high to moderate energy environment. Third, in the upper most part of T3, patch reefs are found associated with MF 6. These patch reefs are indicative of lagoon environment and it can develop in both deep and shallow lagoon (Leinfelder et al., 2005).

### 3.2.5. Sediment Source

As no non carbonate depositional components were identified petrographically, XRF analyses were conducted to test for the presence of such component in representative samples of the studied sections. Elemental analysis of powdered samples using XRF showed the presence of Si, Al, Zr, Ti, and K, which might be indicative for siliciclastic input. In order to examine that cross-plots of Si % vs Al %, Si % vs Zr %, and Al % vs Zr % are generated (Fig. 41). A plot of the amount of silica versus the amount of zircon shows a positive correlation (Fig. 41.b). This positive correlation is showing the signature of detrital silica because the element zircon is associated with the detrital heavy mineral zircon (Tribovillard et al., 2006; Ratcliffe, 2012). In addition, a plot of the amount of silica versus the amount of aluminum (Fig. 41.a) shows a positive correlation that might suggest the presence of detrital silicate (e.g. feldspars or clays). Moreover, the plot of the amount of aluminum versus the amount of zircon (Fig. 41.c) shows a positive correlation that may also suggest the presence of siliciclastic input in the depositional system of TMF in the study area.

This interpretation is agreement with the findings of Al Ibrahim (2014), who used the positive correlation of cross-plots of Si % vs Al %, Si % vs Zr %, Al % vs Zr %, and Ti % vs Zr % as an indicator of the presence of detrital silica and clay input in his study interval of TMF and Hanifa. The source of this siliciclastic input might be a tidal channel that accesses the nearby Arabian shield as proposed by Hughes (2004; 2008 and 2009) and or windblown dust.

### 3.2.6. Comparison with Other Case Studies

Hughes (2004; 2008; and 2009) and Al-Dhubaib (2010) discussed the depositional settings of the TMF constructed a palaeoenvironmental model of the Middle to Late Jurassic in central Saudi Arabia. Hughes (2004; 2008; and 2009) suggested that monaxial and triaxial sponge spicules and thin walled bivalves (*Bositra buchi* sp.) are indicative of deep water intra-shelf basin while Al-Dhubaib (2010) suggested that sponge spicules and thin walled bivalves (*Bositra buchi* sp.) can be also encountered in the deep lagoon environment. Data presented in this study suggests that sponge spicules and thin walled bivalves (*Bositra buchi* sp.) can be also found in deep lagoon settings and not only in a deep water intra-shelf basin. Supporting evidence for this point is that sponge spicules and thin walled bivalves (*Bositra buchi* sp.) are found associated with shallow marine benthic foraminiferas (*Nautiloculina* sp., *Redmondoides* sp., *Pfenderina salernitana* sp., and *Andersenolina alpine* sp., *Riyadhella* sp., *Andersenolina elongata* sp., *Andersenolina cherchiae* sp., *Kurnubia* sp., and *Globovulvulina* sp.,) with no occurrence of any deep marine planktonic foraminiferas. Many authors have made similar suggestion in different case studies all over the world. For instance, Beresi et al. (2017) studied the evolution of the Oxfordian shallow-marine carbonate platform at Portada Covunco, Neuquén Basin in Argentina and suggested that sponge spicules are found in the facies of a restricted shallow subtidal to intertidal lagoon.

## 3.3. Depositional sequences

The information from fieldwork, microfacies and stacking patterns of microfacies can be used to identify the cyclicity in the TMF, and can be used to determine the different factors controlling the deposition of the TMF. In the study area, 2 major medium scale cycles

which are formed of stacked small scale cycles, were identified in the studied section of TMF (Figs. 42, 43, 44, 45 and 46).

### 3.3.1. Small Scale Cycles

#### 3.3.1.1. Deep Lagoon Small Scale Cycles

The thickness of this cycle type (Fig. 42) ranges from 2 to 5 m, and occurs throughout the entire studied section of the TMF. The lower part of the cycle is composed of several decimeters of nodular spiculitic wackstone (MF 4), overlain by bioturbated spiculitic wackstone that ranges in thickness range 50-100 cm. The wackstone grades upward into thick to massive bioturbated coral floatstone (MF 3). In some cases, the middle part of this cycle consists of foraminiferal wack/pack-stone (MF 5).

The MF 4 is interpreted as lagoonal facies which is deposited in a low energy environment and it represents transgressive portion of the cycle. Not like other interpretations (e.g. Tawfik et al., 2016) the upward transition from bioturbated spiculitic wackstone into foraminiferal wack/pack-stone to coral floatstone is interpreted as shallowing upward succession. The contacts between the repeated deep lagoon cycles are typically gradational.

#### 3.3.1.2. Shallow Lagoon Small Scale Cycle

The thickness of this cycle type (Fig. 43) ranges from 2 to 5 m, and occurs in the T2 and T3 members. The lower part of this cycle is composed of 50 to 100 cm of spiculitic wackstone (MF 4) which is overlain by peloidal packstone (MF 7) and or fine grained peloidal grainstone (MF 6). In some cases this cycle contains coral rudstone (MF 2) and or coral peloidal rudstone (MF 1).

The MF 4 is interpreted as a lagoonal facies which was deposited in low energy environment and it represents transgressive portion of the cycle. The upward transition

from low energy spiculitic wackstone to moderate to high energy peloidal packstone and or fine grained peloidal grainstone is interpreted as shallowing upward. The contacts between the repeated shallow lagoonal cycles are typically gradational.

### 3.3.2. Medium Scale Cycles

#### 3.3.2.1. Deep Lagoon Medium Scale Cycle

The thickness of this cycle (Figs. 44, 45 and 46) is around 23-37 m and it is composed of stacking of 6-10 small scale cycles. This cycle is observed in all studied sections. This cycle is capped by coral rudstone facies (MF 1 and MF 2) which represents the shift from a deep lagoon low energy environment to a shallow lagoon moderate to high energy environment

#### 3.3.2.2. Shallow Lagoon Medium Scale Cycle

The thickness of this cycle (Fig. 44, 45 and 46) is around 10 m and it is composed of stacking of 3 small scale cycles. This cycle is observed in the T2 and T3 members. This cycle is capped by the peloidal grainstone facies (MF 8) which represents the shift from restricted shallow lagoon moderate to high energy environment, to a shoal high energy environment

### 3.3.3. Factors Controlling Cyclicity in TMF

The stacking pattern and cyclicity seen in the TMF in the study area reveals a general trend of shallowing upward by shifting from a deep lagoon setting to a shallow lagoon and a shoal environment. Not like other interpretations (e.g. Sharland et al,. 2001 interpreted the TMF to represent TST, which contradicts our study and the studies of Enay et al., 2009 and Al-Husseini, 2009), this trend represents a major regressive cycle of TMF, and agrees with the findings of Enay et al. (2009) who interpreted the TMF as a part of a major regressive

cycle R8 (including the upper most part of D7 member of Dhruma). In this study, the regressive cycle is only representing the TMF without including Dhruma Formation as there is an unconformity between the TMF and Dhruma Formation (Fig. 15).

Throughout the TMF, the coral rich facies (MF 1, 2, 3 and 4) decrease upward, which is interpreted to be due to the general trend of regression from deep lagoon to shallow lagoon and shoal. Coincident with this is a trend upward toward facies that were formed under more restriction and probable more saline conditions. The increase in salinity yields conditions unfavorable for the development of patch reefs, and is suggested to control the facies shifting from coral rich facies (MF 1, 2, 3,4) to grain dominated facies with very few to no coral fragments (MF 6, 7 and 8).

The estimation of the duration of these high frequency cycles (HFC) of TMF is very difficult as there is no accurate geochronology or specific biostratigraphic constrains are available. In addition, the absence of a complete succession of the TMF in the study area showing the complete interval of each member (T1, T2 and T3) and the contacts between the members further hinders the accurate counting of small scale cycles in the TMF. Despite these problems, the available data of facies, stacking patterns and defined cycles can be used to estimate the driving mechanism and time duration of the cyclicity in TMF. According to Hughes (2008), TMF was deposited in a maximum time span of ca. 2 Myr and in this study there at least 40 small scale cycles and 6 medium scale cycles. Based on this information along with the thickness of the small and medium scale cycles, this study suggests that the small and medium scale cycles are possibly belong to 4th and possibly 5th order depositional cycles (of a magnitude of meters to a few tens of meters), respectively which may be accounted for by orbitally driven high frequency eustatic

fluctuations driven by Milankovitch cycles. The interpretation agrees with the findings of Al Ibrahim (2014), who used spectral analysis of TMF cycles to show of Milankovitch cycles.

Dromart et al. (2003) attributes a Middle Callovian sea level rise to a temperature optimum followed by a drastic climatic decline leading to continental ice production during the Late Callovian. Therefore, late Callovian was a part of icehouse episode, in which eustatic fluctuations were probably a moderately high-amplitude and high-rate phenomenon which resulted in the observed scale of cyclicity.

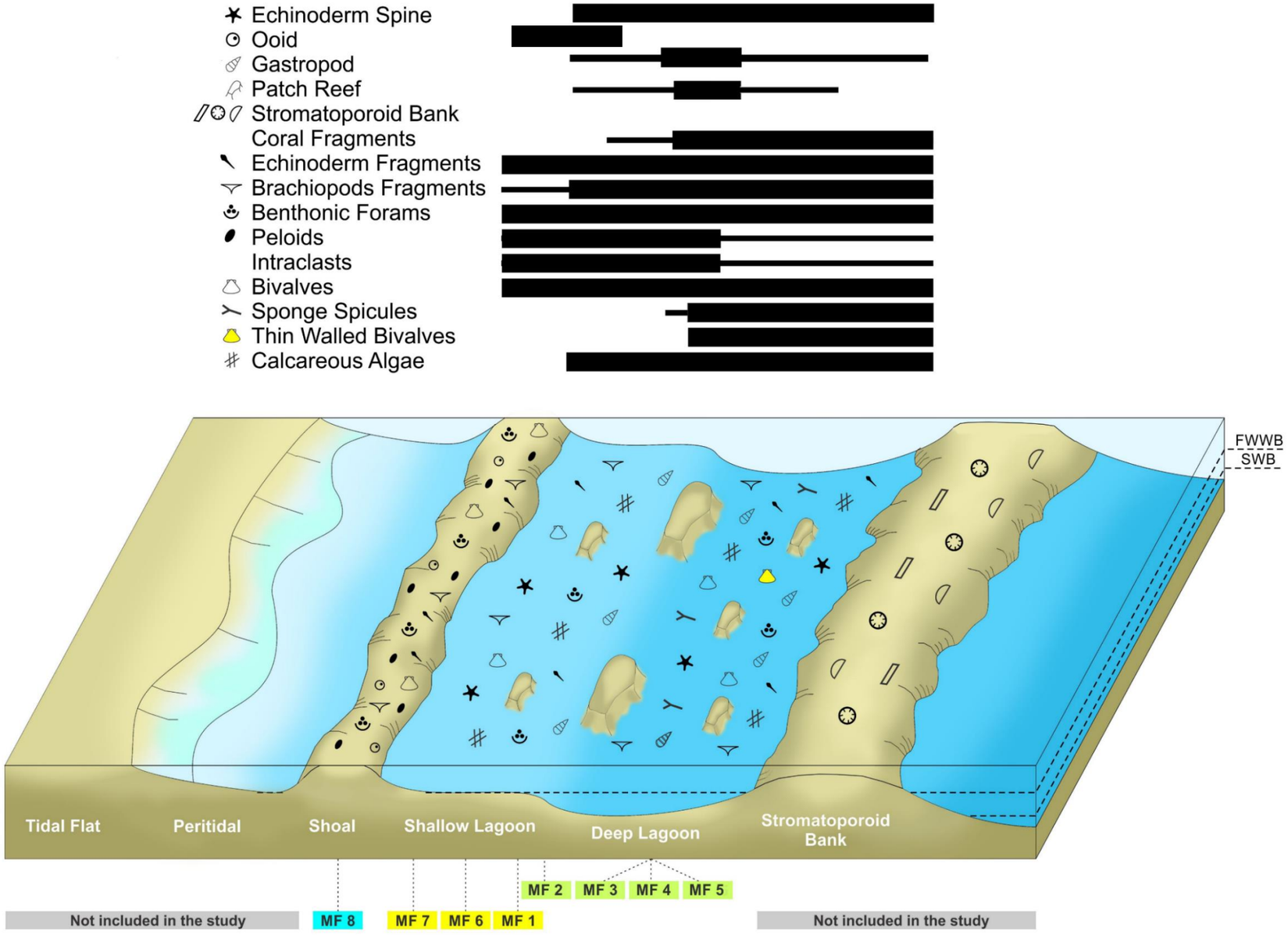


Figure 40 3D conceptual depositional model of TMF in Al Majama'ah area showing different sub environments, distribution of different microfacies and the abundance of different components

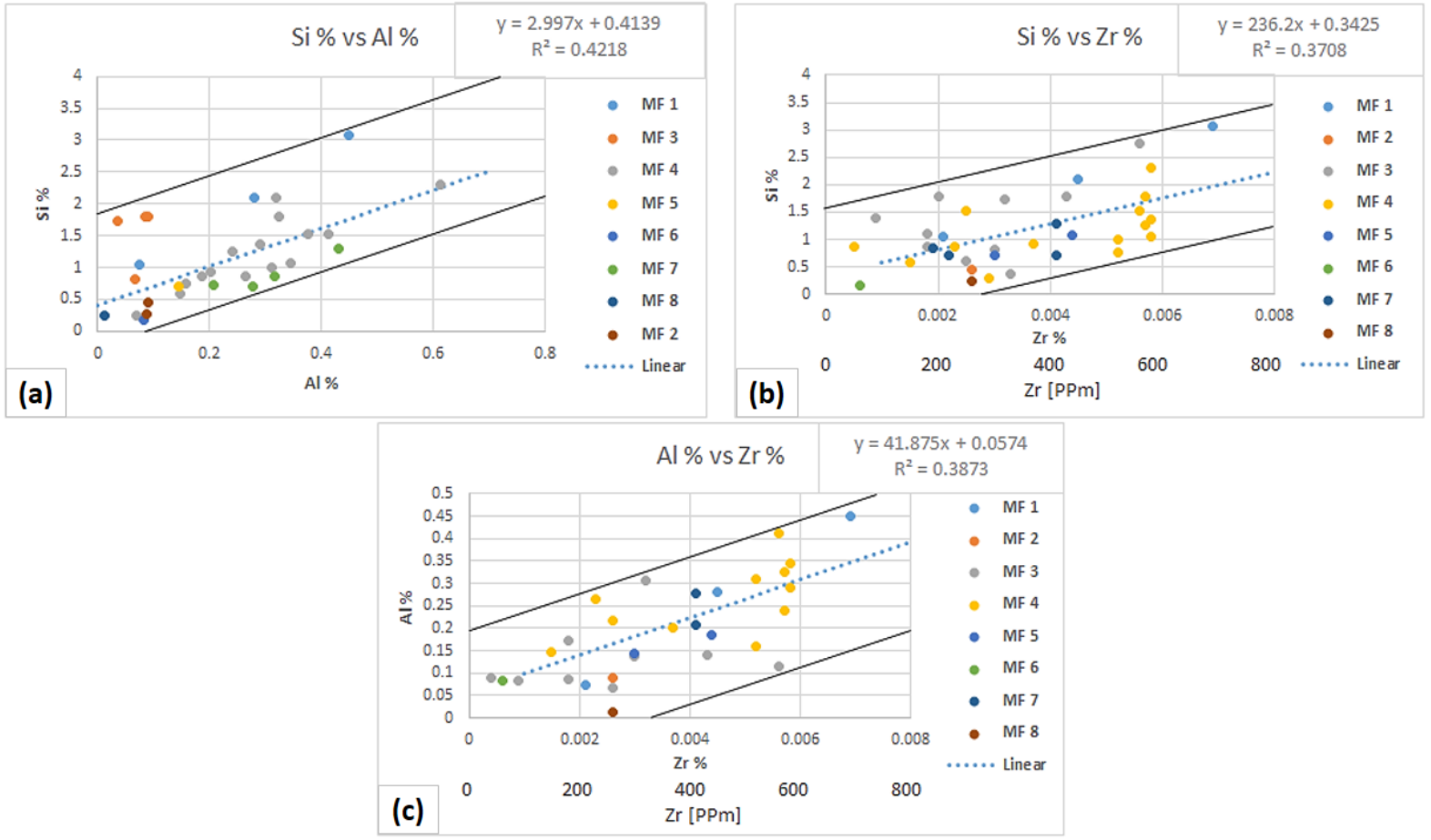


Figure 41 Detrital elements cross plots to examine the presence of siliciclastic input. (a) Cross-plot of Si % vs Al % showing a positive correlation which might be indicative for siliciclastic input. (b) Cross-plot of Si % vs Zr % showing a positive correlation which is indicative for the presence of detrital heavy mineral zircon. (c) Cross-plot of Al % vs Zr % showing a positive correlation which might also be indicative for siliciclastic input.

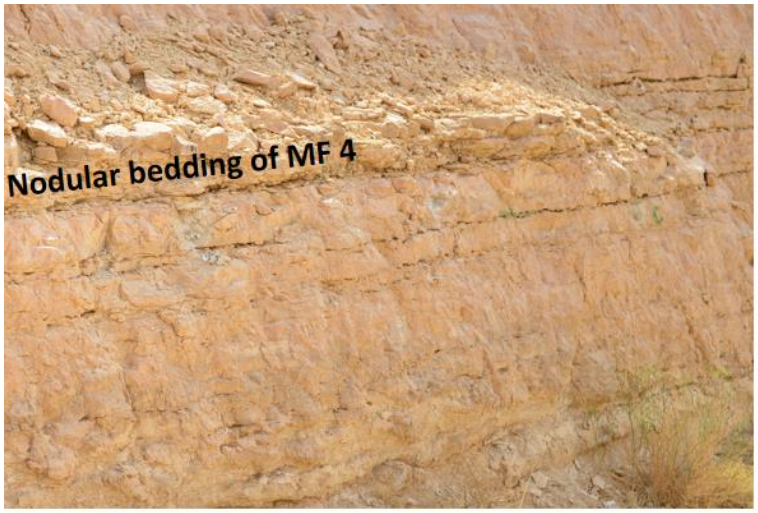


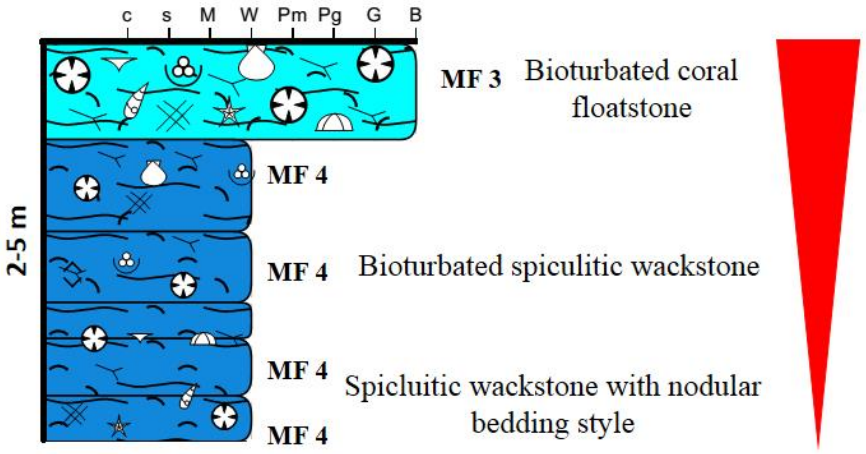


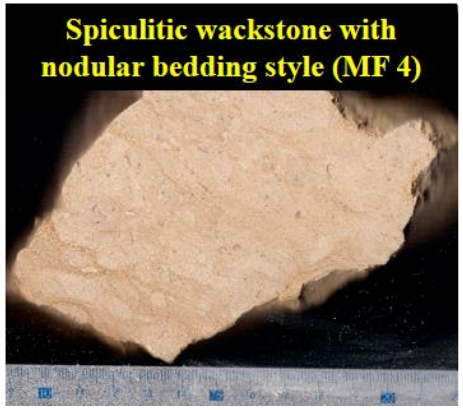




Figure 42 Schematic diagram of deep lagoon small scale cycle, and field and slab photos of the different facies composing this cycle (spicuitic wackstone with nodular bedding, bioturbated spiculitic wackstone and bioturbated coral floatstone).

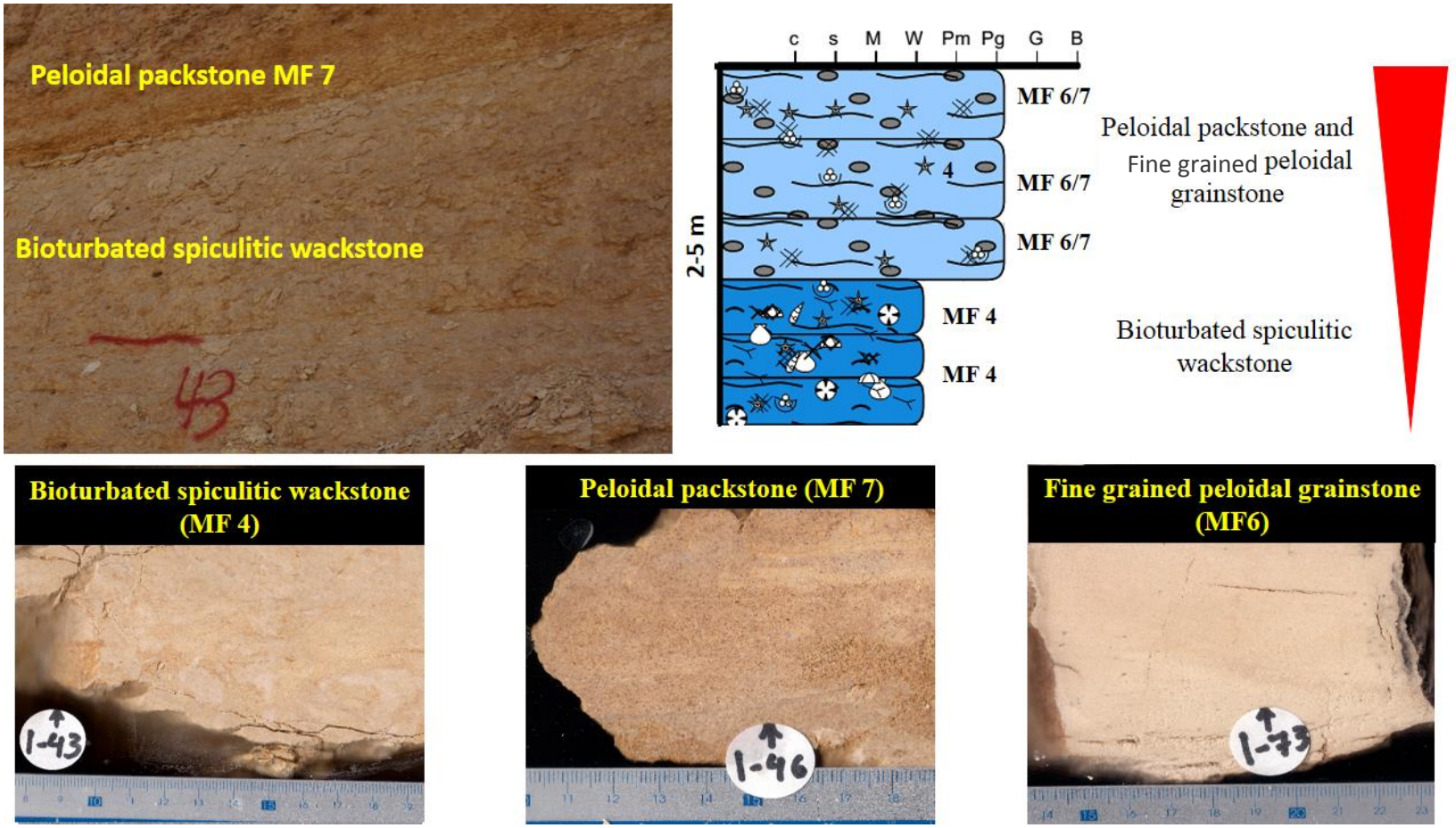


Figure 43 Schematic diagram of shallow lagoon small scale cycle and field and slab photos of the different facies composing this cycle (bioturbated spiculitic wackstone, peloidal packstone and fine grained peloidal peloidal grainstone).

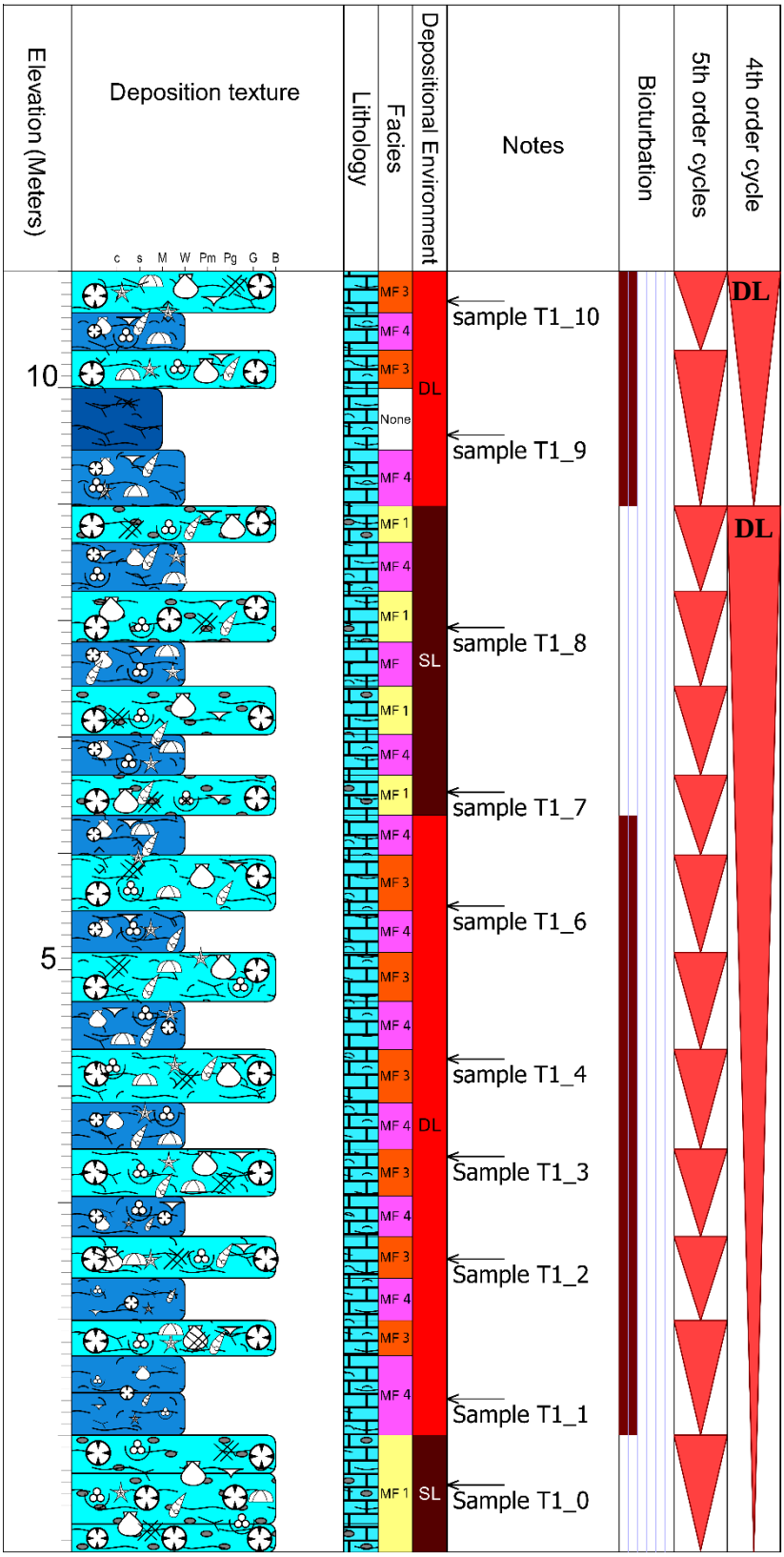


Figure 44 Measured section of the T1 member showing the interpreted 4th and 5th order cycles (note abbreviations of 4th order DL: deep lagoon and SL: shallow lagoon).

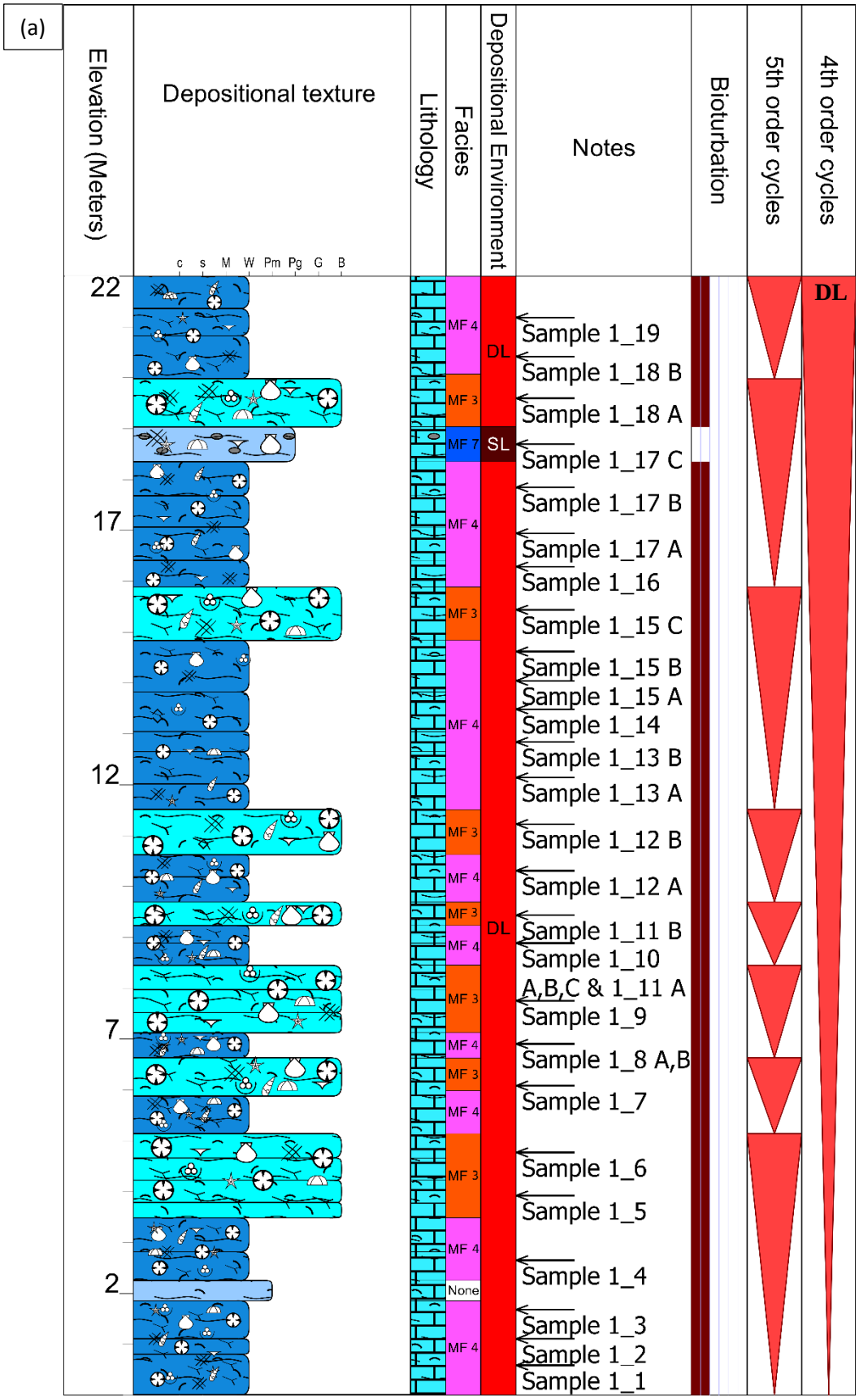
(a)
Elevation (Meters)
Depositional texture
c s M W Pm Pg G B
Lithology
Facies
Depositional Environment
Notes
Bioturbation
5th order cycles
4th order cycles
22
17
12
7
2
MF 4
MF 3
MF 7
SL
None
DL
Sample 1_19
Sample 1_18 B
Sample 1_18 A
Sample 1_17 C
Sample 1_17 B
Sample 1_17 A
Sample 1_16
Sample 1_15 C
Sample 1_15 B
Sample 1_15 A
Sample 1_14
Sample 1_13 B
Sample 1_13 A
Sample 1_12 B
Sample 1_12 A
Sample 1_11 B
Sample 1_10
A,B,C & 1_11 A
Sample 1_9
Sample 1_8 A,B
Sample 1_7
Sample 1_6
Sample 1_5
Sample 1_4
Sample 1_3
Sample 1_2
Sample 1_1

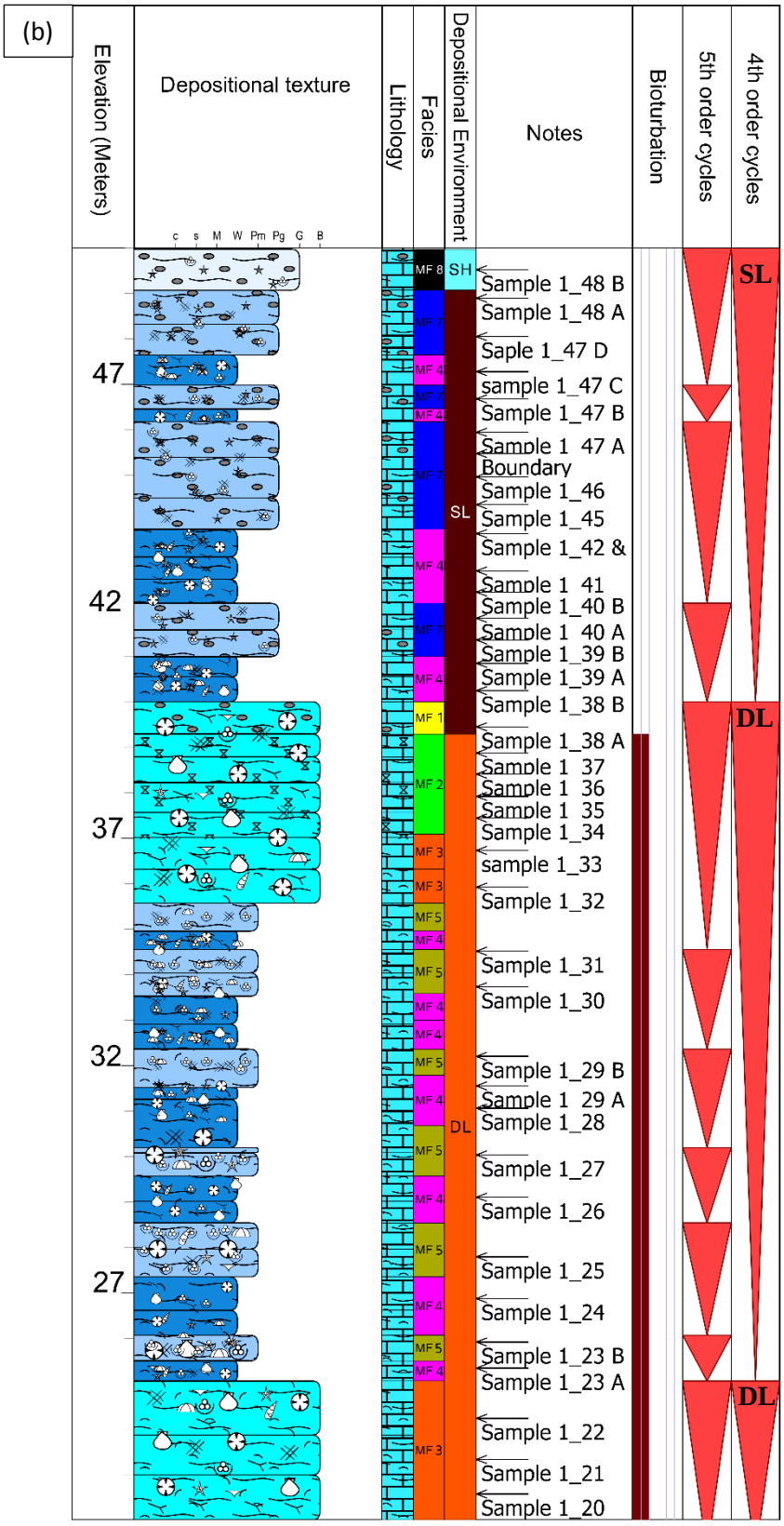


Figure 45 Measured sections of T2 member (part (a) from 0 to 22 m and part (b) from 22 to 50 m) showing the interpreted 4th and 5th order cycles (note abbreviations of 4th order DL: deep lagoon and SL: shallow lagoon).

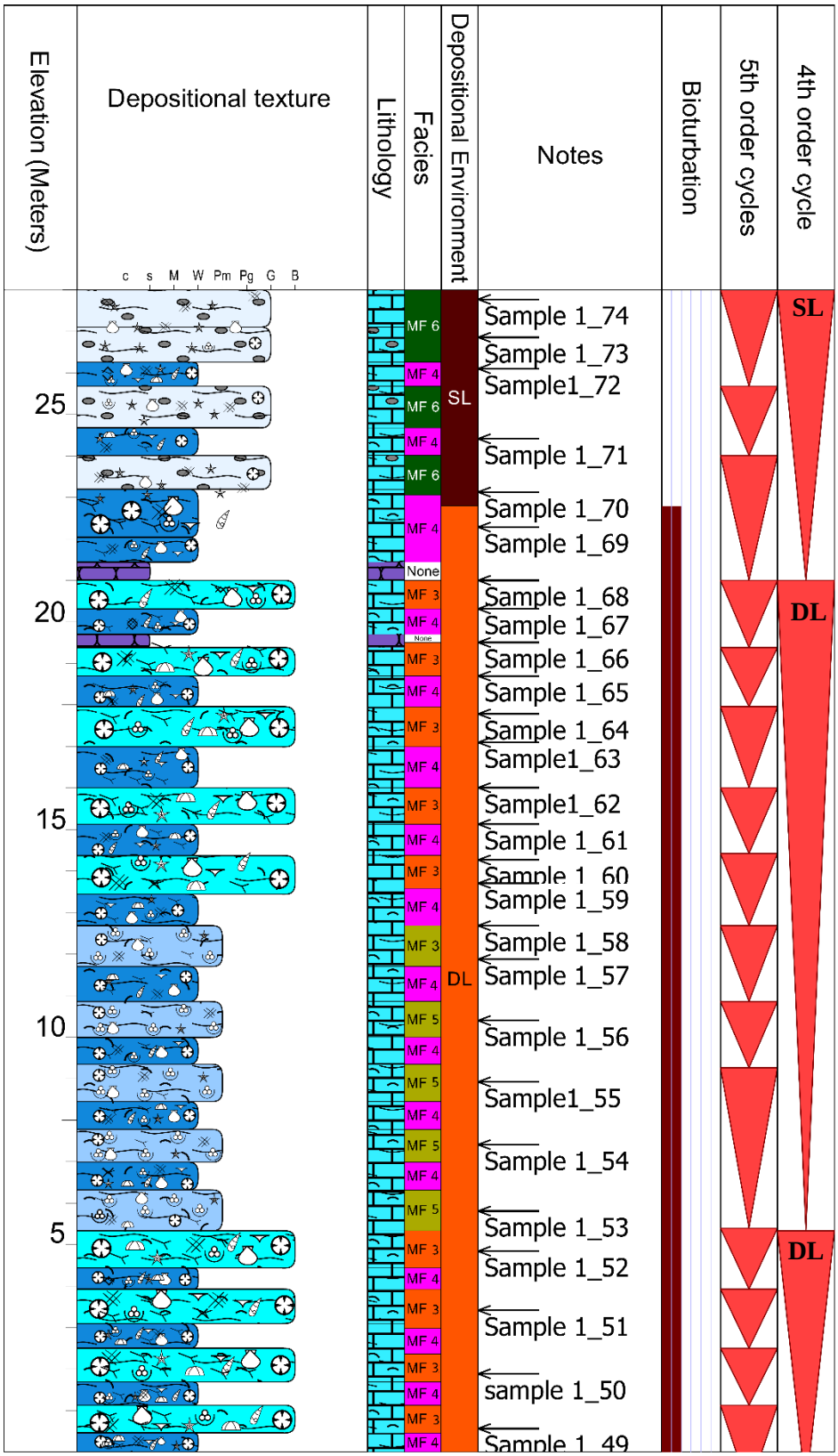


Figure 46 Measured section of T3 member showing the interpreted 4th and 5th order cycles (note abbreviations of 4th order DL: deep lagoon and SL: shallow lagoon).

# CHAPTER 4

# Diagenetic Features and Paragenetic Sequence: Results and Discussion

A comprehensive study on the TMF samples utilizing polarized microscope, reflected microscope, x-ray diffraction (XRD), x-ray fluorescence (XRF), and scanning electron microscope revealed several post-depositional alteration features in the TMF. In this chapter the diagenetic features are described and discussed in a context of the different diagenetic environment affected the TMF, and then a paragenetic sequence established for these diagenetic features based on cross cutting relationships.

## 4.1.Diagenetic Features

Detailed study of TMF revealed the presence of different diagenetic processes, which are microbial micritization, dissolution, recrystallization, cementation, evaporite precipitation, dolomitization, silicification, dolomite dissolution and calcitization. In this part, different diagenetic alterations of TMF carbonates are described

### 4.1.1. Microbial Micritization

Microbial micritization has affected samples of the TMF (Fig. 47) in a variety of ways. The less common way is by formation of micrite envelope where the outer surface of different types of grains are colonized by endolithic microbes which are transformed into fine grained calcite (micrite) to form micrite envelope. Different types of carbonate grains are affected by this process (Fig. 47.a), including brachiopods, mollusk fragments, and foraminiferas. The most common type is the extensive micritization of carbonate grains as

the whole grain is micritized. In that case, some grains would still preserve the internal structure (Fig. 47.c) while most of the grains would lose their internal structure due to the obliteration formed by micritization (Fig. 47.b). Under SEM, the micrite crystals are observed to be less than 10 µm and typically around 2-5 µm (Fig. 47.d). Based on the classification of Deville de Periere et al. (2011), the micrite micofabric is generally subrounded to subhedral crystal shape with punctic to partially coalescent intercrystalline contacts. Intercrystalline microporosity is dominant in micrite, Microbial micritization is observed throughout the entire TMF succession in all microfacies and occurs in both grain dominated facies and mud dominated.

### 4.1.2. Recrystallization and Neomorphism

The recrystallization is a process by which the crystals change from fine crystalline to coarse crystalline. This happens by changing from aragonite to equant calcite crystals (Flok, 1965, Tucker and Wright, 1990). In TMF, the aragonite and high magnesium calcite forming skeletons underwent recrystallization process to crystalline, more stable LMC. Also the lime mud (micrite) filling the septa in some corals underwent recrystallization to microspar with crystal size 5-20 µm and pseudospar with crystal size 30 µm (Fig. 48). Mainly, the micrite and coral fragments (Fig. 48) are mostly affected by recrystallization more than the other components.

### 4.1.3. Dissolution

Dissolution is a process by which carbonate grains, matrix and cements are dissolved due to the chemical disequilibrium between fluids with low $Ca^{2+}$ concentration and aragonite, high magnesium calcite (HMC), and to a lesser extent low, magnesium calcite (LMC). The dissolution process may extend from shallow burial (eogenetic) to deep burial

(mesogenetic) and until uplifting (telogenetic). In the TMF, the dissolution is observed in different forms;

1. Totally or partially dissolved carbonate grains (e.g. different types of bioclasts; Fig. 49.a and d).
2. Molds of carbonate grains (formed originally of aragonite or HMC) filled with LMC sparry cement (Fig. 49.b).
3. Molds of siliceous sponge spicules (originally formed of $SiO_2$) filled with LMC sparry cement (Fig. 49.e).
4. Partially or totally dissolved authigenic minerals such as dolomite and evaporite minerals, e.g. anhydrite) (Fig. 49.c and f).

Various ranges of dissolution, which occur in all microfacies, contribute to the creation of moldic and vuggy secondary porosity.

### 4.1.4. Evaporite Precipitation and Dissolution

In this study, dissolved evaporite crystals were found in samples from the T1 member with crystal sizes ranging from 250 µm to 300 µm. The outline of the molds of totally dissolved evaporite crystals is similar to the anhydrite crystal shape, so it is suggested that the present molds of evaporites in TMF were originally anhydrite (Fig. 50.a and b). Moreover, in T2 and T3 polycrystalline calcite is found filling lenticular mold thought to have formerly been by gypsum crystals (Fig. 50.c). In addition to petrographic analysis, the XRF analysis showed the concentration of sulfur to be relatively high (2100-293 ppm; mean 913 ppm) and persistent throughout all the analyzed samples. XRD data of a chert bed in the T3 member also showed the presence of trace amounts of anhydrite (Fig. 50.d).

### 4.1.5. Dolomitization

Dolomite is a common diagenetic feature in the studied samples of the TMF. Dolomitization in the TMF had been reported earlier by Dabbagh (2006), and EL-Sorogy et al. (2016). In this study, most of the observed dolomite crystals are zoned idiotopic dolomite rhombs with cloudy core and clear rim (CCCR) and often have an iron-rich fill (Figs. 51 and 52). The dolomite crystals occur dispersed as patches in lime mud (Figs. 51.a and 52.a) with a crystal sizes ranging from finely crystalline (30-50 μm) to medium to coarse crystalline (around 250 μm). In corals, skeletal fragments, and burrows coarse crystalline dolomite (Fig. 51.b, c and d) is dominant with crystal size ranges from 200 μm to 500 μm. Dolomite crystals are always either totally or partially dissolved. In the partially dissolved dolomite crystals, mainly the cores and outer rims are typically preserved although locally the cores or the outer rims are dissolved. Under cathodoluminescence, the dolomite crystals display red luminescence (Fig. 52.d), with differences in luminescence between the core and outer rim. In thin section, the concurrent dolomite growth is demonstrated by zoned dolomite in which any two or more self-impinging crystals show their corresponding zones to meet each other along a mutual boundary.

### 4.1.6. Cementation

Cementation is a chemical process where precipitation of cements in carbonate sediments happens when pore-fluids are supersaturated with respect to the cement phase and there are no kinetic factors inhibiting the precipitation (Tucker and Wright, 1990). In this study, calcite cements have several different cement fabrics which are listed below;

- Equant calcite cement: euhedral to subhedral calcite crystals (size > 30 μm) with approximately the same length and width occur filling partially or completely the

intraparticle porosity in skeletal grains and interparticle porosity between the different components in the rock (Fig. 53.a, b and c). This type of cement is found in all facies as a cement filling the interparticle porosity (Fig. 53.b) in grain dominated facies and as a cement filling moldic pores in the dissolved bioclasts (Fig. 53.a) in all facies. Also, it is found as cement filling the fractures. This fabric was observed under SEM (Fig. 53.c). In addition, blocky calcite cement with medium to coarse crystals (may reach more than 1 mm) occur filling the molds of coral fragments and burrowing sites (Fig. 54.c). The crystal size of calcite cement is increasing from walls of coral to the center by increasing the space to be filled with the cement. Under SEM, the blocky calcite cement is showing intercrystalline microporosity (Fig. 54.d).

- Drusy calcite cement: cements in which fabric crystal size is increasing from the pore walls toward the pore center. In this study, drusy cement starts with crystal size of 15-20 μm along the pore walls and ends with coarse crystals in the pore center with crystal size 200-300 μm. It is found as a cement filling the molds of different skeletal components (Fig. 53.d).
- Syntaxial overgrowths: cement that grow in optical continuity with an underlying host grain; such cements are formed exclusively on grains composed of single crystals of calcite (e.g. echinoderm fragments, spines and crinoids) in this study. This type of cement occurs on echinoderm grains filling the burrow and in interparticle porosity. The crystal size of this cement may reach 1 mm (Fig. 54.a). The syntaxial overgrowth is found in all facies as the echinoderms are abundant throughout the studied sections.

- Poikilotopic cement: syntaxial overgrowths in which the overgrowth engulfs several surrounding grains. This type of cement occurs on echinoderm grains infilling burrows as well as in interparticle porosity (Fig. 54.b).

### 4.1.7. Silicification

Silicification is a common diagenetic feature that affects a wide variety of non-siliceous rock type and the degree of silicification varies from minor to pervasive (Hesse, 1989). In this study, most of the samples showed partial silicification. This silicification happens either as a pore filling cement, where the pores are filled with equigranular microcrystalline quartz (Fig. 55.d), or as a replacement phase (Fig. 55.a, b, c, e, and f), where the calcite has been replaced by spherulitic chalcedony. In addition to petrographic analysis, XRF analysis revealed significant variation in the concentration of silicon. In samples containing partially silicified corals, the silicon concentration of these corals ranged from around 30 % to 50 %. In whole rock analyses, the silicon concentration was 3 % - 1 % and mean 1726 ppm. Typical partially silicified components included corals, echinoderms and brachiopods.

### 4.1.8. Dolomite Dissolution and Calcitization

In this study, different fabrics of dolomite dissolution and calcitization are recognized. These fabrics are:

- Partially dissolved dolomite crystals with core and outer rim or with outer rim only preserved (Fig. 56.a).
- Completely dissolved dolomite crystals without any calcite relics remaining (Fig. 56.b).

- Completely dissolved dolomite crystals with calcite relics along the rim (Fig. 56.c).
- Completely dissolved dolomite crystals filled completely with equant calcite crystals (Fig. 56.c and d).

### 4.1.9. Fracturing and Fracture Filling

In this study, fractures were observed as a large scale features in outcrop (Fig. 57.a) as well as local microscopic fractures in thin section and SEM (Fig. 57.b, c, and d). In outcrops, most of the large scale fractures are open with 3-5 cm apertures. In fact it doesn't add much to the porosity and permeability because the formation is not highly fractured. Regarding the orientation, most of the large scale fractures are vertically oriented to the bedding plane. In thin section, some of the microscopic fractures are open which add to the porosity and permeability while others are totally filled calcite cement and reduce porosity and permeability. Under SEM, the calcite cement filling the fracture is equant calcite cement with crystal sizes ranging from 15-25 μm (Fig. 57.c and d) and intercrystalline microporosity between equant calcite crystals. The apertures of microscopic fractures range from 10-20 μm and the orientation ranges from parallel to vertical to bedding.

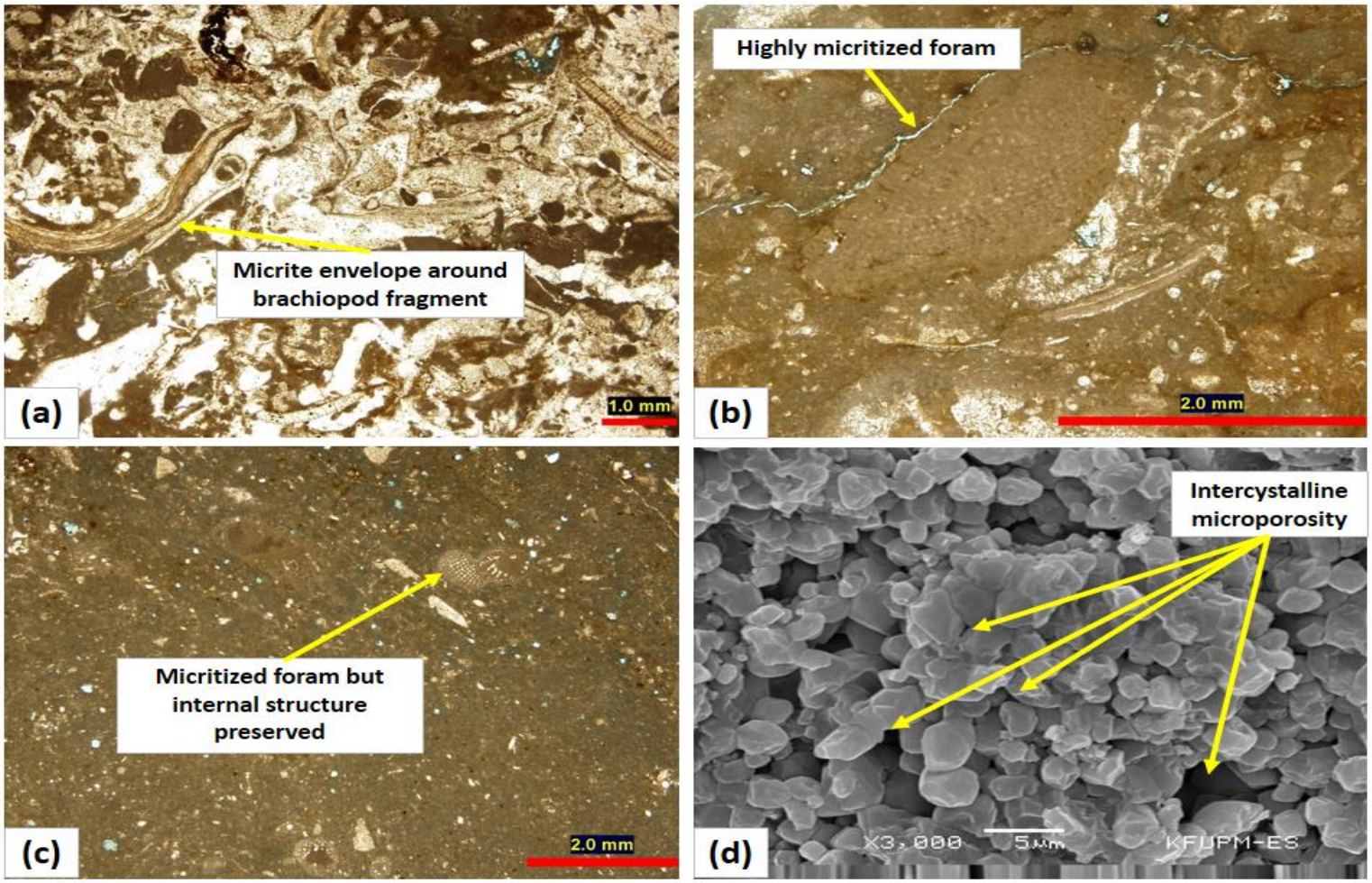


Figure 47 Thin section photomicrographs (a-c) and SEM image (d) of different intervals within the TMF documenting the different effects of microbial micritization and characteristics of micrite and showing: (a) Micrite envelop on a brachiopod fragment (PPL). (b) Intensive micritization effect of a foraminiferas that totally obliterated internal structure (PPL). (c) Micritized foraminiferas but with preserved internal structure (PPL). (d) Micrite with subrounded to subhedral crystal shape with punctic to partially coalescent intercrystalline contacts and intercrystalline microporosity.

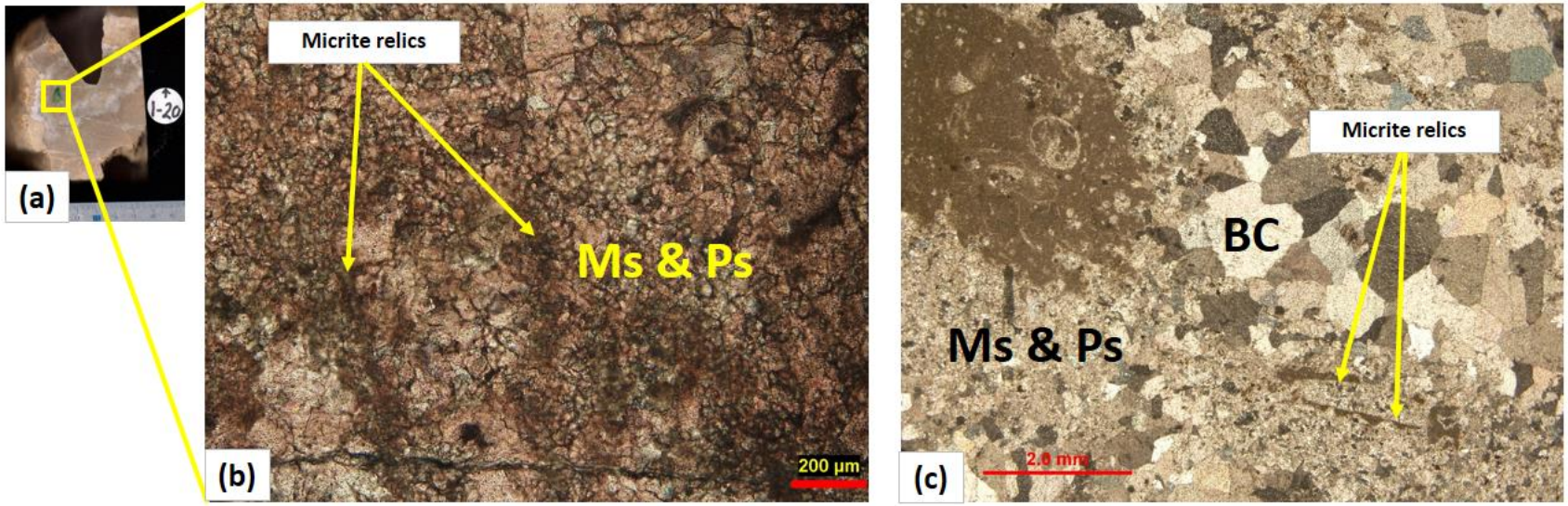


Figure 48 Slab (a) and thin section photomicrographs (b-c) of coral floatstone showing: (a) coral fragment filled with calcite as a mold. (b and c) recrystallization and neomorphism of micrite into microsparite (Ms) and pseudosparite (Ps) of the slab in photo (a). Note the micrite relics surrounded by Ms, Ps and blocky calcite (Bc) (PPL).

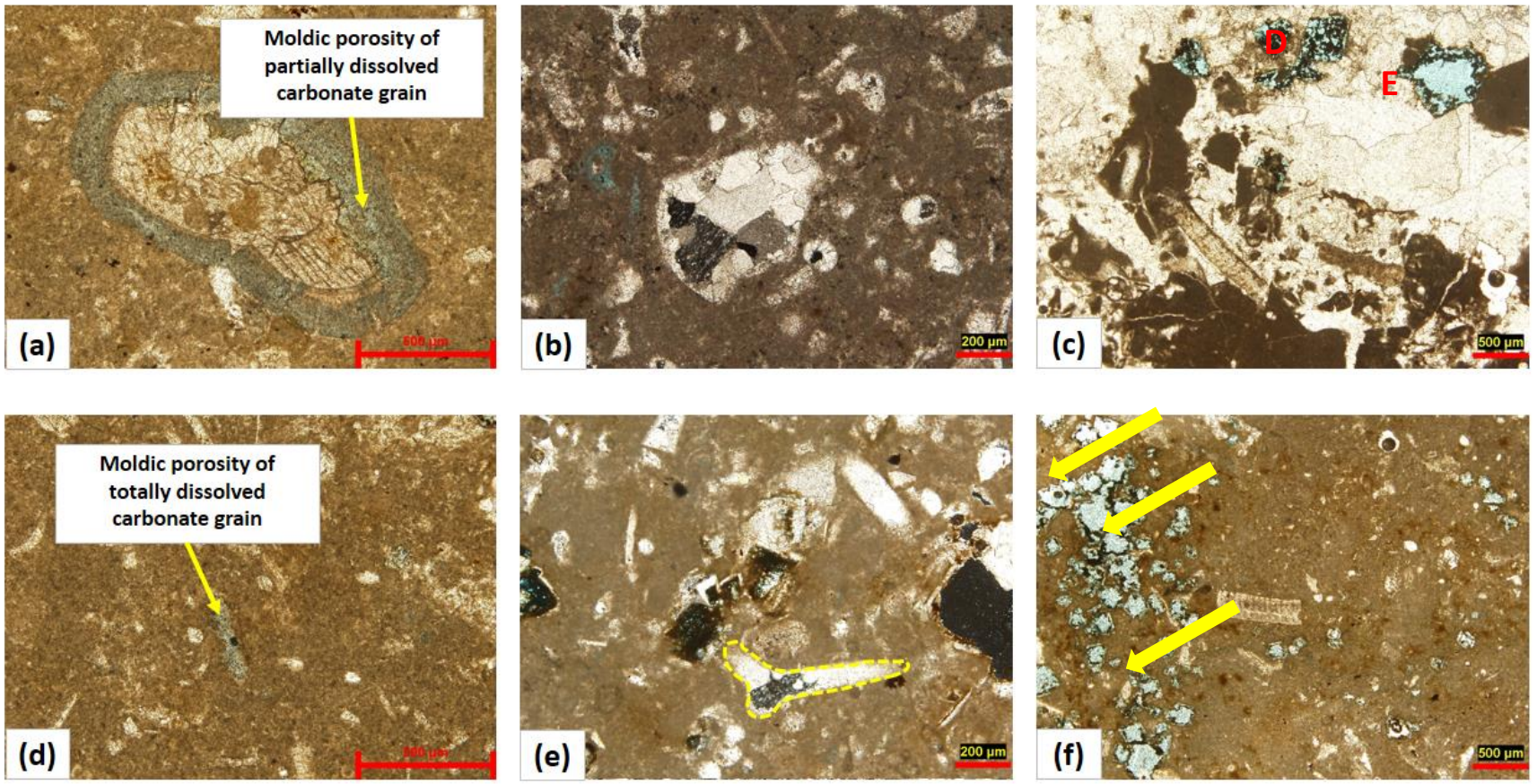


Figure 49 Thin section photomicrographs of different intervals within the TMF documenting the different effects of grain dissolution and showing: (a) Moldic porosity formed by partial dissolution of carbonate grains (PPL). (b) Completely dissolved aragonite carbonate grain and later LMC sparry cement filled the pore developed by dissolution (XPL). (c and d) Moldic pores formed by dissolution of dolomite (D), evaporite (E) and undifferentiated carbonate grain. (e) Mold of totally dissolved siliceous sponge spicule filled with equant calcite cement (note the yellow dashed line around the siliceous sponge spicules, XPL). (f) Vuggy porosity by intensive dissolution of cluster of dolomite crystals (note the arrows pointing to the vuggy and moldic pores formed by dissolution of dolomite, PPL).

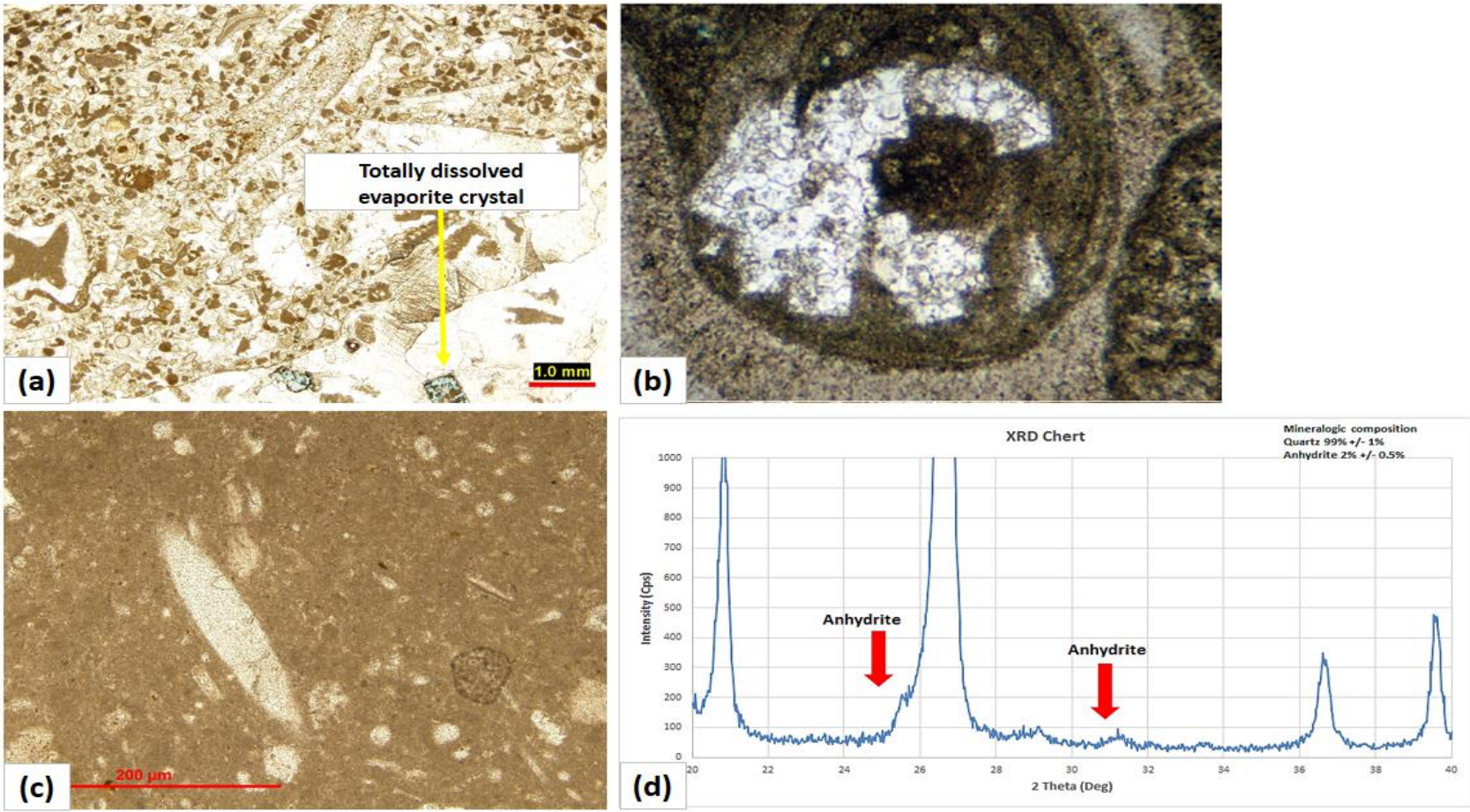


Figure 50 Thin section photomicrographs (a-c) and XRD results indicating the presence of evaporites in the TMF and showing: (a) The totally dissolved evaporite crystals within the TMF (PPL). (b) Thin section photomicrograph from Scholle and Ulmer-Scholle (2003) showing anhydrite replacing pisoid and later replaced by calcite but still keeping the original fabric and outline. This photomicrograph shows similar outline to the evaporite crystals in TMF samples. (c) Polycrystalline calcite filling lenticular mold formerly occupied by gypsum crystals (PPL). (d) XRD results of chert bed in T3 showing the presence of relics of anhydrite (note the low intensity which reflects low percentage).

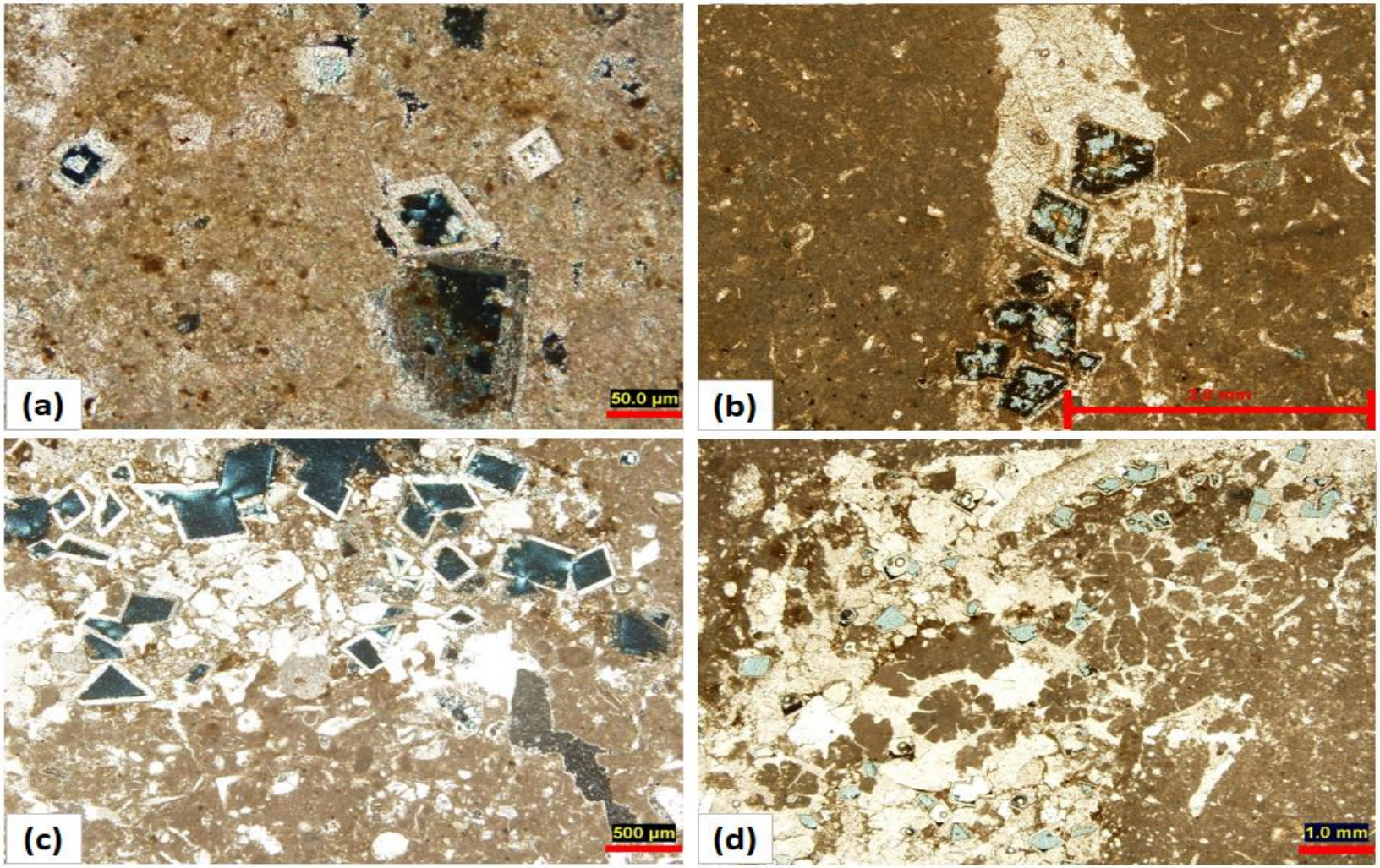


Figure 51 Thin section photomicrographs of different intervals within the TMF indicating the presence of dolomite and showing: (a) Finely crystalline partially dissolved dolomite crystals within a muddy matrix (XPL). (b) Large partially dissolved dolomite crystals with CCCR (PPL). (c and d) Large dolomite crystals with preserved outer rims only found replacing calcite cement filling the coral fragments (c; XPL and d; PPL)

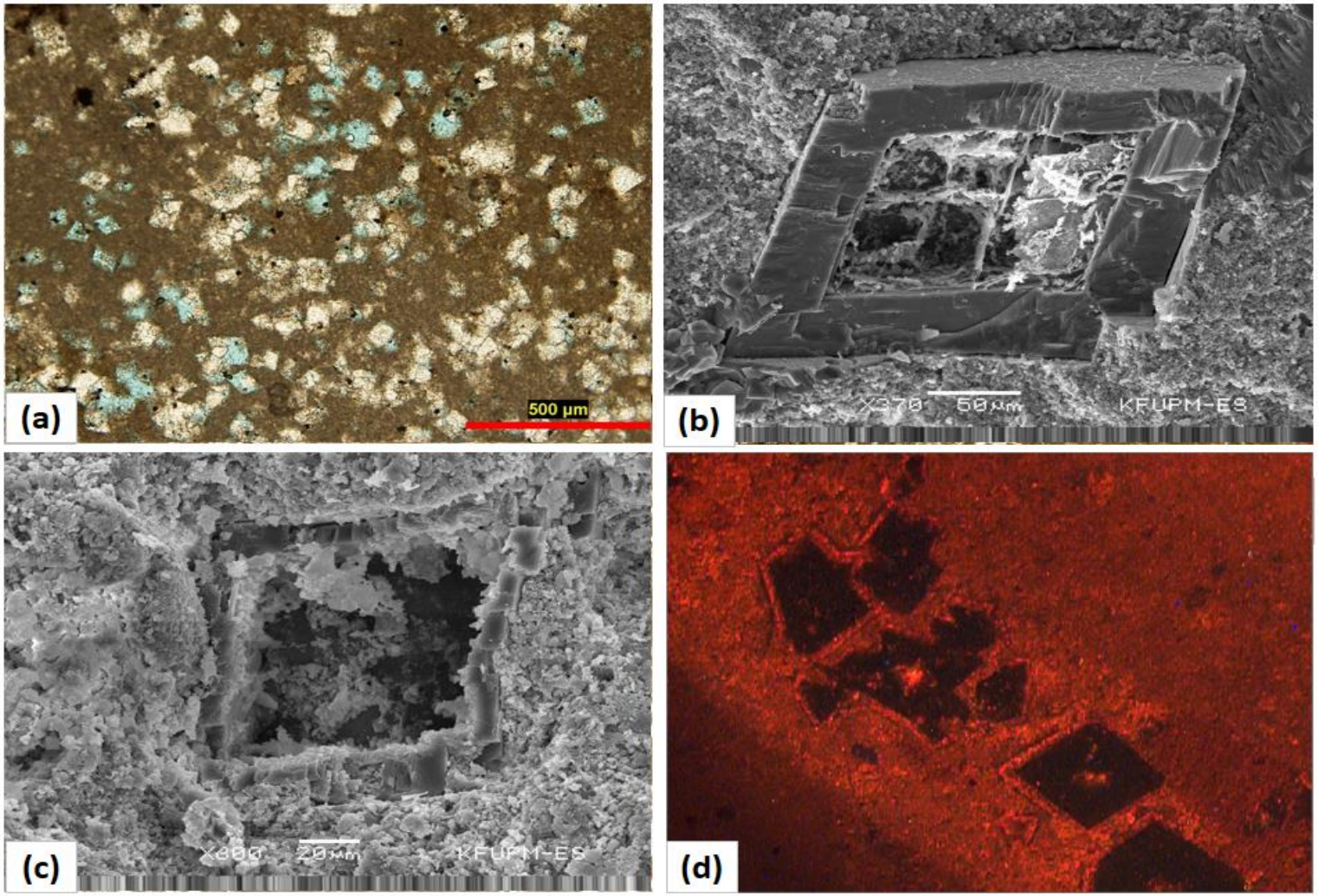


Figure 52 Thin section photomicrograph (a), SEM images (b-c) and CL image (d) of dolomites in the TMF and showing: (a) Small dolomite crystals within a muddy matrix. Some of the crystals are totally dissolved and others are filled with calcite (PPL). (b and c) Partially dissolved dolomite crystals with only outer rim preserved and iron oxide filling the pore space developed by dissolution of core. (d) Red luminescence of dolomite crystals, with a difference in luminescence between core and outer rims.

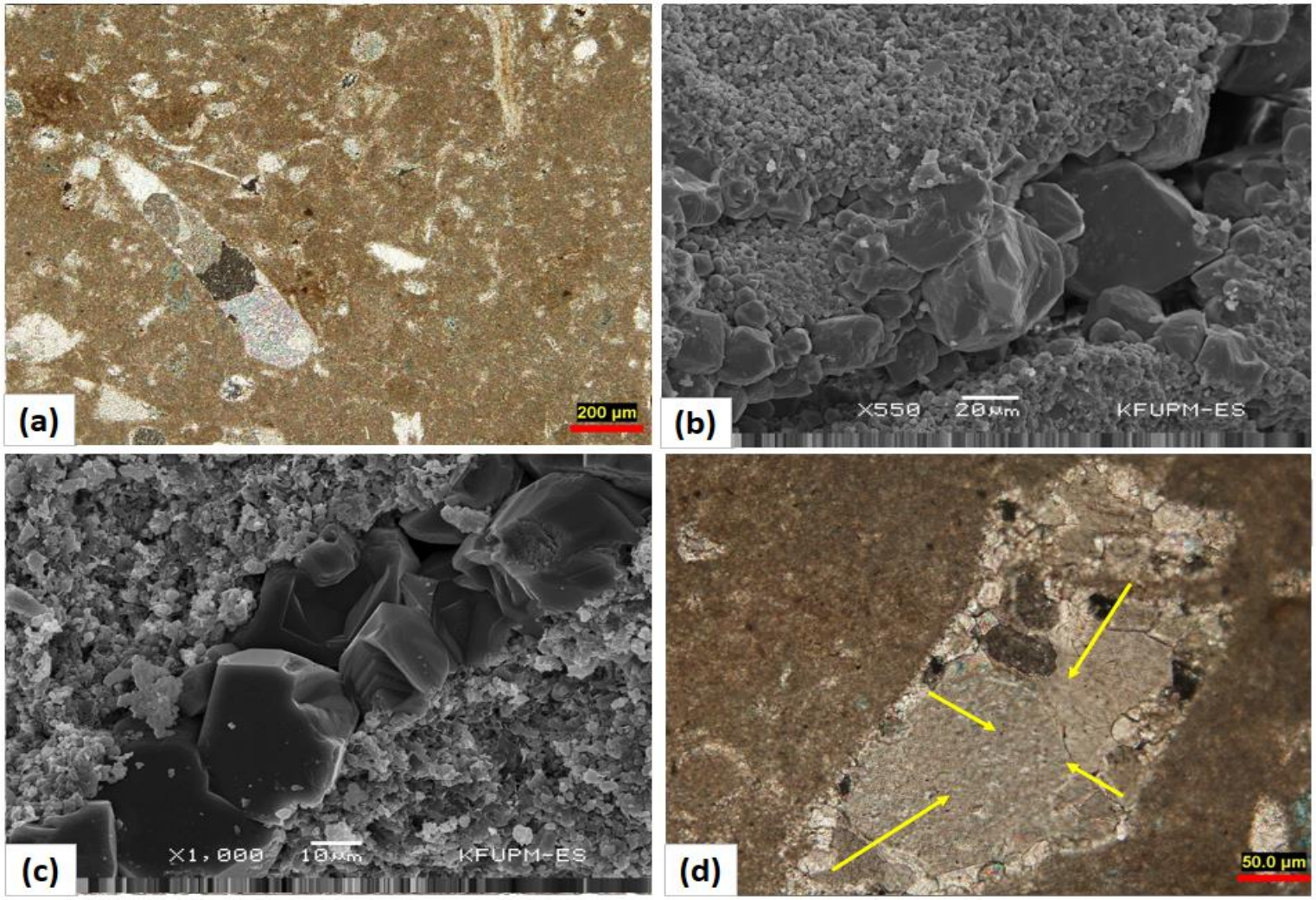


Figure 53 Thin section photomicrographs (a and d) and SEM images (b and c) of equant and drusy calcite cement showing: (a) Equant LMC calcite cement filling the pore formed by dissolution of an originally aragonitic skeletal fragment (XPL). (b) Equant calcite cement filling interparticle porosity between different grains. (c) Equant calcite cement filling a fracture. (d) Drusy calcite cement (XPL). Note the direction of crystal enlargement (arrow).

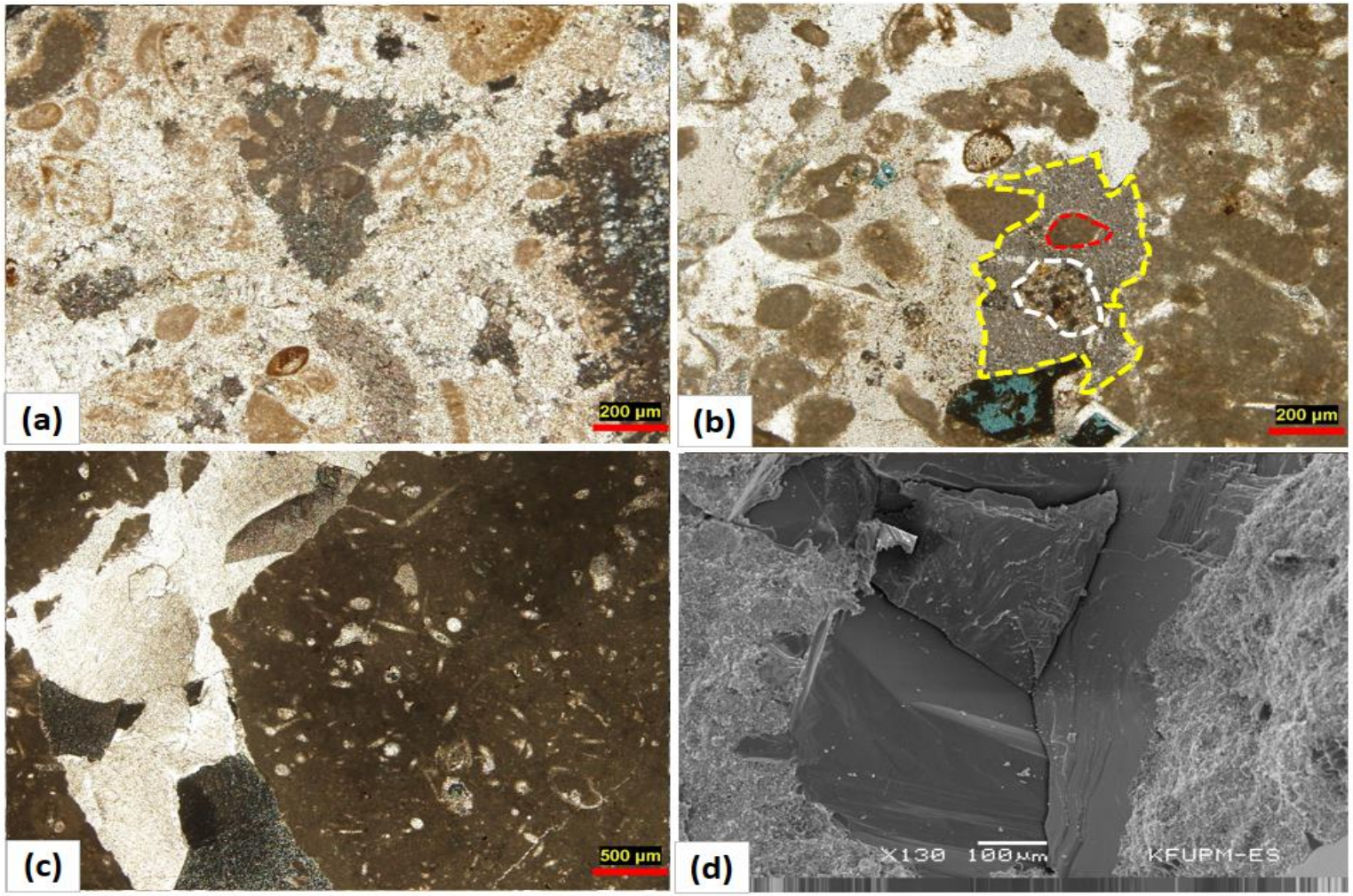


Figure 54 Thin section photomicrographs (a-c) and SEM image (d) of different calcite cements in the TMF showing: (a) Syntaxial overgrowth of echinoderm spine (XPL). (b) Poikilotpoic cementation formed by syntaxial overgrowth of an echinoderm (XPL). The yellow dashed line represents the outline of the poikilotopic cement, the red dashed line highlights an engulfed peloid, and the white dashed line highlights the echinoderm fragment which underwent syntaxial overgrowth. (c) Blocky calcite cement filling a pore formed by dissolution of an originally aragonitic coral fragment (XPL). (d) Large crystals of blocky calcite filling a leached coral fragment.

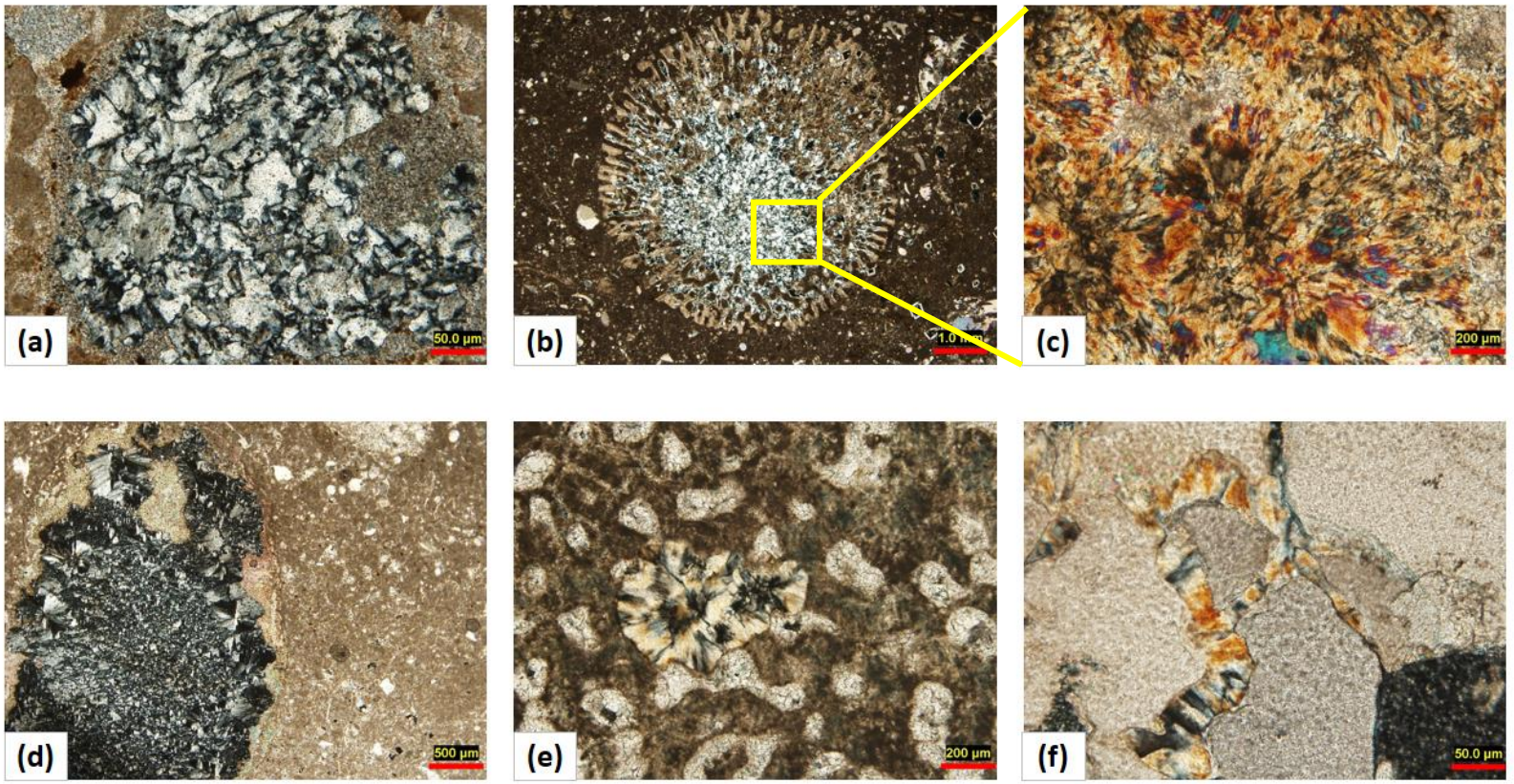


Figure 55 Thin section photomicrographs of different intervals within the TMF revealing the effect of silicification and showing: (a) The silicification as a replacement in echinoderm fragment. The calcite has been replaced by chalcedony (XPL). (b) The silicification of coral as a replacement phase (XPL). Note the inclusions of calcite in the center. (c) The silica replacement of calcite as chalcedony (XPL). The calcite cement is engulfed by chalcedony. (d) The microcrystalline quartz cement filling the pores in echinoderm fragment (XPL). (e) Silica replacement of coral by chalcedony (XPL). (f) The silica replacement of calcite as chalcedony in a coral (XPL)

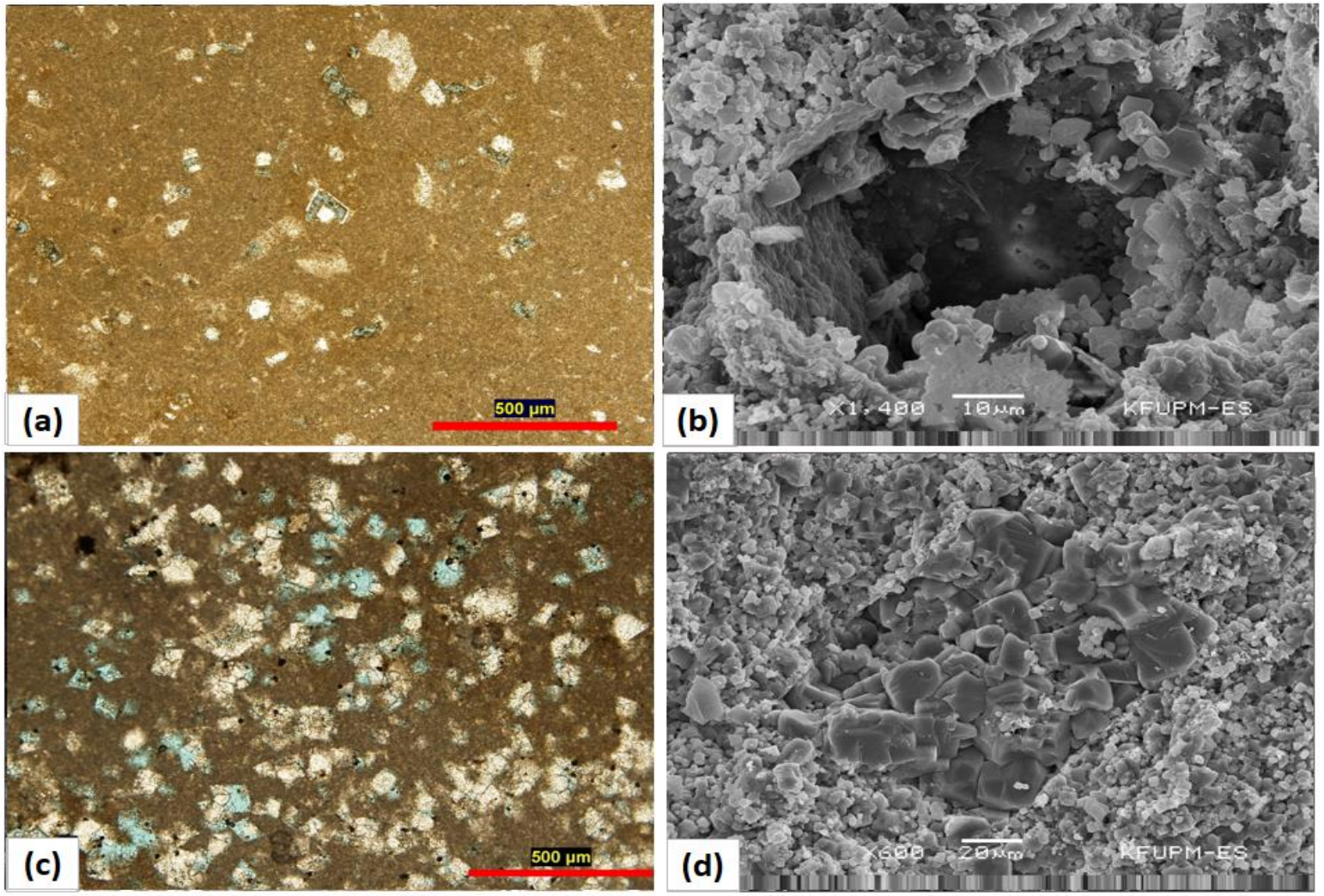


Figure 56 Thin section photomicrographs (a and c) and SEM images (b and d) documenting the effect of dolomite calcitization and showing: (a) Partially dissolved dolomite crystals with core and outer rim only preserved (PPL). (b) Totally dissolved dolomite crystal with no calcite filling the resulting moldic porosity. (c) Totally dissolved dolomites with some crystals filled with calcite cement (PPL). (d) Calcitized dolomite with equant calcite crystals filling the rhombohedral pore of a totally dissolved dolomite precursor.

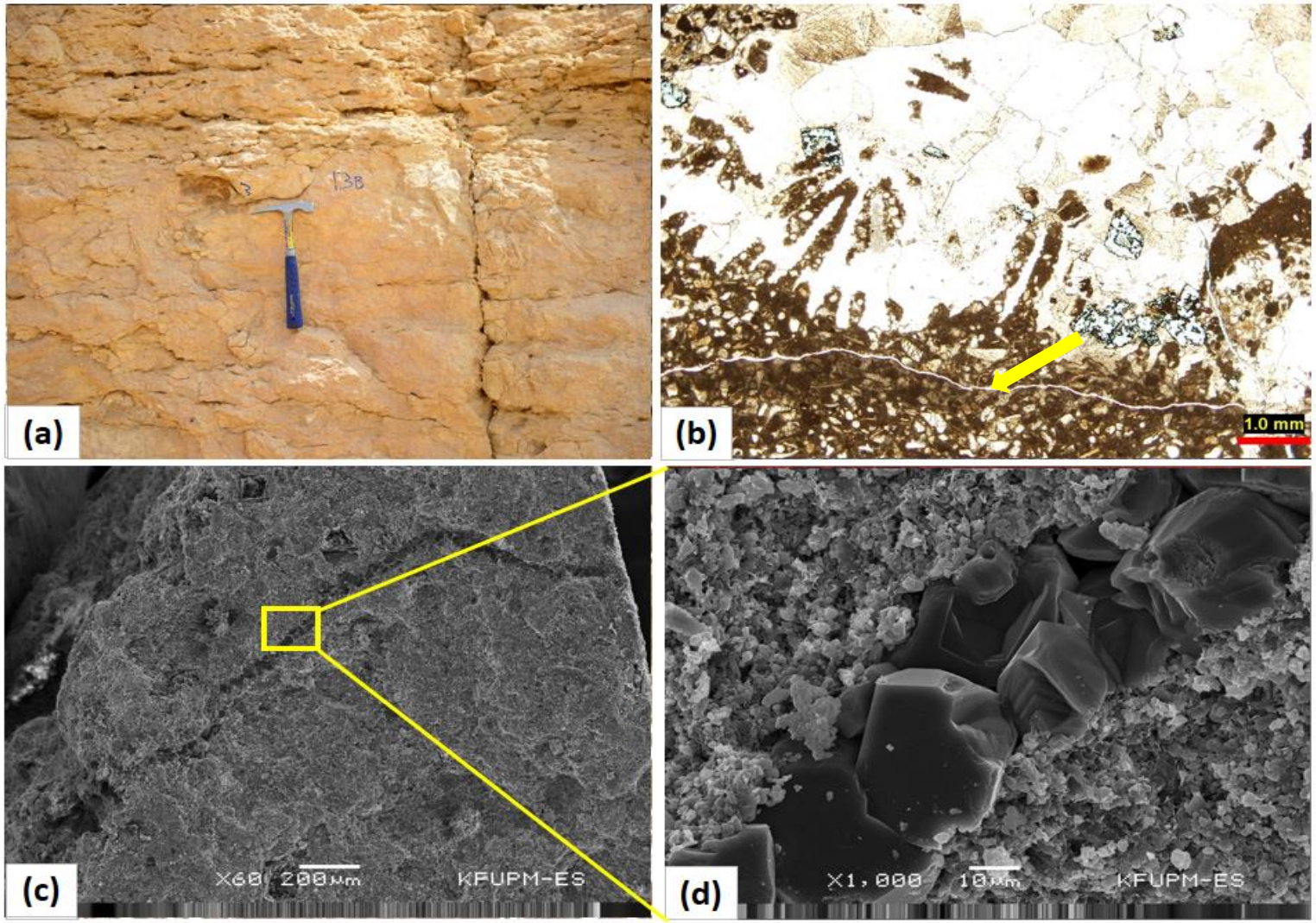


Figure 57 Field photo (a), thin section photomicrograph (b) and SEM images (c-d) of fractures and fracture filling showing: (a) Vertically oriented fracture in the outcrop. (b) Fracture (arrow) filled with sparry calcite cement (PPL). (c) Fracture filled with calcite cement. (d) The equant calcite cement filling the fracture space.

## 4.2.Discussion

The three diagenetic stages described by Choquette and Pray (1970) including eogenetic, mesogenetic, and telogenetic are used to interpret the timing and sequence of observed diagenetic alterations of the studied carbonate sequence. The lack of early marine cementation has allowed some compaction to occur even though these rocks were never deeply buried (as evidenced by lack of significant compaction features as stylolitization and burial cements (Fig. 58). Based on the petrographic characteristics of the diagenetic products previously described and their elemental compositions, the timing of diagenetic events in the TMF can be inferred (Fig. 59). The studied sequence was subjected mainly to eogenetic processes, to some extent shallow mesodiagenetic processes, and to telodiagenetic processes.

### 4.2.1. Eogenetic Environment

#### 4.2.1.1. Marine Environment

The marine diagenetic environment is occurs within the eogenetic realm, and the major diagenetic process observed in the TMF that is thought to have occurred there is micritization. Micritization occurs at the seafloor or just below by boring of the grain margins by micro-organisms such as endolithic algae, fungi and bacteria. The borings were then filled with fine grained cement or sediment forming a micrite envelope (Reid & Macintyre, 2000). In the TMF, microbial micritization is observed throughout the succession in all microfacies (Fig. 47). Micritization process plays an important role in porosity reduction as it fills the intraparticle porosity (Fig. 47.b). In TMF, no evidence is observed of marine cements.

#### 4.2.1.2. Meteoric Environment

The meteoric diagenetic environment is an important diagenetic stage that directly impact the development and evolution of the carbonates reservoir quality (Moore, 2013). Meteoric waters are chemically dilute, typically undersaturated and in disequilibrium with respect to most carbonate minerals (aragonite and HMC). Therefore, meteoric waters are strongly aggressive toward metastable carbonate minerals and have ample opportunity to dissolve these minerals. This strong aggressiveness is attributed to the fact that meteoric waters have access to large $CO^2$ reservoirs that are present in the atmosphere as well as in the vadose zone as the waters percolate downward toward the meteoric phreatic zone (Morse and Mackenzie, 1990).

##### 4.2.1.2.1. Recrystallization and Neomorphism

Recrystallization is a process by which the crystals change from fine crystalline to coarsely crystalline. This happens by changing from aragonite to equant calcite crystals (Flok, 1974, Tucker and Wright, 1990). In the TMF, most of the skeletal components were originally composed of aragonite or HMC, with only the brachiopods being originally composed of LMC. Both aragonite and HMC are stable under marine conditions, but become unstable under meteoric conditions. Therefore, during meteoric diagenesis, all aragonitic and HMC components transformed to LMC. In some coral fragments, micrite relics are found and this may suggest recrystallization into microsparite and pseudosparite. Many authors discussed (Sandberg, 1983; Gill et al., 2008; Hopley et al., 2009 and Basyoni and Khalil, 2011) in their case studies the recrystallization process of aragonite or HMC to LMC by the removal of $Mg^{2+}$. Mainly they referred that removal of magnesium ions can happen in two places either in a brackish water (mixing zone) or in fresh water percolation in the

vadose zone. So in both cases it happens in early meteoric stage. Therefore, it is suggested that recrystallization happened in the early meteoric stage and started before cementation process.

#### 4.2.1.2.2. Dissolution

The extensive dissolution of most of skeletal grains suggests that they were dissolved by undersaturated water with respect to aragonite, which suggests dissolution by meteoric water (James and Jones, 2015). This preferential dissolution of skeletal grains (e.g. bivalves, corals and gastropods) is due to the instability of their mineral composition under meteoric water while brachiopods are more stable under meteoric water as they are composed of LMC. In the TMF, all the samples show the dissolution of different skeletal fragments and, in some cases, the only record of the grains is the micrite envelope that still preserves the outer shape of the skeletal fragments. The dissolution process continued throughout eodiagenetic, mesodiagenetic, and telodiagenetic stage.

#### 4.2.1.2.3. Meteoric Cementation

As meteoric water passes through the carbonate succession, it dissolves the metastable carbonate minerals which are formed of aragonite and HMC forming moldic and vuggy porosity. This secondary porosity is observed to be filled with equant calcite cement that precipitated from supersaturated meteoric water with respect to calcite mineral. As a result, equant calcite cement precipitates both in the interparticle porosity surrounding the grains as well as within the molds (Longman, 1980; Moore, 2013). In the TMF, initially undersaturated meteoric fluids dissolved aragonite skeletal components, gradually leading to an increase in saturation to the point where carbonate calcite is precipitated. Therefore, the moldic porosity of skeletal fragments were later filled with either equant calcite or

drusy calcite cement (Figs. 53 and 54). The other two types (poikilotopic cement and syntaxial overgrowth) along with equant calcite cement were found filling the interparticle porosity and burrows (Figs. 53 and 54). Mainly the corals are the only skeletal fragments where blocky calcite cement occurs filling the moldic pores, while the other skeletal fragments are mainly filled with either drusy or equant calcite cement. According to Braithwaite and Montaggioni (2009), the actue scalenohedral or obtuse-angled rhombohedral terminations are interpreted as the products of pores that were flooded in the meteoric zone (Figs. 53.a, b, c and 54.c and d). This type of cement resulted in the decrease of interparticle, moldic, and vuggy porosity.

#### 4.2.1.3. Shallow Burial

As discussed earlier, TMF is thought not to have been buried deeply before being uplifted, and this is suggested due to the absence of any burial cementation, stylolitization, concave convex grain contact, and dissolution seems (Fig. 58). Further suggesting that there is only minimal pre-cement compaction has occurred. Therefore, all burial diagenesis is thought to have happened at shallow depths.

### 4.2.2. Mesogenetic Environment

#### 4.2.2.1. Dolomitization and Evaporite Precipitation

Dolomite crystals are found replacing the calcite cements either in the skeletal fragments or in the burrows filled with calcite cement (Fig. 51.b, c and d). Also, patches of dolomites are found dispersed within and replacing the lime mud (Figs. 51.a and 52.a). Basyoni and Khalil (2013) indicated that, such dolomitization took place during or after the introduction of late, post-compaction cement, and consequently the replacement process must be of

burial diagenetic origin, though not necessarily at great depth. Therefore, it is suggested that dolomitization happened during or after the post compaction cementation process.

In order to suggest a mechanism of dolomitization in the TMF, thin section petrography, SEM and chemical data (XRF and XRD data) are integrated together. In thin section and SEM the dolomite crystals have a size range from fine to coarsely crystalline (Lumsden & Chimahusky, 1980 classification) with a texture of planar-e euhedral zoned idiotopic with cloudy core and clear rim (CCCR) (Figs. 51 and 52). Planar crystals tend to develop around the so called critical roughening temperature (CRT), which appears to be about 50-60$^{o}$C for dolomites (Gregg and Sibley, 1984). These temperatures are considerably lower than those likely to have been generated during dolomitization of limestones at deep burial temperature (70-90$^{o}$C) or by hydrothermal waters (100-220$^{o}$C) (Warren, 2000). The concentrations of Sr in the studied dolomites range from 800 ppm to 1200 ppm which is around those in hypersaline evaporites (Veizer, 1983; Warren, 2000). In addition, the thin section petrography revealed the presence of evaporites within the studied interval (Fig. 50), as well as anhydrite relics in chert beds (Fig. 50.d). Thus, most evidence points to hypersaline fluids to have been the fluid and mechanism of dolomitization in the studied interval of the TMF. Such hypersaline fluids that are associated with evaporite precipitation can be potent mechanism for dolomitization. So, during the precipitation of evaporites $Ca^{+2}$ ions are consumed and $Mg^{2+}/Ca^{2+}$ ratio increases in the pore fluids, which triggers the dolomitization process (Tucker and Wright, 1990). Another related factor facilitating dolomitization is that evaporite minerals precipitation reduces the sulphate content of the pore fluids which represents removal of dolomite formation inhibitor (Tucker and Wright, 1990; James and Jones, 2015).

#### 4.2.2.2. Silicification

In this study, silicification is suggested to be of burial origin as it replaces partially post-compaction cement and is also observed engulfing these post-compaction cements in coral fragments. It is suggested that dissolution of sponge spicules results in water that are saturated with respect to $SiO^{2+}$, which results in the precipitation of silica into the forms described (chalcedony and microcrystalline silica). Many authors consider that the source of silicification in carbonates can best be attributed to a biogeneic source (Lawrence, 1994; Gimenez-Montsant et al. 1999). The question here is from what was this biogeneic source? The most plausible answer is that it was sourced from the formation itself as it contains abundant sponge spicules, and many authors have previously discussed such a scenario of an intra-formational source of silica (e.g., Coniglio, 1987; Loope and Maliva and Siever, 1988a; Loope and Watkins, 1989). The timing of silicification is difficult to determine because the lack of cutting relationships but in thin section chalcedony is observed to engulf the post-compaction equant calcite cement within a coral fragment (Fig. 55.f). This suggest that silicification formation postdated calcite cementation; in addition, it seems likely that silicification occurred before evaporite and dolomite dissolution since the resulting moldic pores would have been filled with silica cement if silicification postdated this dissolution

### 4.2.3. Telogenetic Environment

#### 4.2.3.1. Dolomite Dissolution and Calcitization

In this study, two dolomite fabrics are observed, one in which dolomite crystals are partially (with outer rim and or core) or totally dissolved (Fig. 56.a and b), and a second

where dolomite crystals are totally dissolved then filled partially or completely with equant calcite crystals (Fig. 56.c and d).

In the first fabric, the remaining parts (zones) of the dolomite crystal is more resistant than the dissolved parts (zones) of the crystal. This observation suggests that zoning in dolomite in the TMF reflects differences in the chemical composition of the different zones, which is reflected in their stability against dissolution. This observation is supported by CL images (Fig. 52.d) which showed differences in the luminescence between the core and outer rim.

In the second fabric, the rhombohedral pores of dissolved dolomites are filled partially or totally with equant calcite crystals (Fig. 56.d)., a process that has been termed dolomite calcitization (Coniglio, 1978). Calcitized dolomites preserve the rhombohedral shape of dolomite, even though they have been completely replaced by calcite. This preservation of a rhombohedral shape suggests that the dissolution process and calcite precipitation happened concomitantly where the dissolution and precipitation are closely spatially coupled at the interface between the dolomite and calcite (Altree-Williams, 2015).. according to Folk (1974), Lahann (1978) and Moore & Wade (2013), freshwater calcite cement crystals tend toward equant shapes, while marine calcite and aragonite cement crystals tend toward elongate fibrous shapes. Therefore, the crystal morphology of the calcite filling rhombohedral pores of dissolved dolomites suggests that dolomite calcitization process is of meteoric origin.

The mechanism of dolomite calcitization in thr TMF is a controversial issue. Dabbagh (2006) suggested that the dissolution of anhydrite deposits of the Arab and Hith Formations is responsible for the dolomite calcitization in TMF. In this study, it is suggested the source

of evaporites is intraformational as there was evaporite content within TMF. This suggestion relies on three supporting lines of evidence. First, the observation of totally dissolved anhydrite crystals (Fig. 50.a) and polycrystalline calcite filling lenticular mold formerly occupied by gypsum crystals (Fig. 50.c). Second, XRD results of chert bed (Fig. 50.d) showed the presence of relics of anhydrite within the chert bed which suggest was anhydrite nodules occurred as a precursor of the chert and, with later chert nodules replacing the dissolved anhydrite nodules. Finally, the high Sr concentrations in the studied dolomites (800-1200 ppm) matche values seen in other hypersaline evaporative dolomites (Veizer, 1983; Warren, 2000).

#### 4.2.3.2. Fracturing and Fracture Filling

Since fractures cross cut all other depositional and diagenetic features of the TMF, it was clearly one of the last event to have occurred and is suggested to be associated with late-stage uplift of this succession. TMF was deposited during the Middle to Late Callovian, a time when the Arabian plate was passive margin with no significant tectonic activity influencing sedimentation patterns. Therefore, it is suggested that these fractures are local within Majma'ah graben and affected the formation during uplifiting. During the uplift dissolution of calcitic component occurred due to water rock interaction with undersaturated water with respect to calcite. When the water became saturated, equant calcite cement filled some of the fractures as a fracture filling.

## 4.3. Geochemical Signature of Diagenesis in the TMF

Brand and Veizer (1981), Winefield et al. (1996) and many other authors discussed the geochemical signatures of different diagenetic environments on the trace elements of carbonate rocks. Modern aragonite sediments in tropical warm shallow-marine waters have

low Mn and Fe (20 ppm), moderate Na (2500 ppm) and high Sr (10,000 ppm) concentrations (Milliman, 1974). Modern temperate shallow-marine calcite sediments on average have low Sr (3000 ppm) and high Na (5000 ppm), Mn (150 ppm) and Fe (1000 ppm) concentrations (Rao, 1990). In this study, concentrations of Sr (875-1520 ppm; mean 1127 ppm), Fe (917-22000 ppm; mean 8924 ppm) and Mn (26-890 ppm; mean 208 ppm) in TMF suggest appreciable loss of Sr and a gain of Mn and Fe during diagenesis when compared with modern tropical aragonite and temperate calcite sediments. The increase in Fe result from result from meteoric diagenetic processes. Transformation and stabilization of aragonite and HMC calcite into LMC decreases Sr values and enhances Mn concentration which can be observed here in TMF by comparing the concentrations of analyzed samples and modern tropical and temperate calcite sediment. This indicates that meteoric diagenesis has affected the TMF.

Cross-plots of trace elements including Mg % vs Fe %, Mn % vs Fe %, Sr % vs Mn% and 1000Sr/Ca vs Mn % are used to reveal the geochemical signatures of diagenesis in the TMF (Fig.60). Winefield et al. (1996) discussed the correlation scenarios of Mg % vs Fe %, Mn % vs Fe %, Sr % vs Mn% cross-plots and mentioned that the positive correlation of these cross plots represents a signature of meteoric diagenesis. Therefore, the Positive correlation in the cross-plots of Mg % vs Fe %, Mn % vs Fe % and Sr % vs Mn% suggest that the TMF is affected severely by meteoric diagenesis (Fig. 60.a,b and c) and previous workers (Brand and Veizer, 1980; Rao, 1991; Winefield et al., 1996) have shown that increasing iron and manganese concentrations and high manganese concentrations compared to the modern carbonate sediments, can be attributed to meteoric diagenesis because of the high manganese content in the meteoric waters (Brand and Veizer, 1980; Rao, 1991; Winefield

et al., 1996). In addition, bivariate plot of Sr/Ca vs Mn % shows (Fig. 60.d) that the limestones have been stabilized by meteoric fluids in an open diagenetic system (Brand and Veizer, 1980).

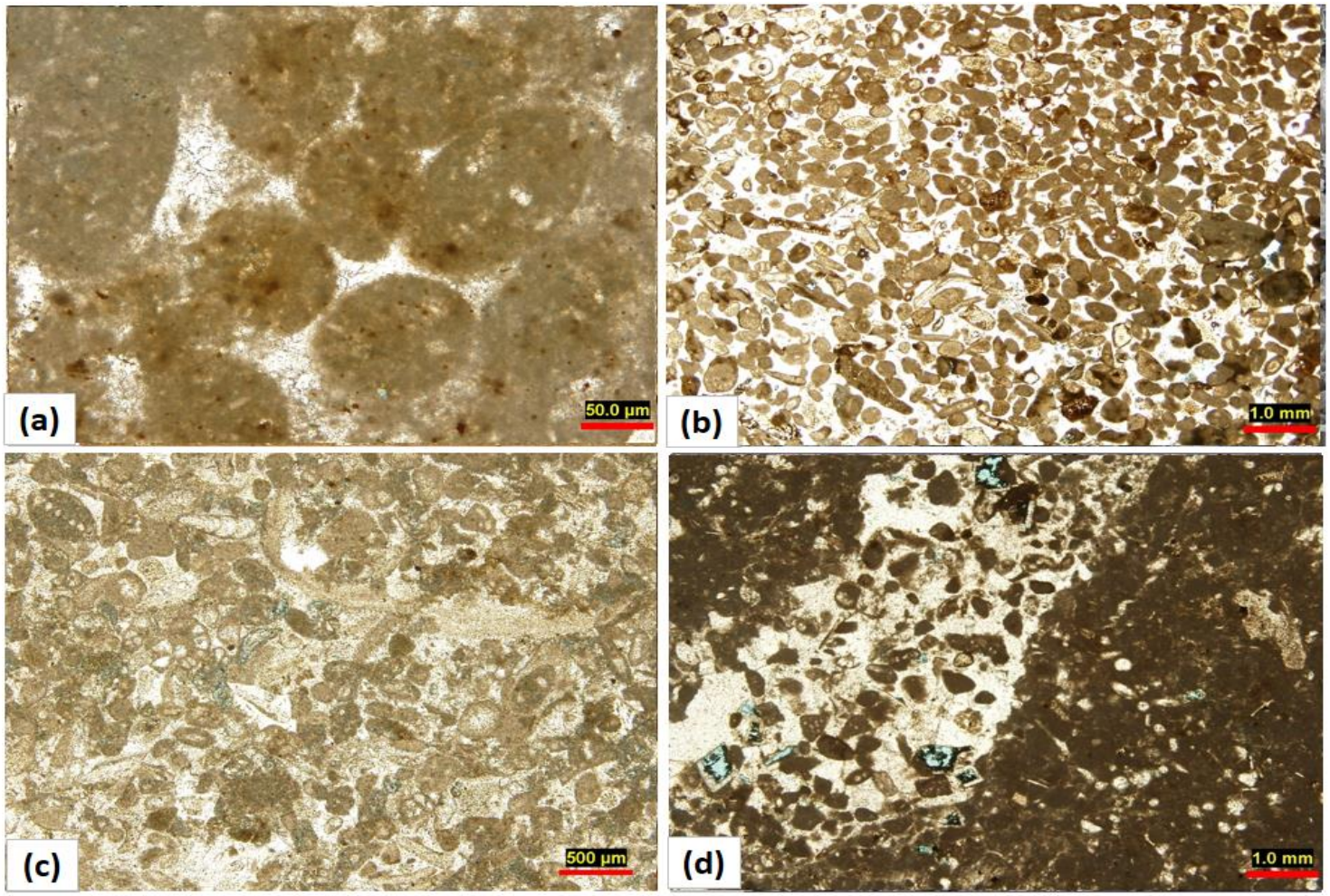


Figure 58 Thin section photomicrographs of different microfacies in different intervals within TMF showing the pre-cementation mechanical compaction. These photomicrographs are showing the lack of early marine cementation which allowed some compaction to occur but these rocks were never deeply buried (as evidenced by the lack of stylolitization and burial cements).

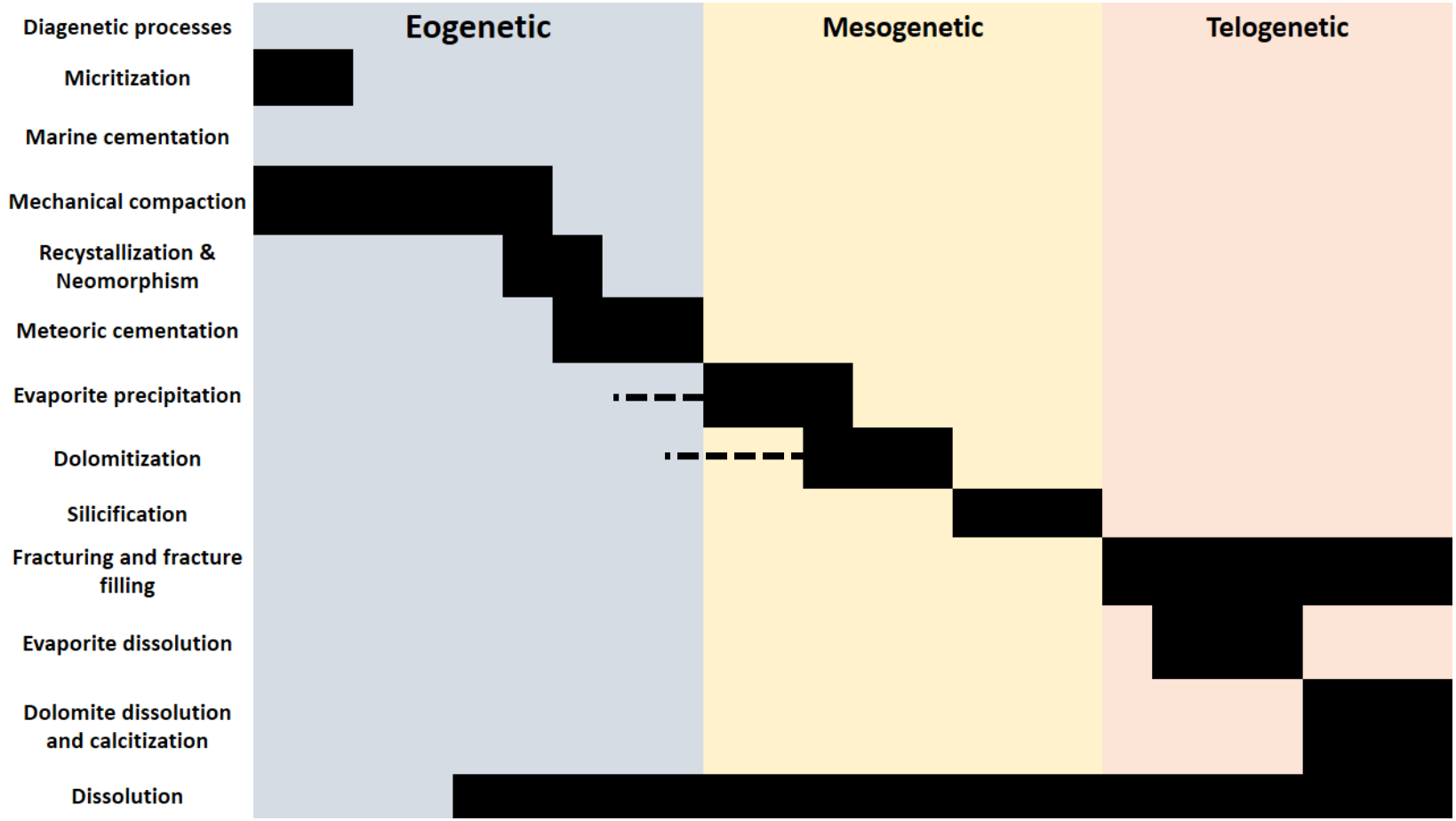


Figure 59 Paragenetic sequence of TMF.

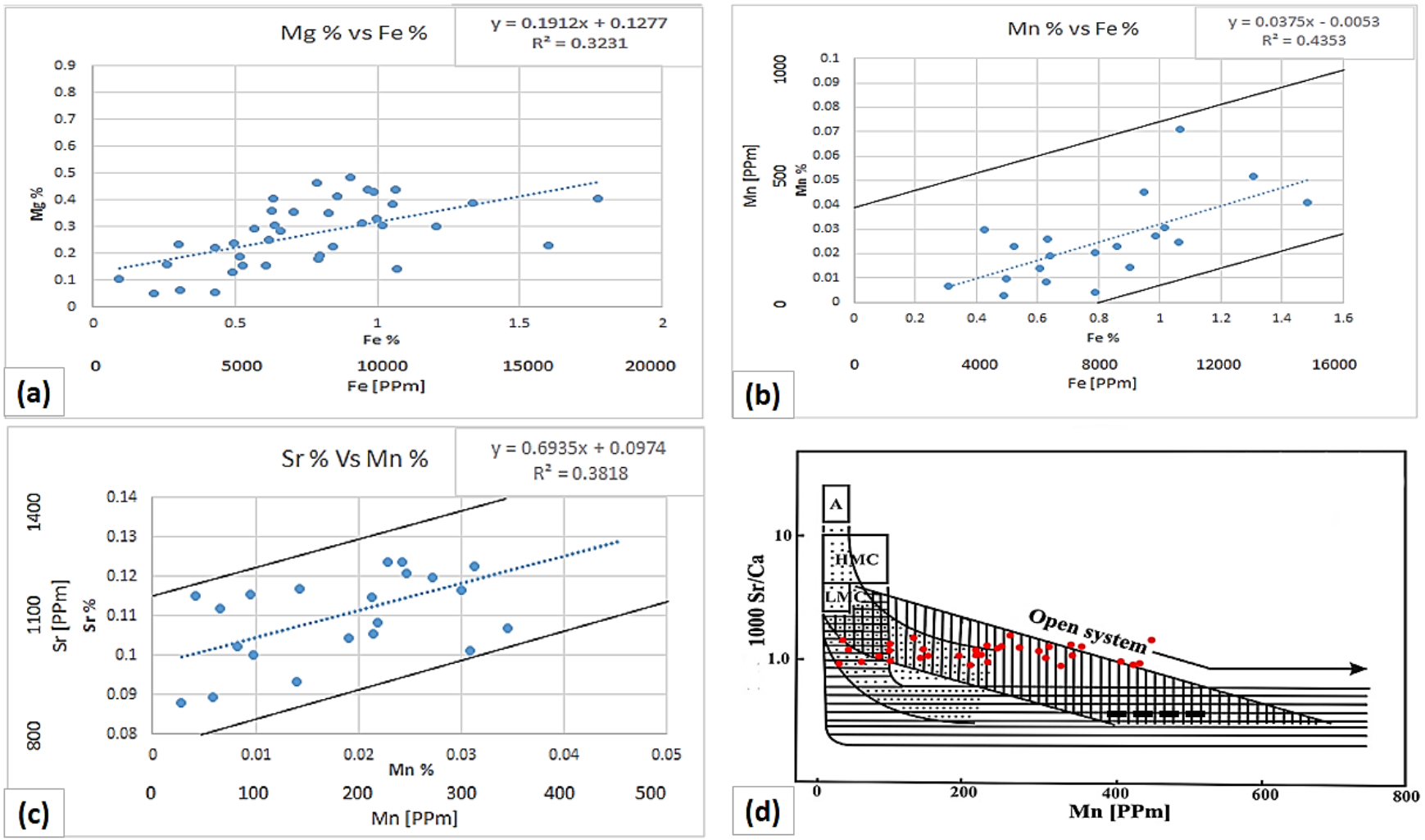


Figure 60 Cross-plot between various trace elements. (a), (b) and (c) Cross-plots of Mg % vs Fe %, Mn % vs Fe % and Sr % vs Mn %, respectively showing the severe effect of meteoric diagenesis (Winefield et al., 1996). (d) Bivariate plot of Sr/Ca vs Mn % showing the effect of meteoric fluids in an open diagenetic system (Brand and Veizer, 1980).

# CHAPTER 5

# Controls on the Development of Petrophysical Properties of TMF microfacies: Results and Discussion

In this chapter the interplay between depositional processes and diagenetic alteration of the rock and how they control the petrophysical properties of each microfacies will be discussed. Understanding the controls on reservoir quality and the development of petrophysical properties in the TMF is a very crucial issue as it encompasses two reservoir intervals in the Khurais and the Ghawar fields (Upper Fadhili reservoir and Hadriya reservoir), one source rock interval, and one unconventional reservoir interval in the Jafura basin. In addition, contact angle measurements were conducted on five microfacies to determine the effect of rock chemistry and lithology on wettability and contact angle measurements.

In this chapter, porosity (ø) and permeability (K) are also evaluated using the reservoir quality index (RQI, in microns), which is equal $0.0314[\sqrt{(K/ø)}]$ (Amaefule et al., 1993)

## 5.1. Porosity and Permeability of the TMF

The impact of biological and physical depositional processes in combination with diagenetic overprints can make the distribution of porosity and permeability in carbonates much more heterogeneous than in siliciclastics.

Porosity and permeability measurements of samples from the TMF (including the three studied sections of T1, T2, and T3 members) are plotted to determine the variations and controls on the petrophysical properties. Cross-plot of porosity vs permeability (Fig. 61)

shows a positive correlation and clustering of different textures. This clustering shows that the decrease in mud content and the shifting from mud supported textures (wackstone and floatstone) to grain supported texture (packstone and grainstone) has a positive impact in increasing porosity and permeability. Therefore, it is suggested that there is a positive correlation between depositional environment energy and the values of porosity, and permeability. The cross-plot shows that the grain dominated facies (MF 8 and MF 7) have the highest porosity, and permeability compared with the other facies (MF 3, 4 and 5) which are mud dominated facies. While, the rudstones (MF 1 and MF 2) have very low porosity, and permeability compared with the other grain dominated facies (MF 7 and MF 8) because the major component of MF 1 and MF 2 is highly cemented calcite molds of originally aragonitic coral fragments.

To recognize the stratigraphical impact on porosity and permeability evolution, 3 cross-plots of porosity vs elevation, permeability vs elevations, and RQI vs elevation (Fig. 62) are constructed within the depositional (texture, facies) and stratigraphical (medium scale cycles) frameworks of the studied intervals of the TMF. The cross plots showed that the TMF succession is divided into 3 units (highlighted by pink, yellow, and blue color). These units have different porosity, permeability and RQI values and the boundaries of these units fit with the identified medium scale cycles. The lower unit and upper unit (highlight by pink and blue, respectively) have a similar poor petrophysical properties as they are composed of similar microfacies (MF1, 2, 3, 4, and 5), while the middle unit (highlighted by yellow) has higher petrophysical properties. The studied succession of TMF represents a major regressive cycle of shifting from deep lagoon to shallow lagoon. This shift impacted the petrophysical properties of TMF in a way that there is a general trend of

upward increase in porosity, permeability, and RQI. It is suggested that this upward increase is attributed to the shift from low energy depositional environment (deep lagoon) to high energy depositional environment (shallow lagoon) and to the increase in meteoric dissolution in shallower units (shallow lagoon units) compared with the deeper units (deep lagoon units).

The coral rudstone facies (MF 1) is very tight with poor porosity (2.3-5.3 %; mean 3.4 %), permeability (0.005- 0.12 mD; mean 0.04 mD) and RQI (0.01-0.05; mean 0.03) values. The pore type distribution column chart shows the relative abundance of different pore types in MF 1 (Fig. 63). Intercrystalline microporosity, vuggy and moldic porosity are the abundant pore types while fracture and intraparticle porosity are less abundant. The intercrystalline microporosity in MF 1 has two types; intercrystalline microporosity within micrite and between crystals of calcite cement. The latter is more dominant than the microporosity within micrite as this facies has low lime mud content

The coral rudstone with coated grains and intraclasts (MF 2) shows similar petrophysical properties to MF 1 as it has very poor porosity (3-5.7 %; mean 4.4 %), permeability (0.006-0.13 mD; mean 0.05 mD) and RQI (0.01-0.05; mean 0.03) values. The pore type distribution column chart shows the relative abundance of different pore types in MF 2 (Fig.64). Visual porosity in the studied thin sections of this facies is very low and is primarily moldic porosity caused by partial dissolution of dolomite. Although not optically resolvable in thin section, intercrystalline microporosity is the most volumetrically significant pore type and occurs between the crystals of calcite cement and as micropores in micrite.

The spiculitic wackstone (MF 3) and coral floatstone (MF 4) have similar petrophysical properties as both have the same mud dominated texture but are differentiated on the basis of the percentage of large coral fragments dispersed with a wackstone texture. These facies have poor petrophysical properties, with poor to moderate porosity values (4.4-14.9 %; mean 9.6 %), but very poor permeability (0.022-1 mD; mean 0.2 mD), and RQI (0.02-0.1; mean 0.04) values. The pore type distribution column chart shows the relative abundance of different pore types in MF 3 and 4 (Fig.65). As these facies have a mud dominated texture, the major part of the porosity occur as intercrystalline microporosity (Fig. 66). The micropores in micrite is more significant volumetrically than the intercrystalline microporosity that occurs between the crystals of calcite cement. In addition, there is minor part of microporosity occurs as microporosity between the boundaries of dolomite crystals and surrounding micrite as in figure 52.b. In T3, these facies were affected by dolomite calcitization, which has led to the development of intercrystalline microporosity between equant calcite crystals that fill rhombohedral pore of dissolved dolomite crystals. The second major macropore types are moldic and vuggy porosity created by dissolution of dolomite and skeletal fragments. Fracture and intraparticle porosity also occur but are rare.

The worn and coated foraminiferal wack/pack-stone facies (MF 5) has a mud dominated texture with very poor petrophysical properties as it has moderate porosity values (10.1-11.8 %; mean 11.2 %) but very poor permeability (0.15-0.4 mD; mean 0.8 mD) and RQI (0.04-0.08; mean 0.05) values. The pore type distribution column chart shows the relative abundance of different pore types in MF 5 (Fig. 67). As it has a mud dominated texture, the major part of porosity in this facies occurs as intercrystalline microporosity. Most of this type of porosity is within the micropores micrite, although intercrystalline

microporosity also occurs between equant calcite crystals that fill the rhombohedral pores of dissolved dolomites. Visual porosity in thin section is rare, and occurs primarily as fracture porosity and moldic porosity within different components.

The fine grained peloidal grainstone facies (MF 6) has a grain dominated texture with moderate porosity values (15-20 %; visually estimated from thin sections). No permeability measurements were done on this facies as the samples are inadequate for this purpose but thin section examined revealed the pores are isolated and not well connected which would probably produce low permeability and RQI values. The pore type distribution column chart shows the relative abundance of different pore types in MF 6 (Fig.68). Moldic porosity of dissolved dasycladacean algae is common, while vuggy porosity is less abundant. Fracture porosity is rare. The relative abundance of microporosity cannot be measured in this facies as there are no air porosity measurements from this facies but SEM examination reveals that this facies has two types of intercrystalline microporosity, between the micrite of micritized grains, and intercrystalline microporosity between equant crystals of calcite cement.

The peloidal packstone (MF 7) has a grain dominated texture with moderate to good porosity values (10-19.2 %; mean 16.4 %) but poor permeability (0.13-8.8 mD; mean 3 mD) and RQI (0.04-0.2; mean 0.12) values. The pore type distribution column chart shows the relative abundance of different pore types in MF 7 (Fig. 69). The major pore types in this facies are vuggy, moldic, interparticle porosity and intercrystalline microporosity while fracture and intraparticle porosity are less abundant (Figs. 70 and 71). Intercrystalline microporosity in this facies occurs in three ways: as intercrystalline microporosity within

micrite, intercrystalline microporosity between cement crystals, and intercrystalline microporosity within micrite of peloids (micritized grains).

The peloidal grainstone (MF 8) has a grain dominated texture and moderate to good porosity value (15.8 %) but poor permeability (6 mD) and RQI (0.2) value. The pore type distribution column chart shows the relative abundance of different pore types in MF 8 (Fig. 72). Predominant pore types are vuggy porosity and moldic porosity is and microporosity is rare. Microporosity in this facies occurs in two forms, intercrystalline microporosity within micrite of peloids (micritized grains) and between the cement crystals.


Figure 61 Porosity-permeability cross-plot of different facies.

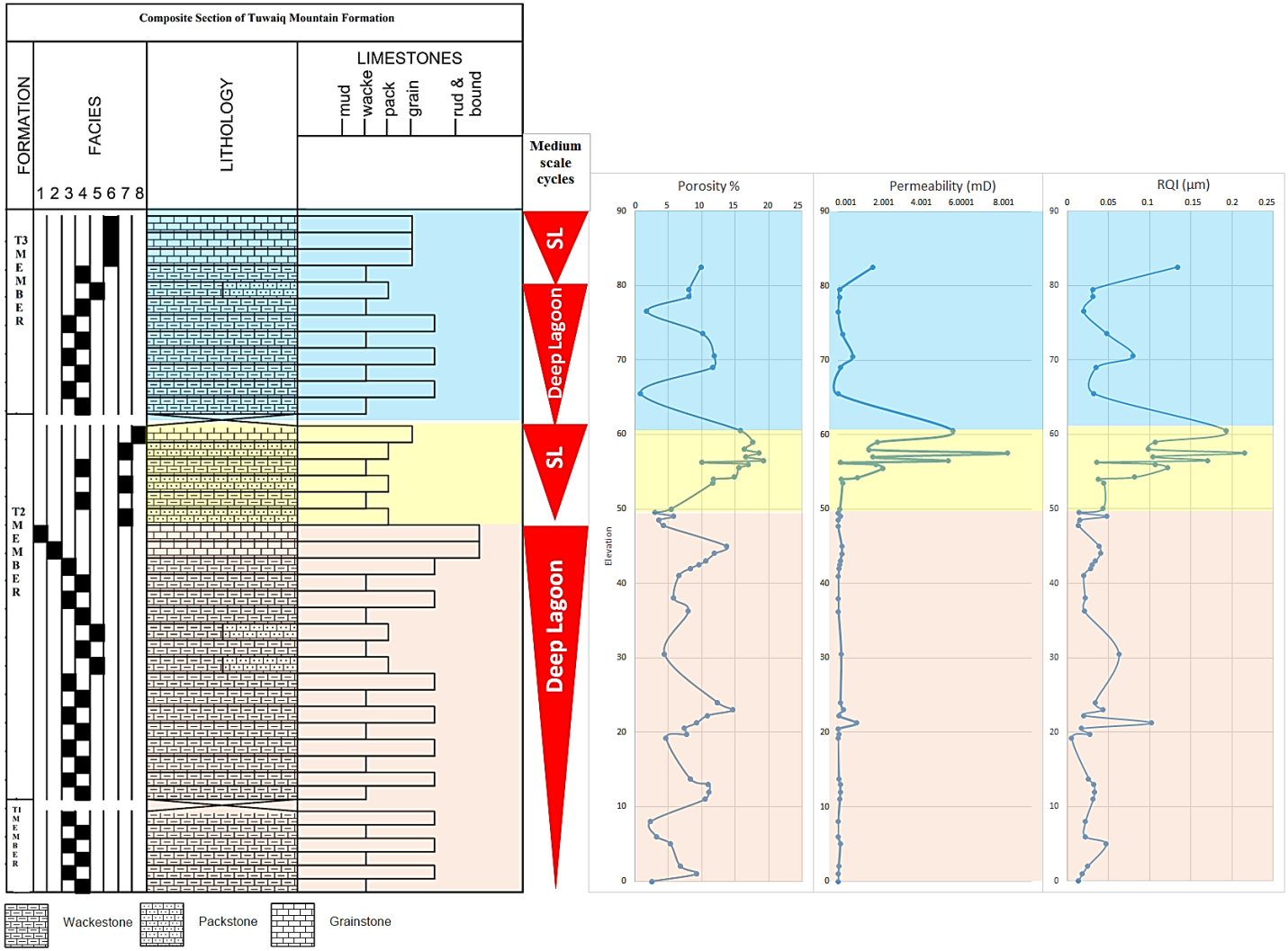


Figure 62 Cross-plots of porosity, permeability and RQI within the depositional (texture) and stratigraphical (cyclicity) frameworks showing the three distinct petrophysical units. SL: Shallow lagoon

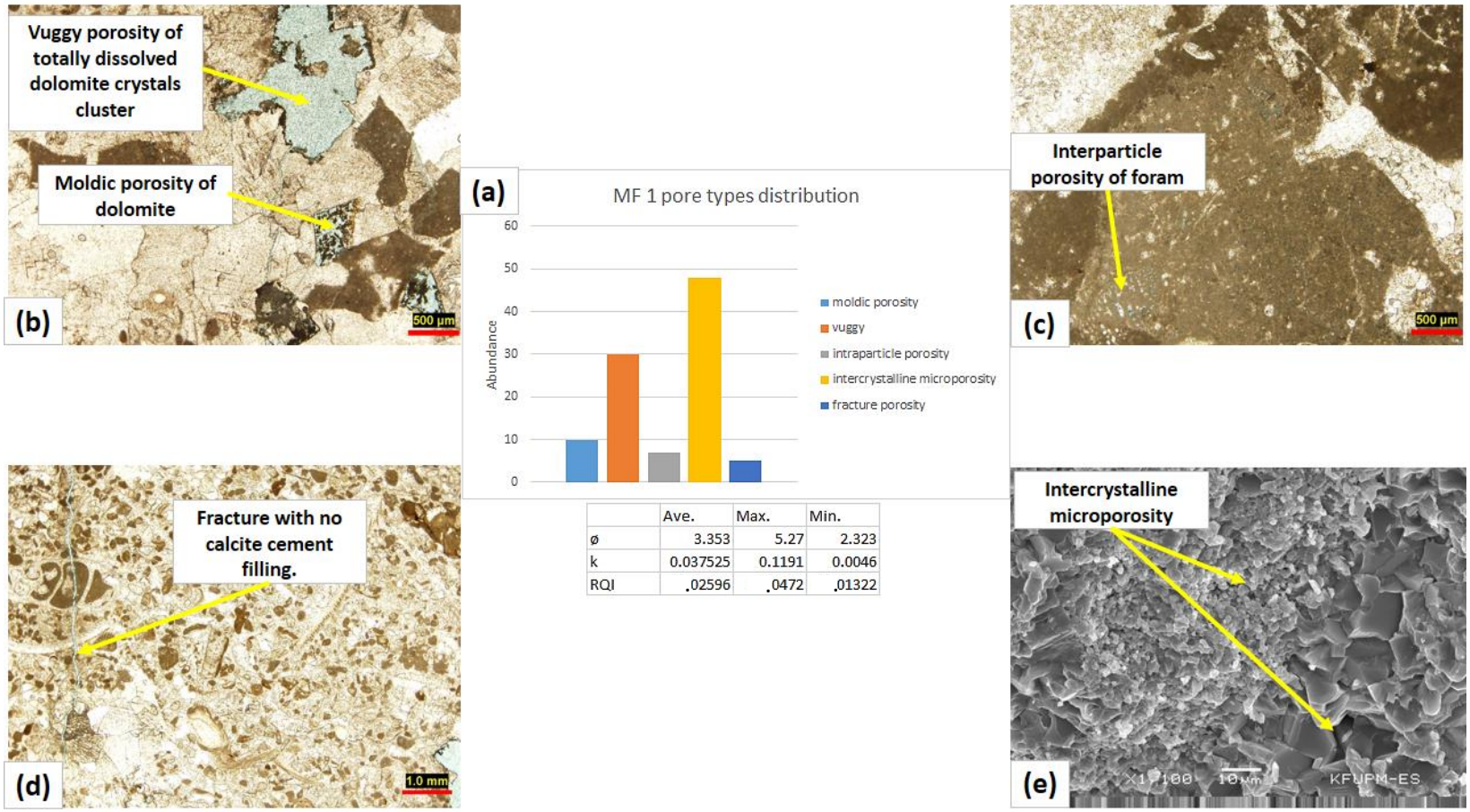


Figure 63 Column chart (a), thin section photomicrographs (b-d) and SEM image (e) of different pore types of MF 1 coral rudstone showing: (a) Pore types distribution of MF 1. (b) Vuggy and moldic porosity (PPL). (c) Intraparticle porosity within *Kurnubia* sp. (PPL). (d) Open fracture (PPL). (e) Intercrystalline microporosity within micrite and cement.

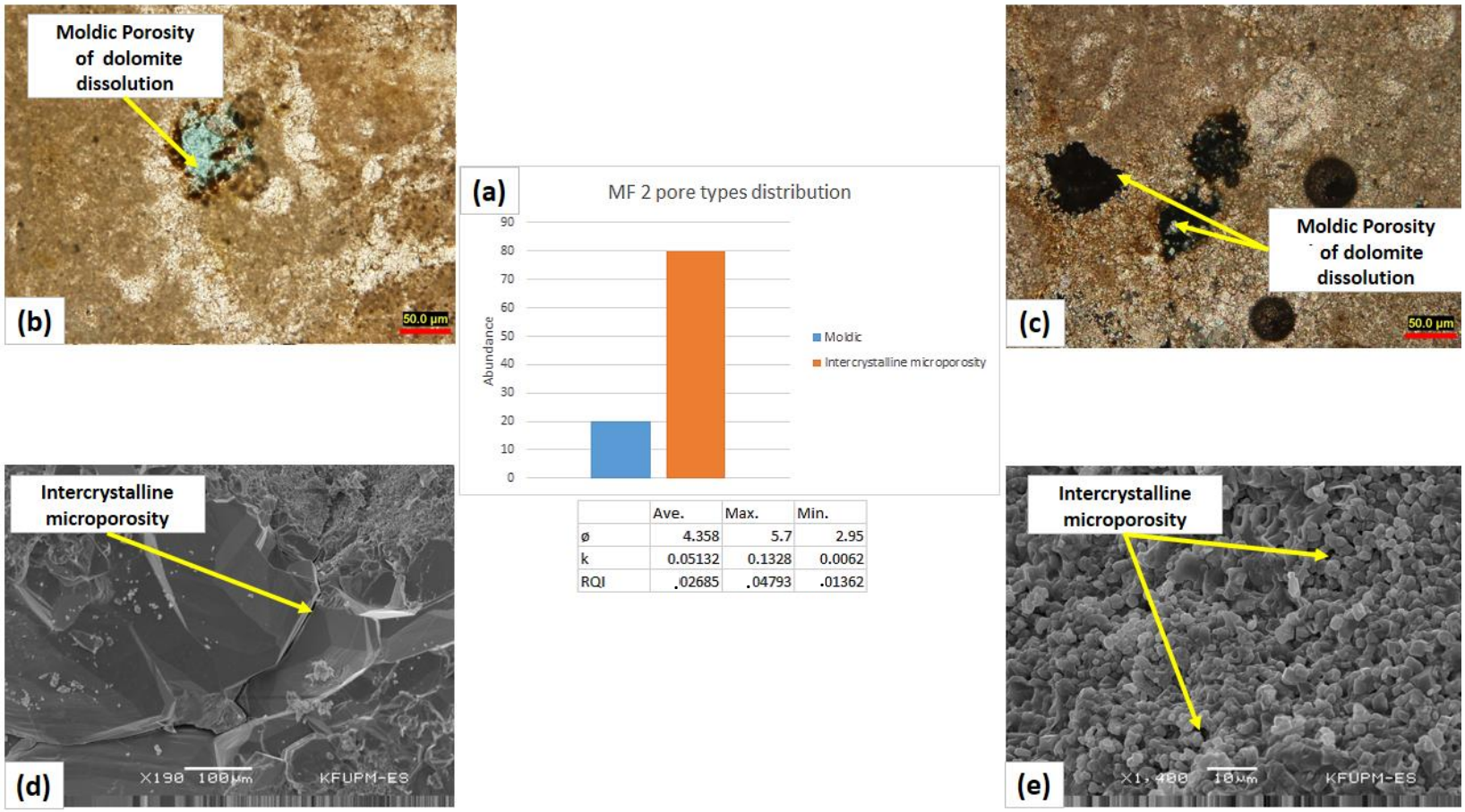


| | Ave. | Max. | Min. |
|---|---|---|---|
| ø | 4.358 | 5.7 | 2.95 |
| k | 0.05132 | 0.1328 | 0.0062 |
| RQI | .02685 | .04793 | .01362 |

Figure 64 Column chart (a), thin section photomicrographs, (b-c) and SEM images (d-e) of different pore types of MF 2 coral rudstone with coated grains and intraclasts showing: (a) Pore types distribution of MF 2. (b and c) Moldic porosity of dissolved dolomites (b; PPL, c; XPL). (d and e) Intercrystalline microporosity between cement crystals and within micrite, respectively.

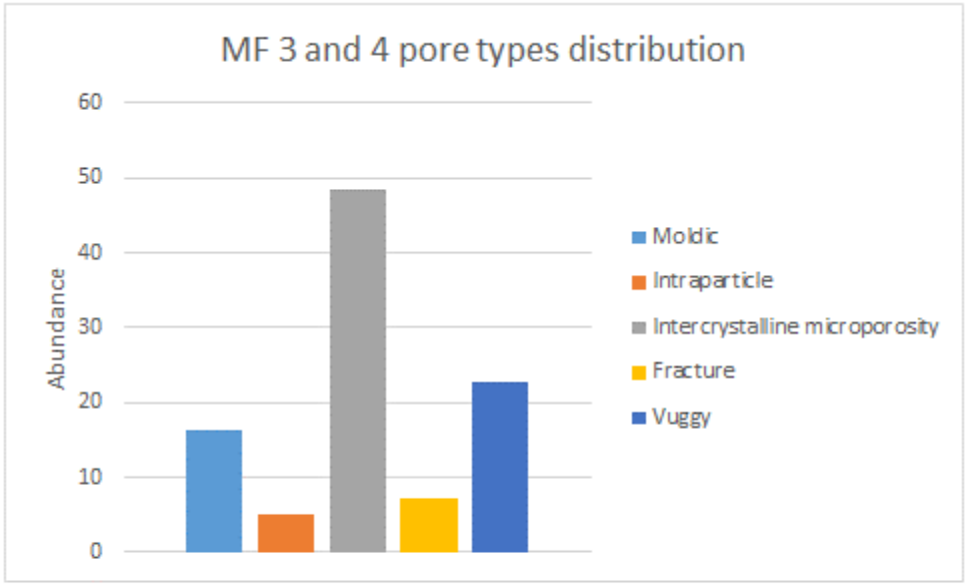


| | Ave. | Max. | Min. |
|---|---|---|---|
| ø | 9.61908 | 14.903 | 4.411 |
| k | 0.17512 | 1.0135 | 0.022 |
| RQI | 0.03591 | 0.102482 | 0.017161 |

Figure 65 Column chart of different pore types of MF 3 and 4.

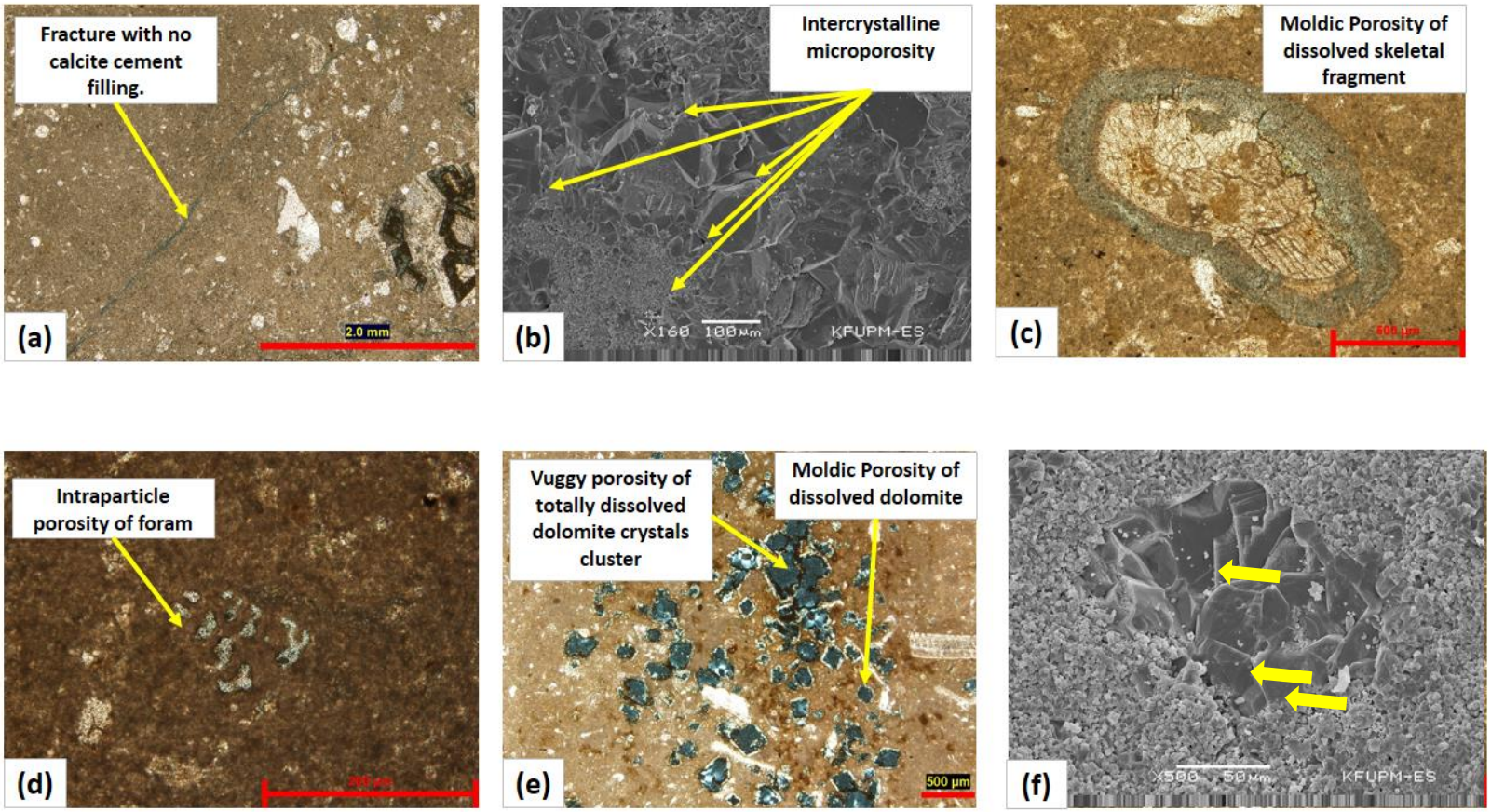


Figure 66 Thin section photomicrographs (a, c, d-e) and SEM images (b and f) of different pore types in MF 3 and MF 4 showing: (a) Fracture porosity (XPL). (b) The intercrystalline microporosity within micrite and cement crystals. (c and e) Moldic and vuggy porosity of different dissolved components (PPL). (d) Intraparticle porosity within a foram (XPL). (f) The rhombohedral pores of dissolved dolomites in T3 member are filled with equant calcite cement with intercrystalline microporosity between crystals (arrows).

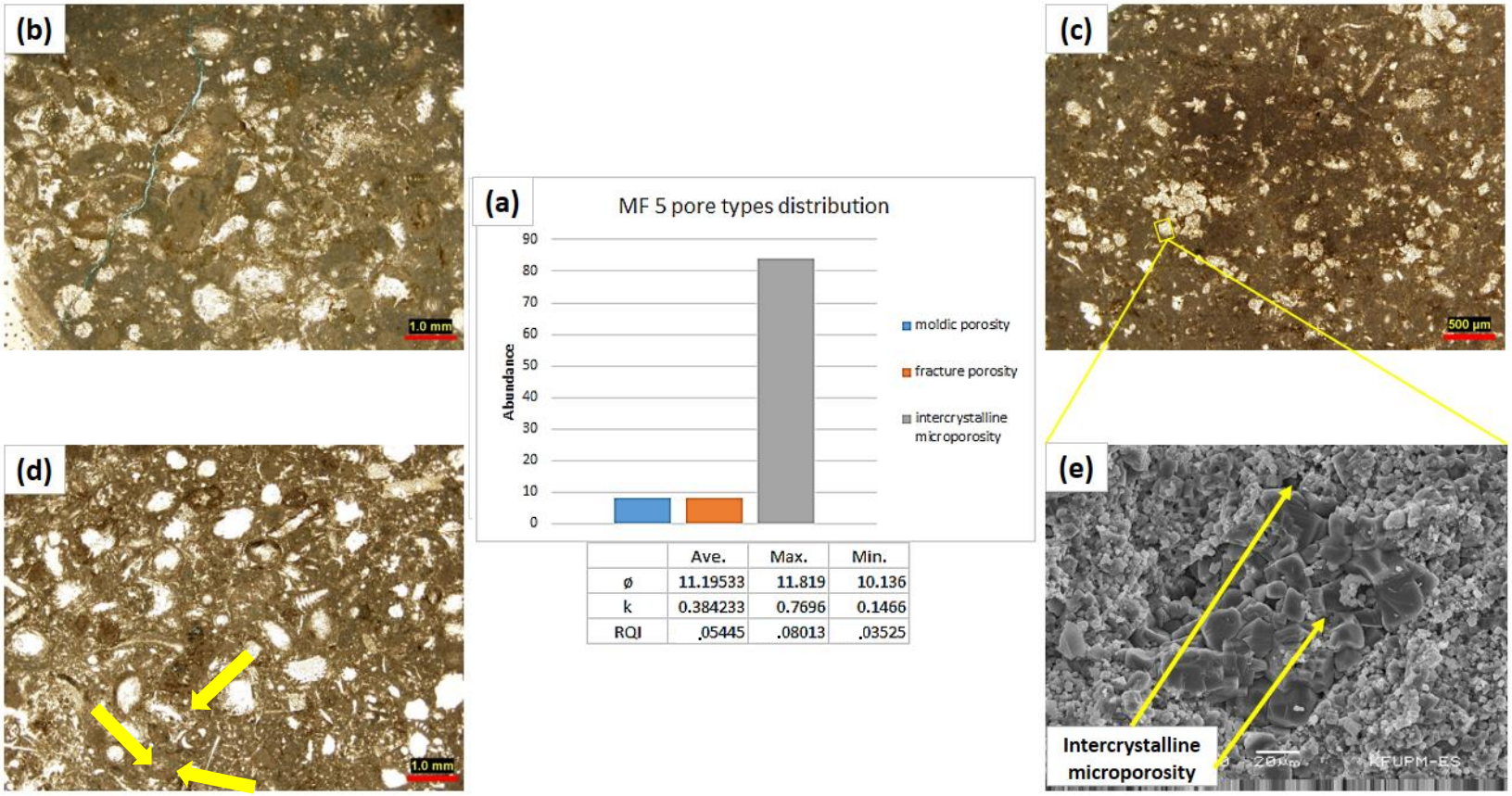


| | Ave. | Max. | Min. |
|---|---|---|---|
| ø | 11.19533 | 11.819 | 10.136 |
| k | 0.384233 | 0.7696 | 0.1466 |
| RQI | .05445 | .08013 | .03525 |

Figure 67 Column chart (a), thin section photomicrographs (b-d) and SEM image (e) of different pore types of MF 5 worn and coated foraminiferal wack/pack-stone showing: (a) The different pore types present in MF 5. (b) Fracture porosity (PPL). (c and e) Thin section photomicrograph (PPL) of calcitized dolomite and SEM image showing intercrystalline microporosity. (d) Moldic porosity (arrows) (PPL).

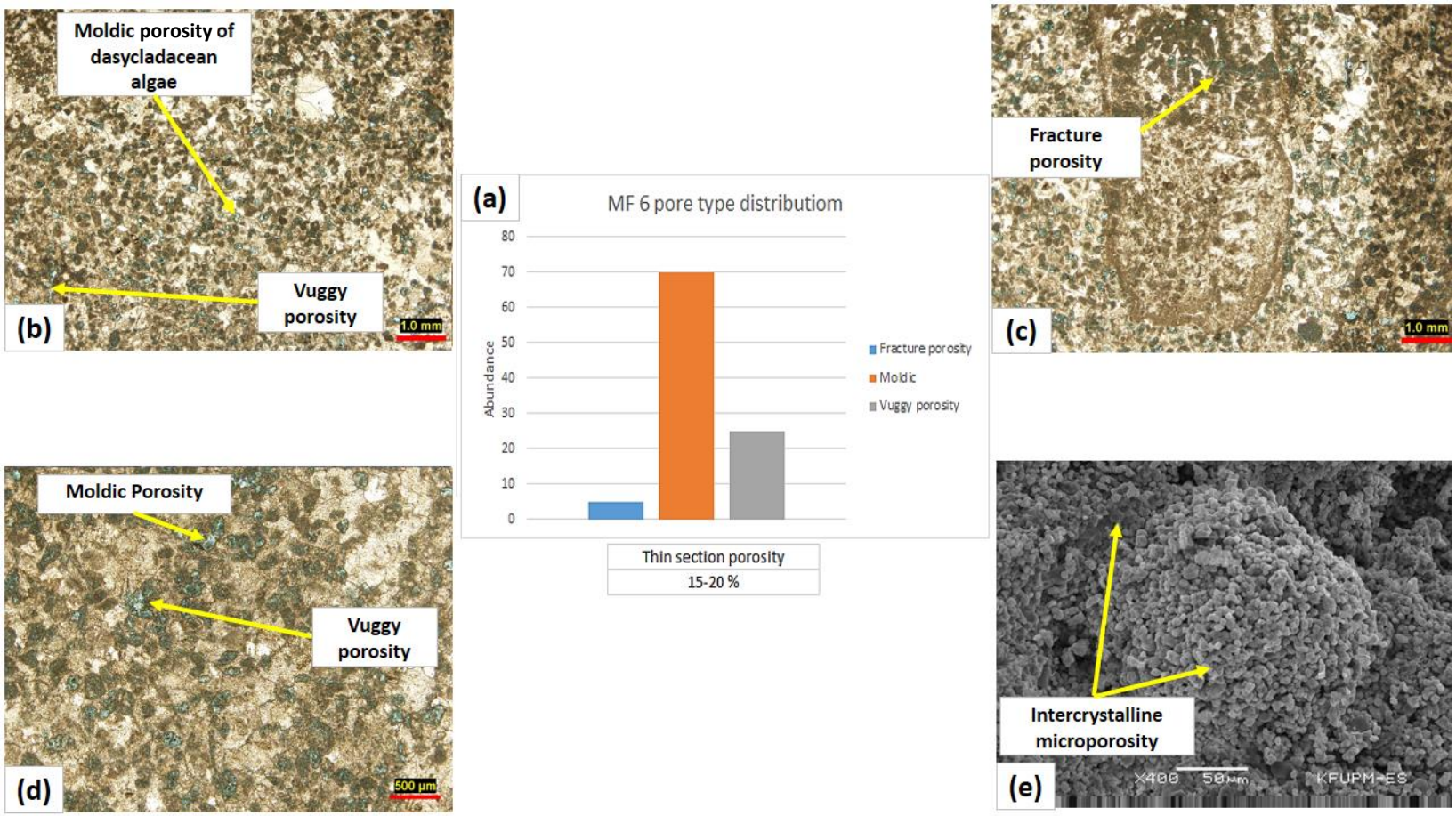


Figure 68 Column chart (a), thin section photomicrographs (b-d) and SEM image (e) of different pore types of MF 6 fine grained peloidal grainstone showing: (a) The different pore types of MF 6. (b and d) Moldic and vuggy porosity (PPL). (c) Fracture porosity (PPL). (e) Intercrystalline microporosity within micrite of peloids and between cement crystals.

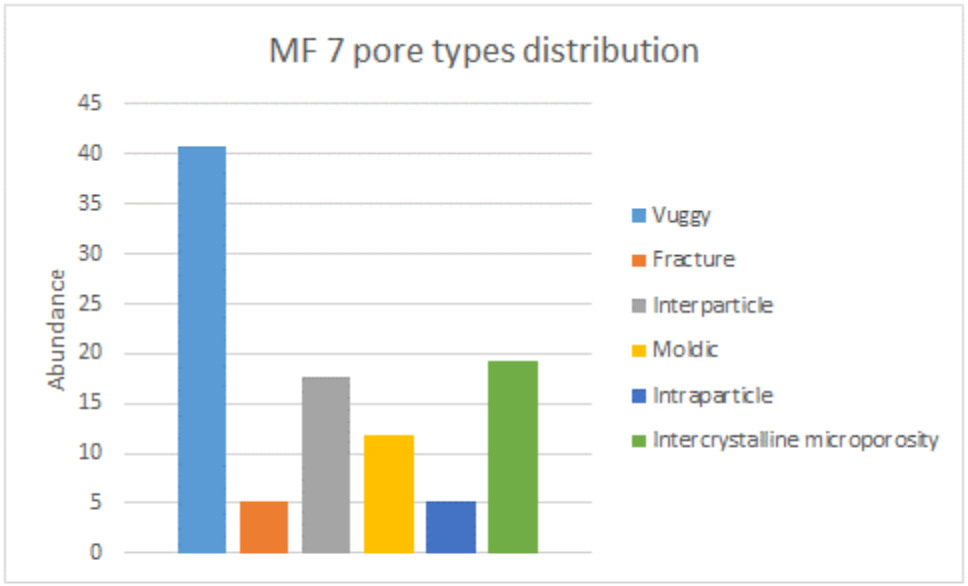


| | Ave. | Max. | Min. |
|---|---|---|---|
| ø | 16.36688 | 19.242 | 10.04 |
| k | 3.04095 | 8.751 | 0.1331 |
| RQI | .11998 | .21536 | .03615 |

Figure 69 Column chart of different pore types distribution of MF 7

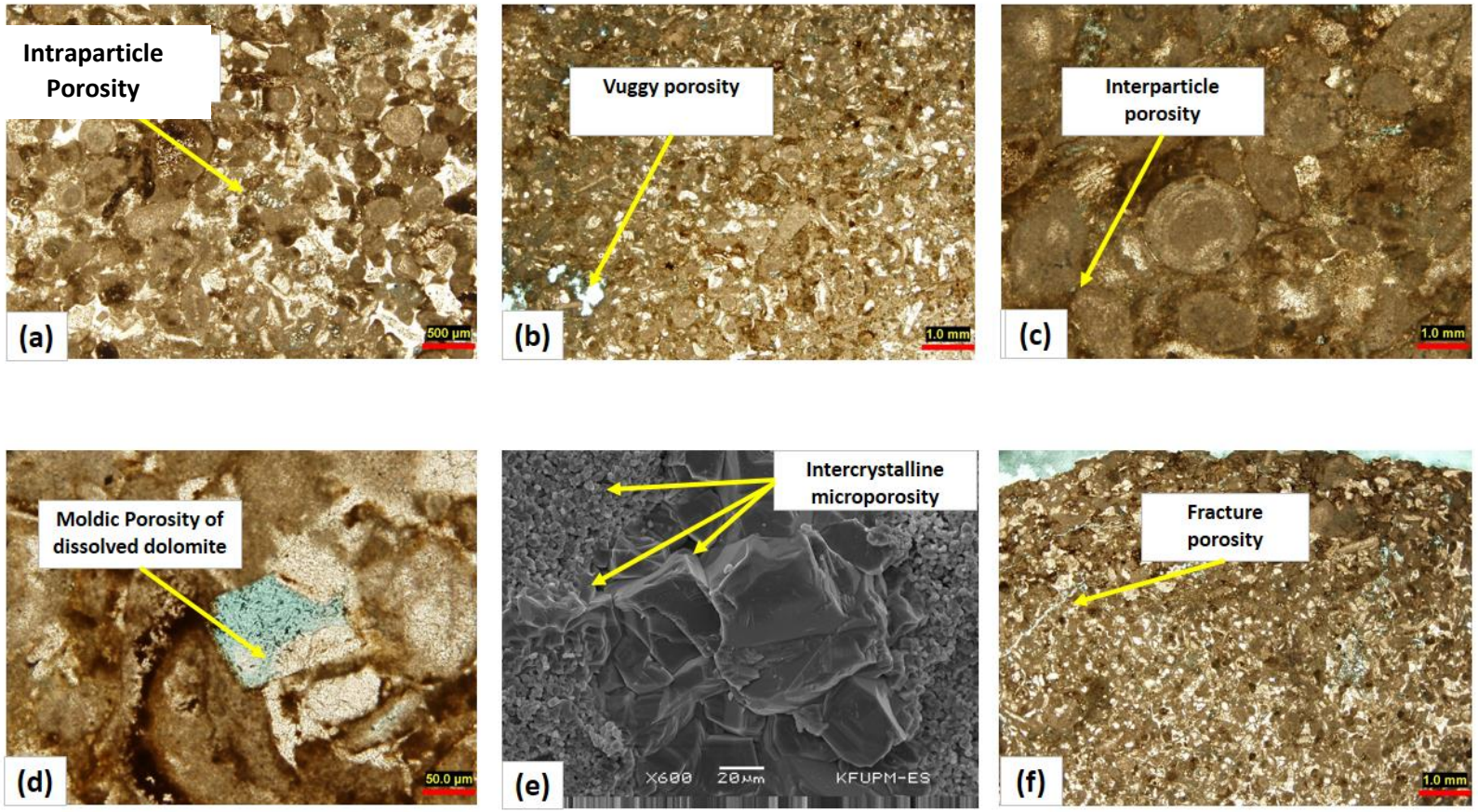


Figure 70 Thin section photomicrographs (a-d and f) and SEM image (e) of different pore types in MF 7 peloidal packstone showing: (a) Intraparticle porosity within a foram (PPL). (b) Vuggy porosity (PPL). (c) Interparticle porosity between peloids and ooids (PPL). (d) Moldic porosity of dissolved dolomite (PPL). (e) Intercrystalline microporosity within micrite and cement crystals. (f) Fracture porosity (PPL).

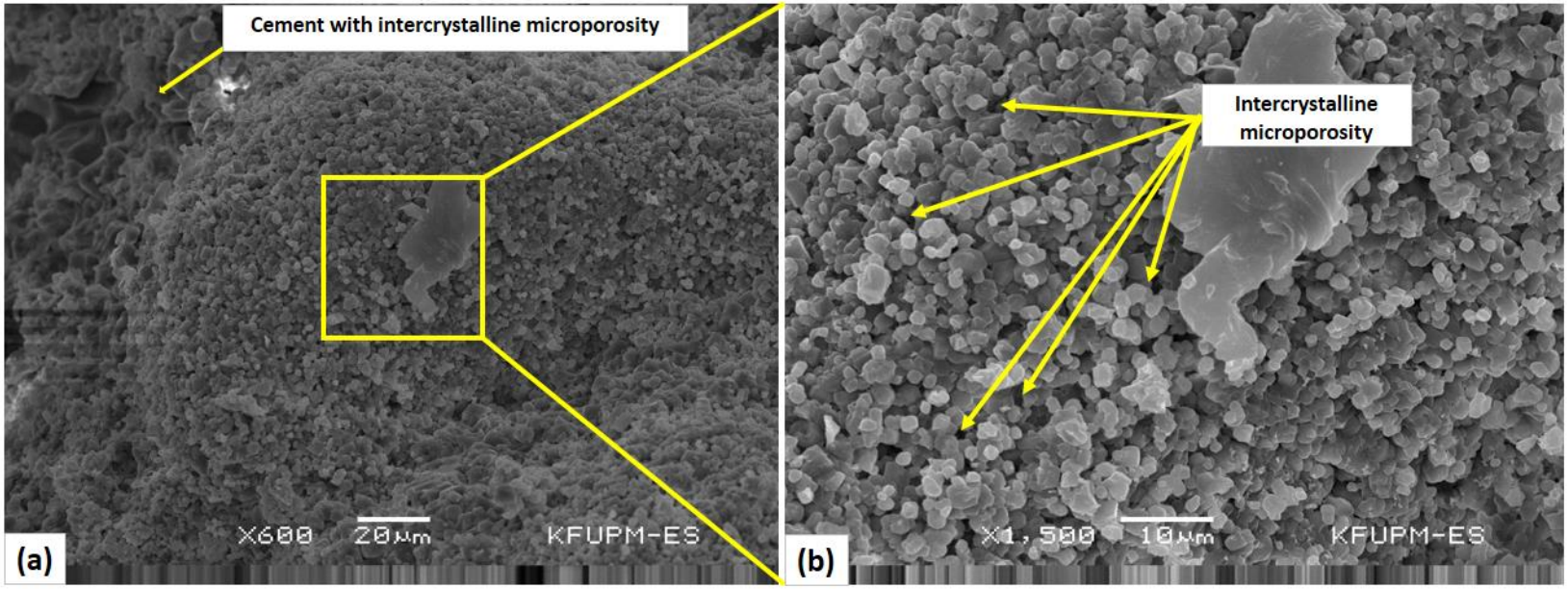


Figure 71 SEM images of peloids in MF 7 showing the microporosity within micrite of peloids (micritized grains).

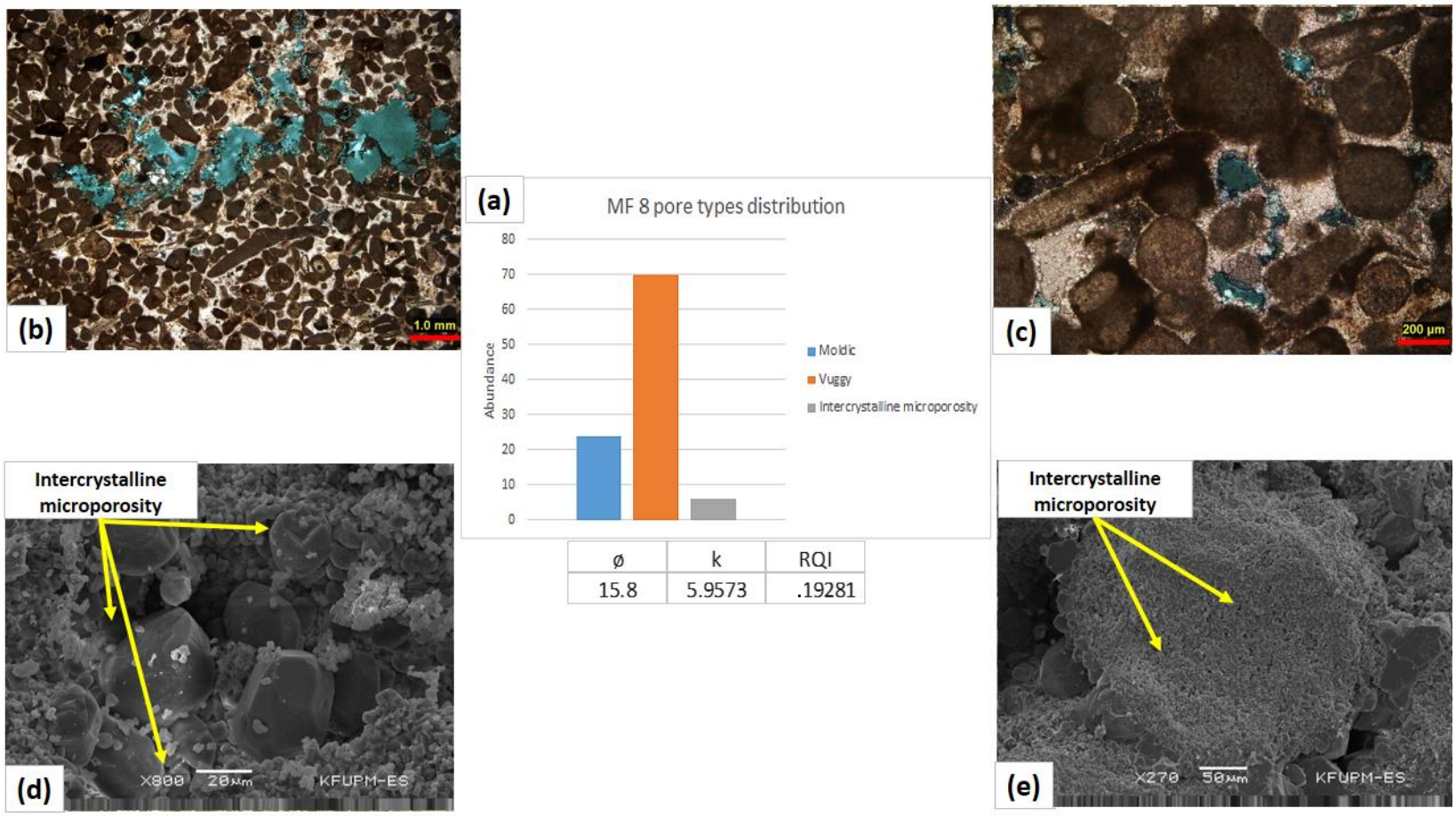


Figure 72 Column chart (a), thin section photomicrographs (b and c) and SEM image (d-e) of different pore types of MF 8 peloidal grainstone showing: (a) The different pore types distribution. (b) Vuggy porosity (XPL). (c) Moldic porosity (XPL). (d) Intercrystalline microporosity between cement crystals. (e) Intercrystalline microporosity within micrite of peloids (micritized grains).

## 5.2.Discussion

The porosity and permeability evolution of the studied samples of the Tuwaiq Mountain Formation reflects a complex history of interplay between diagenetic and depositional factors. Different imprints were seen at different stratigraphic levels in the TMF, and this section explores the interplay of depositional and diagenetic controls of porosity and permeability development.

Starting with depositional and stratigraphic controls, the Tuwaiq Mountain Formation succession displays depositional patterns that are similar to the other formations of the Middle to Late Jurassic in Saudi Arabia. In the study area, the TMF displays a general trend of shallowing upward (Figs. 44, 45 and 46), in that, by moving upward in the TMF the facies changes from deep lagoon mud supported facies to shallow lagoon grain supported facies with little mud to shoal grain dominated facies with no mud at all. This depositional history reflects porosity enhancement by increasing depositional water energy as one moves upsection. This enhancement is due to the replacement of mud supported facies with grain supported facies upsection. This imprint is clear in figures 61 and 62 as the cross plots of porosity, permeability and RQI shows a positive correlation with the increasing dominance of grain supported facies and hence, water energy.

The micritization affected this primary porosity negatively. This reduction was resulted from filling the intraparticle porosities with micrite by the action of boring organisms and this can be seen on the highly micritized grains (Fig. 47.b).

Diagenesis, and especially meteoric diagenesis, has both enhanced and destroyed porosity. Porosity enhancement occurred due to the dissolution of different carbonate grains and

matrix, however, these voids developed by dissolution were then typically filled with meteoric cement, which resulted in porosity reduction. Also, meteoric cements filled the primary porosity, which further reduced porosity. Porosity enhancement occurred mainly in the grain dominated facies at cycle top, as meteoric fluids passed through the sediments forming dissolution-related porosity there (Figs. 68, 70 and 72). Mechanical compaction has had a minimal effect on porosity evolution; while grains are touching and locally display some grain interpenetrations and concavo-convex boundaries, these are typically rare, and no stylolites, suture, or dissolution seams are observed.

Later, hypersaline fluids precipitated evaporate and dolomite which represents a porosity destructive process, although subsequent dissolution of these evaporites enhanced porosity. Evaporite dissolution event further enhanced porosity by the serving as a source of Ca-rich fluids which then dissolved dolomite.

The silicification was also destructive for porosity, in that microcrystalline quartz served as pore filling cement (Fig. 55.d). Dissolved dolomite crystals are filled partially or totally be equant calcite cement, this calcitization process is porosity destructive, as the early developed pores became occluded by calcite crystals. This process has stratigraphic control as it increases upsection in the upper part of T2 to T3 members.

It can be concluded that intensive cementation played a significant role in porosity and permeability destruction. Dolomite dissolution enhanced porosity but added little to permeability. Meteoric dissolution played an important role in porosity enhancement by dissolution of different components, especially in the grain dominated facies (MF 6, 7 and 8). Later dolomite calcitization which is more prominent in the upper part of the T2 member and T3 member resulted in additional porosity destruction. Compaction only had a minimal

effect on porosity. Fracturing contributed to porosity enhancement in some cases but, since the TMF is not highly fractured, provided only a minor contribution to the reservoir quality of the TMF. Fracturing also resulted in local porosity destruction, as cement filled the fracture can act as barriers to fluid flow.

## 5.3. Contact Angle Measurements

In order to determine the effect of texture, lithology, and rock chemistry on wettability, contact angle measurements were performed on four different microfacies (MF 1, 3, 4 and 5). XRD and XRF results of the disks used in the analysis show generally similar mineralogical and chemical composition (around 98% calcite). Porosity and permeability measurements were conducted on disks.

The conditions of the experiments are constant and the only variable is the microfacies. The bulk fluid is a low salinity brine (7125 ppm), and the drop fluid is Arabian oil. The cell pressure is around 130 psi and the temperature is 60$^{o}$C. Figure 73 shows the results of these experiments.

### 5.3.1. Discussion

In most of the publications, authors are dealing with limestones as calcite without paying attention to rock heterogeneity in terms of different microfacies and rock textures. In this study, figure 73 shows the different contact angles of different microfacies under the same test conditions. The measurements show how important the effect of microfacies on contact angle measurements as the mineralogical and chemical composition exhibit different wettability. MF 4 and 5 are oil wet, although the degree of wettability is different as MF 4 is more oil wet than MF 5. Both microfacies have similar petrophysical properties but

different wettability. This observation may suggest that the rock texture of different microfacies has a great impact on wettability and so contact angle. MF 1 and 3 are intermediate wetting. Sultan (2009) studied the binding energy between different metal cations and the carboxylate Oxygens, M−OC, and water Oxygen, $M-OH_2$, in M(-OAc)n.(6-n)$H_2O$ complexes. From his study, he found that M−O bond distance is very short with $Al^{3+}$, $Mn^{3+}$ and $Fe^{3+}$ as they have high binding energy compared with $Mg^{2+}$, $Na^{+}$ and Zn (Fig. 9). These binding energies of $Al^{3+}$, $Mn^{3+}$ and $Fe^{3+}$ have a direct impact on the adhesion of polar substances of oil (Resins and Asphaltenes) on rock and thus contact angle. To explore, the effect of surface rock chemistry ($Al^{+3}$ and contact angle) on contact angle, cross-plot of $Al^{3+}$ % vs contact angle (Fig. 74) showed a negative correlation, and hence, as the aluminum concentration increases the rock becomes more oil wet and so it is suggested that the surface rock chemistry of each microfacies affects the contact angle. The variation in surface rock chemistry comes from different components and diagenetic alteration that affected different microfacies. Therefore, it can be concluded that contact angle measurements showed that the microfacies of the studied limestone has a great impact on wettability and contact angle and thus will have an impact on reservoir performance.

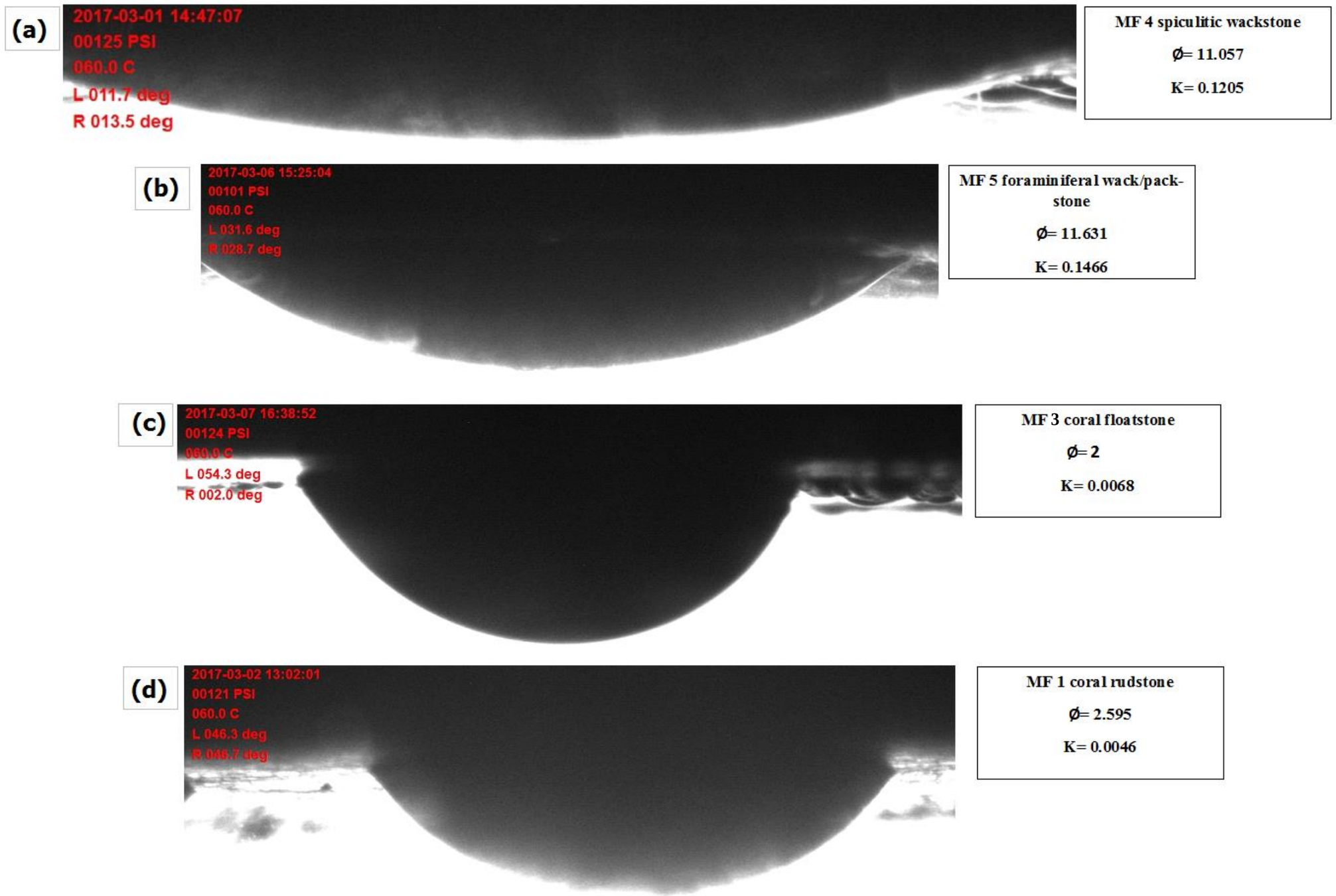


Figure 73 Capture photos of contact angles of four different microfacies. (a) Contact angle of MF 4 spiculitic wackstone (approximately $11^0$). (b) Contact angle of MF 5 worn and coated foraminiferal wack/pack-stone (approximately $30^0$). (c) Contact angle of MF 3 coral floatstone (approximately $54^0$). (d) Contact angle of MF 1 coral rudstone (approximately ($46^0$).

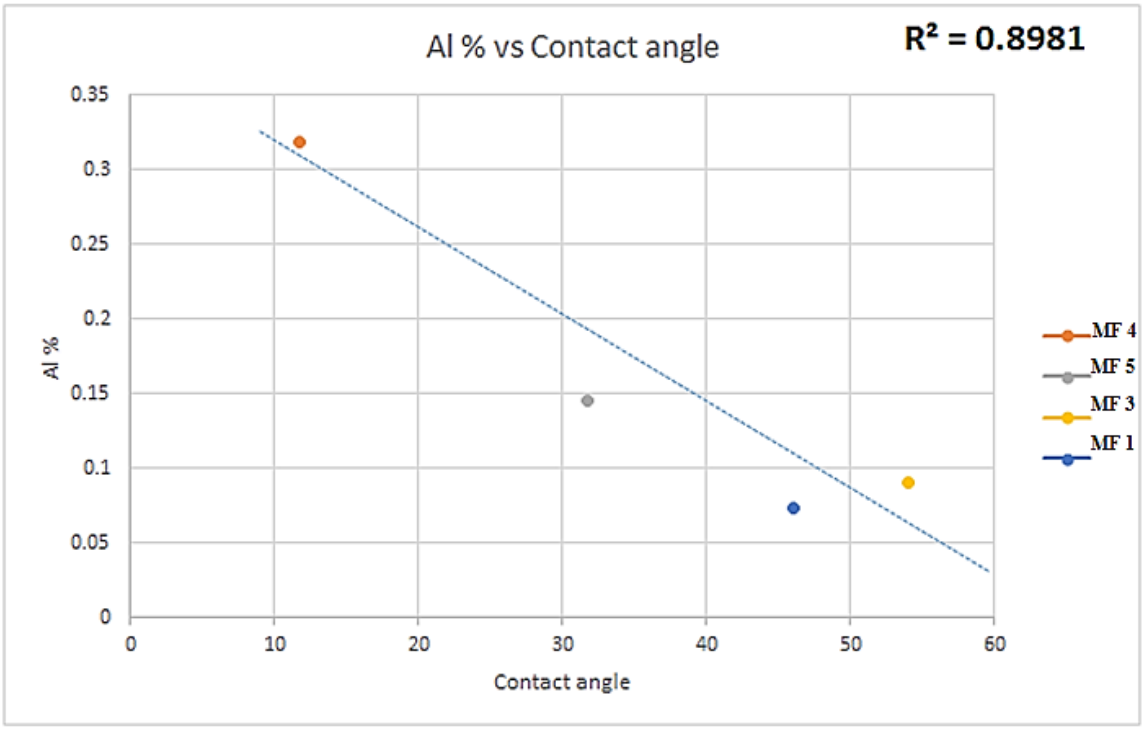


Figure 74 Cross-plot of $Al^{+3}$ concentration vs contact angle showing a negative correlation with $R^2$= 0.8981 which shows that the $Al^{3+}$ concentration plays a significant role in rock wettability.

# CHAPTER 6

# Conclusions and Recommendation

## 6.1.Conclusions

- The studied sections of TMF in Shaqra quadrangle were deposited in the interior part of rimmed carbonate platform that existed during the Middle to late Jurassic in Central Saudi Arabia.
- This succession is composed of eight microfacies (MF 1 coral rudstone, MF 2 coral rudstone with coated grains and intraclast, MF 3 coral floatstone, MF 4 spiculitic wackstone, MF 5 worn and coated foraminiferal wack/pack-stone, MF 6 fine grained peloidal packstone, MF 7 peloidal packstone and MF 8 peloidal grainstone).
- The TMF in the study area was deposited in the following depositional environments (from distal to proximal): deep lagoon, shallow lagoon and shoal.
- The depositional environments show shift to (from deep lagoon to shoal) shallower settings toward the west and this coincides with the paleofacies maps of Ziegler (2001).
- The geochemical analysis of studied samples showed a signature of siliciclastic input. This siliciclastic input is suggested to be from siliciclastic input by a tidal channel or windblown dust.
- Stratigraphically, TMF contains two medium scale cycles ($4^{th}$ order; shallow lagoon medium scale cycle and deep lagoon medium scale cycle) and two small

scale cycles ($5^{th}$ order; shallow lagoon small scale cycle and deep lagoon small scale cycle).

- The general stacking pattern of facies in the TMF is shallowing upward, which suggests that TMF represents a regressive cycle.
- The diagenetic history of the TMF is very complex, and includes: micritization, marine cementation, recrystallization, dissolution, meteoric cementation, evaporite precipitation, dolomitization, silicification, evaporite dissolution, dolomite dissolution and calcitization, fracturing and fracture filling.
- Trace element geochemical analyses revealed the meteoric diagenesis has had a significant input on the TMF sediments.
- Dolomitization is suggested to have originated from hypersaline fluids.
- Fabric selective silicification affected brachiopods, echinoderms and coral fragments of the TMF.
- The source of silica required for silicification is suggested to be intraformational because the formation contain abundant sponge spicules (e.g. deep lagoon sequences).
- Meteoric cementation has had a destructive impact on porosity and permeability by occluding both primary depositional porosity and secondary porosity with four different types of cements; equant, drusy, and syntaxial calcite cement.
- Meteoric diagenesis has had a constructive impact on porosity and permeability, by dissolution and especially in grain dominated facies.
- Evaporite dissolution by meteoric waters formed Ca-rich solution which attacked dolomite and caused dolomite dissolution and calcitization.

- The calcitized dolomite is formed of equant calcite crystals filling the rhombohedral pores developed by dissolved dolomite crystals.
- Porosity, permeability and RQI values revealed poor reservoir quality in the studied interval because of intensive meteoric cementation in grain dominated facies, while in mud dominated facies reservoir quality is poor due to both meteoric cementation and original mud dominated texture are the main reasons.
- Contact angle measurements showed that wettability varies between the different microfacies identified in the studied limestones.

## 6.2.Recommendations

- Isotope analysis of microsampled different types of the cement would reveal a better results, which would indicate the different diagenetic fluids and environment.
- Studying additional outcrops of the TMF in different localities would add greater derail to our understanding of the regional depositional environment and paleogeography of the TMF.
- Analysis of insoluble residue should be conducted as XRF results show the presence of Al, K, Si in samples that is not silicified which might indicate the presence of clay minerals whether authegenic or detrital.

# REFERENCES


Agbalaka, C. C., Dandekar, A. Y., Patil, S. L., Khataniar, S., & Hemsath, J. (2008, January). The effect of wettability on oil recovery: a review. In *SPE Asia Pacific Oil and Gas Conference and Exhibition*. Society of Petroleum Engineers.

AI-Husseini, M. (2009). Update to Late Triassic-Jurassic stratigraphy of Saudi Arabia for the Middle East geologic time scale. *GeoArabia*, 14(2), 145

Al Ibrahim, M. A. H. (2014). *Multi-scale sequence stratigraphy, cyclostratigraphy, and depositional environment of carbonate mudrocks in the Tuwaiq Mountain and Hanifa Formations, Saudi Arabia.* COLORADO SCHOOL OF MINES.

Al-Dabbas, M. A., Jassim, J. A., & Qaradaghi, A. I. (2012). Sedimentological and depositional environment studies of the Mauddud Formation, central and southern Iraq. *Arabian Journal of Geosciences, 5*(2), 297-312.

Al-Dhubaib, A. (2010). *Taxonomy and palaeoenvironments of Middle and Late Jurassic foraminifera and its associations of* Saudi Arabia (Doctoral dissertation, UCL (University College London)).

Al-Husseini, M. I. (1997). Jurassic sequence stratigraphy of the western and southern Arabian Gulf. *GeoArabia*, *2*(4), 361-382.

Al-Maamari, R. S., & Buckley, J. S. (2003). Asphaltene precipitation and alteration of wetting: the potential for wettability changes during oil production. *SPE Reservoir Evaluation & Engineering*, *6*(04), 210-214.

Alsharhan, A. S., & Magara, K. (1994). The Jurassic of the Arabian Gulf Basin: facies, depositional setting and hydrocarbon habitat.

Altree-Williams, A., Pring, A., Ngothai, Y., & Brugger, J. (2015). Textural and compositional complexities resulting from coupled dissolution–reprecipitation reactions in geomaterials. *Earth-Science Reviews, 150*, 628-651.

Amaefule, J. O., Altunbay, M., Tiab, D., Kersey, D. G., & Keelan, D. K. (1993, January). Enhanced reservoir description: using core and log data to identify hydraulic (flow) units and predict permeability in uncored intervals/wells. In *SPE annual technical conference and exhibition.* Society of Petroleum Engineers.

Anderson, W. G. (1986). Wettability literature survey-part 1: rock/oil/brine interactions and the effects of core handling on wettability. *Journal of petroleum technology*, *38*(10), 1-125.

Arkell, W. J., Bramkamp, R. A., & Steineke, M. (1952). Jurassic ammonites from jebel Tuwaiq, central Arabia. *Philosophical Transactions of the Royal Society of London. Series B, Biological Sciences*, 241-313.

Basyoni, M. H., & Khalil, M. (2013). An overview of the diagenesis of the Upper Jurassic carbonates of Jubaila and Hanifa formations, central Saudi Arabia. *Arabian Journal of Geosciences*, *6*(2), 557-572.

Beresi, M. S., Cabaleri, N. G., Löser, H., & Armella, C. (2017). Coral patch reef system and associated facies from southwestern Gondwana: paleoenvironmental evolution of the Oxfordian shallow-marine carbonate platform at Portada Covunco, Neuquén Basin, Argentina. *Facies*, *63*(1), 4.

BP. (2008). BP Statistical Review of World Energy, June. Retrieved from http://www.bp.com/liveassets/bp_internet/china/bpchina_english/STAGING/local_assets/downloads_pdfs/statistical_review_of_world_energy_full_review_2008.pdf

Brand, U., & Veizer, J. (1980). Chemical diagenesis of a multicomponent carbonate system--1: Trace elements. *Journal of Sedimentary Research*, *50*(4).

Bustin, R. M., Bustin, A. M., Cui, A., Ross, D., & Pathi, V. M. (2008, January). Impact of shale properties on pore structure and storage characteristics. In *SPE shale gas production conference*. Society of Petroleum Engineers.

Choquette, P. W., & Pray, L. C. (1970). Geologic nomenclature and classification of porosity in sedimentary carbonates. *AAPG bulletin*, 54(2), 207-250.

Coniglio, M. (1978). Dedolomitization. In *Sedimentology* (pp. 300-303). Springer Netherlands.

Coniglio, M. (1987). Biogenic chert in the Cow Head Group (Cambro- Ordovician), western Newfoundland. *Sedimentology, 34*(5), 813-823.

Craig, F. F. (1971). *The reservoir engineering aspects of water flooding* (Vol. 3, pp. 45-47). HL Doherty Memorial Fund of AIME.

Dabbagh, M. E. (2006). Diagenesis of Jurassic Tuwaiq Mountain Limestone, Central Saudi Arabia. *Journal of King Saud University (Science)*, *19*(1), 31-58.

Dandekar, A. Y. (2013). *Petroleum reservoir rock and fluid properties*. CRC press.

De Periere, M. D., Durlet, C., Vennin, E., Lambert, L., Bourillot, R., Caline, B., & Poli, E. (2011). Morphometry of micrite particles in cretaceous microporous limestones of the Middle East: Influence on reservoir properties. *Marine and Petroleum Geology*, *28*(9), 1727-1750.

Dromart, G., Garcia, J. P., Gaumet, F., Picard, S., Rousseau, M., Atrops, F., ... & Sheppard, S. M. (2003). Perturbation of the carbon cycle at the Middle/Late Jurassic transition: geological and geochemical evidence. *American Journal of Science, 303*(8), 667-707.

Edgell, H. S. (2006). *Arabian deserts: nature, origin and evolution*. Springer Science & Business Media.

Ehrenberg, S. N., & Nadeau, P. H. (2005). Sandstone vs. carbonate petroleum reservoirs: A global perspective on porosity-depth and porosity-permeability relationships. *AAPG bulletin, 89(*4), 435-445.

El-Asa'ad, G. M. (1989). Callovian colonial corals from the Tuwaiq Mountain Limestone of Saudi Arabia. *Palaeontology, 32*(3), 675-684.

El-Asa'Ad G.M.A. (1992). Late Callovian Ammonites from the Tuwaiq Mountain Limestone of Saudi Arabia. *Journal of King Saud University, 4*(2), 173-184.

El-Hedeny, M., Hewaidy, A. and Al-Kahtany, Kh. (2012) Shallow-marine trace fossils from the Callovian-Oxfordian Tuwaiq Mountain Limestone and Hanifa Formations, central Saudi Arabia. *Australian Journal of Basic and Applied Sciences, 6*(3): 722-733

El-Sorogy, A. S., Al-Kahtany, K. M., & El-Asmar, H. M. (2014). Marine benthic invertebrates of the upper Jurassic Tuwaiq Mountain Limestone, Khashm Al-Qaddiyah, central Saudi Arabia. *Journal of African Earth Sciences, 97*, 161-172.

EL-Sorogy, A. S., Almadani, S. A., & Al-Dabbagh, M. E. (2016). Microfacies and diagenesis of the reefal limestone, Callovian Tuwaiq Mountain Limestone Formation, central Saudi Arabia. *Journal of African Earth Sciences, 115*, 63-70.

Enay, R., Le Nindre, Y. M., Mangold, C., Manivit, J., & Vaslet, D. (1987). Le Jurassique d'arabie saoudite centrale: Nouvellesdonnées sur la lithostratigraphie, les paléoenvironnements, les faunes d'Ammonites, les âges et les corrélations. *Geobios, 20*, 13-65.

Enay, R., Mangold, C., Almeras, Y., & Hughes, G. W. A. G. (2009). The Wadi ad Dawasir" delta", central Saudi Arabia: A relative sea-level fall of Early Bathonian age. *GeoArabia, 14*(1), 17-52.

Fischer, J. C., Le Nindre, Y. M., Manivit, J., & Vaslet, D. (2001). Jurassic gastropod faunas of central Saudi Arabia. . *GeoArabia, 6*, 63-100.

Flügel, E., & Munnecke, A. (2010). Microfacies of carbonate rocks: analysis, interpretation and application. Springer-Verlag.

Folk, R. L. (1974). The natural history of crystalline calcium carbonate: effect of magnesium content and salinity. *Journal of Sedimentary Research, 44(*1).

Gill, B. C., Lyons, T. W., & Frank, T. D. (2008). Behavior of carbonate-associated sulfate during meteoric diagenesis and implications for the sulfur isotope paleoproxy. *Geochimica et Cosmochimica Acta*, 72(19), 4699-4711.

Giménez- Montsant, J., Calvet, F., & Tucker, M. E. (1999). Silica diagenesis in Eocene shallow- water platform carbonates, southern Pyrenees. *Sedimentology, 46*(6), 969-984.

Giménez-Montsant, J., Calvet, F., & Tucker, M. E. (1999). Silica diagenesis in Eocene shallow-water platform carbonates, southern Pyrenees. *Sedimentology*, *46*(6), 969-984.

Gregg, J. M., & Sibley, D. F. (1984). Epigenetic dolomitization and the origin of xenotopic dolomite texture. *Journal of Sedimentary Research*, *54*(3).

Halawani, M. A. (2012). Stratigraphic column for the Phanerozoic rocks of Saudi Arabia, a compilation and synthesis with comments. Saudi Geological Survey Technical Report SGS-TR-2001-3, 189.

Haq, B. U., Hardenbol, J., & Vail, P. R. (1988). Mesozoic and Cenozoic chronostratigraphy and eustatic cycles: SEPM Special Publication 42.

Hesse, R. (1989). Silica diagenesis: origin of inorganic and replacement cherts. *Earth-Science Reviews*, 26(1-3), 253-284.

Hewaidy, A. G. A., El-Moghny, M. W. A., Farouk, S., & El Kahtani, K. Microfacies and depositional environments of Jurassic (Callovian) Tuwaiq Mountain Formation in central Saudi Arabia. *Carbonates and Evaporites*, 1-16.

Hewaidy, A. G. A., Farouk, S., & El-Kahtany, K. M. (2016). Macrofauna and paleobiogeography of the Callovian Tuwaiq Mountain Formation in central Saudi Arabia. *Arabian Journal of Geosciences*, *9(*4), 1-24.

Hirasaki, G., & Zhang, D. L. (2004). Surface chemistry of oil recovery from fractured, oil-wet, carbonate formations. *SPE Journal*, *9*(02), 151-162.

Hughes, G. (2004). Middle to Upper Jurassic Saudi Arabian carbonate petroleum reservoirs: biostratigraphy, micropalaeontology and palaeoenvironments. *Geoarabia*, *9*, 79-114.

Hughes, G. (2008). Biofacies and palaeoenvironments of the Jurassic Shaqra group of Saudi Arabia. *Volumina Jurassica*, *6*, 33-45.

Hughes, G. W. (2009). Using Jurassic micropaleontology to determine Saudi Arabian carbonate paleoenvironments. *Geologic Problem Solving with Microfossils. SEPM, Special Publications, 93*, 127-152.

Imlay, R. W., & Jones, D. L. (1970). *Ammonites from the Buchia zones in northwestern California and southwestern Oregon* (No. 647-B). US Govt. Print. Off.,.

James, N. P., & Jones, B. (2015). *Origin of Carbonate Rocks*. John Wiley & Sons.

Jerauld, G. R., & Rathmell, J. J. (1997). Wettability and relative permeability of Prudhoe Bay: A case study in mixed-wet reservoirs. *SPE Reservoir Engineering*, *12*(01), 58-65.

Johansen, R. T., & Dunning, H. N. (1958). *Relative wetting tendencies of crude oils by the capillarimetric method* (No. TID/BERC-68). Bureau of Mines, Bartlesville, Okla.(USA). Bartlesville Petroleum Research Center.

Krause, F. F., Collins, H. N., Nelson, D. A., Machemer, S. D., & French, P. R. (1987). Multiscale anatomy of a reservoir: geological characterization of Pembina-Cardium pool, west-central Alberta, Canada. *AAPG Bulletin, 71*(10), 1233-1260.

Lahann, R. W. (1978). A chemical model for calcite crystal growth and morphology control. *Journal of Sedimentary Research, 48*(1), 337-347.

Lahann, R. W. (1978). A chemical model for calcite crystal growth and morphology control. *Journal of Sedimentary Research*, 48(1), 337–347.

Le Nindre, Y. M., Manivit, J., Manivit, H., & Vaslet, D. (1990). Stratigraphie sequentielle du Jurassique et du Cretace en Arabie Saoudite. *Bulletin de la Societe geologique de France, 6*(6), 1025-1034.

Leinfelder, R. R., Schlagintweit, F., Werner, W., Ebli, O., Nose, M., Schmid, D. U., & Hughes, G. W. (2005). Significance of stromatoporoids in Jurassic reefs and carbonate platforms—concepts and implications. *Facies, 51*(1-4), 288-326.

Li, K., & Horne, R. N. (2003, January). A decline curve analysis model based on fluid flow mechanisms. In *SPE Western Regional/AAPG Pacific Section Joint Meeting.* Society of Petroleum Engineers.

Lo, H. Y., & Mungan, N. (1973, January). Effect of temperature on water-oil relative permeabilities in oil-wet and water-wet systems. In *Fall Meeting of the Society of Petroleum Engineers of AIME*. Society of Petroleum Engineers.

Longman, M. W. (1980). Carbonate diagenetic textures from near surface diagenetic environments. *AAPG bulletin, 64*(4), 461-487.

Longman, M. W. (1980). Carbonate diagenetic textures from near surface diagenetic environments. *AAPG Bulletin, 64*(4), 461-487.

Loope, D. B., & Watkins, D. K. (1989). Pennsylvanian fossils replaced by red chert: early oxidation of pyritic precursors. *Journal of Sedimentary Research, 59*(3).

Loope, D. B., & Watkins, D. K. (1989). Pennsylvanian fossils replaced by red chert: early oxidation of pyritic precursors. *Journal of Sedimentary Research, 59*(3).

Lumsden, D. N. & Chimahusky, J. S. (1980). Relationship between dolomite nonstoichiometry and carbonate facies parameters. In SEPM Special Publication 28 (pp. 123 – 137.).

Lumsden, D. N., & Chimahusky, J. S. (1980). Relationship between dolomite nonstoichiometry and carbonate facies parameters.

Machel, H. G., & Hunter, I. G. (1994). Facies models for Middle to Late Devonian shallow-marine carbonates, with comparisons to modern reefs: a guide for facies analysis. *Facies, 30*(1), 155-176.

Maliva, R. G., & Siever, R. (1988). Diagenetic replacement controlled by force of crystallization. *Geology*, *16*(8), 688-691.

Manivit, J., Pellaton, C., Vaslet, D., Le Nindre, Y. M., Brosse, J. M., & Fourniguet, J. (1985). Geologic map of the Wadi al Mulayh quadrangle, sheet 22H, Kingdom of Saudi Arabia. *Saudi Arabian Deputy Ministry for Mineral Resources Geosciences Map, GM-92, scale, 1*(250,000), 1-32.

Manivit, J., Pellaton, C., Vaslet, D., Le Nindre, Y. M., Brosse, J. M., Breton, J. P., & Fourniguet, J. (1985). Geologic map of the Darma quadrangle, sheet 24 H. Kingdom of Saudi Arabia (with text): *Saudi Arabian Deputy Ministry for Mineral Resources, Jeddah, Geosciences Map GM*-101A, Kingdom of Saudi Arabia.

Manivit, J., Vaslet, D., Berthiaux, A., Le Start, P., & Fourniguet, J. (1986). Geologic map of the Buraydah quadrangle, sheet 26G. Kingdom of Saudi Arabia: DGMR, Geoscience Map GM-114A.

Mehrabi, H., Rahimpour-Bonab, H., Enayati-Bidgoli, A. H., & Navidtalab, A. (2014). Depositional environment and sequence stratigraphy of the Upper Cretaceous Ilam Formation in central and southern parts of the Dezful Embayment, SW Iran. *Carbonates and Evaporites, 29*(3), 263-278.

Milliman, J. D., Förstner, U., & Müller, G. (1974). *Recent sedimentary carbonates. P. 1, Marine carbonates*. Springer.

Milliman, J. D., Müller, G., & Förstner, U. (1974). Carbonates and the ocean. In *Recent Sedimentary Carbonates* (pp. 3-15). Springer Berlin Heidelberg.

Mirza, T. A., Mohialdeen, I. M., & Awadh, S. M. (2016). Iron mineralization in the Garagu Formation of Gara Mountain, Duhok Governorate, Kurdistan, NE Iraq: geochemistry, mineralogy and origin. *Arabian Journal of Geosciences, 9*(6), 1-13.

Montaggioni, L. F., & Braithwaite, C. J. (2009). *Quaternary coral reef systems: history, development processes and controlling factors* (Vol. 5). Elsevier.

Moore, C. H. (2001). Carbonate Reservoirs Porosity and Diagenesis in a Sequence Stratigraphic Framework: Porosity Evolution and Diagenesis in a Sequence Stratigraphic Framework (Vol. 55). Elsevier.

Moore, C. H., & Wade, W. J. (2013). *Carbonate reservoirs: porosity and diagenesis in a sequence stratigraphic framework* (Vol. 67). Newnes.

Morse, J. W., & Mackenzie, F. T. (1990*). Geochemistry of sedimentary carbonates* (Vol. 48). Elsevier.

Nelson, R. C., Lawson, J. B., Thigpen, D. R., & Stegemeier, G. L. (1984, January). Cosurfactant-enhanced alkaline flooding. In *SPE Enhanced Oil Recovery Symposium*. Society of Petroleum Engineers.

Okla, S. M. (1986). Litho- and Microfacies of Upper Jurassic Carbonate Rocks Outcropping in Central Saudi Arabia. *Journal of Petroleum Geology, 9*(2), 195-206.

Okla, S. M. (1987). Algal microfacies in upper tuwaiq mountain limestone (Upper Jurassic) near Riyadh, Saudi Arabia. *Palaeogeography, palaeoclimatology, palaeoecology, 58*(1), 55-61.

Phillips, M. C., & Riddiford, A. C. (1965). The Evaluation of Free Surface Energies of Solids from Contact Angle Measurements. *Zeitschrift für Physikalische Chemie, 47*(1_2), 17-19.

Poston, S. W., Ysrael, S., Hossain, A. K. M. S., & Montgomery III, E. F. (1970). The effect of temperature on irreducible water saturation and relative permeability of unconsolidated sands. *Society of Petroleum Engineers Journal, 10(*02), 171-180.

Powers, R. W. (1968). Saudi Arabia: Lexique stratigraphique international: Paris. France, *Centre National de la Recherche Scientifique, 3*, 171.

Powers, R. W., Ramirez, L. F., Redmond, C. D., & Elberg, E. L. (1966). Geology of the Arabian Peninsula. *Geological survey professional paper*, *560*, 1-147.

Rao, C. P. (1990). Petrography, trace elements and oxygen and carbon isotopes of Gordon Group carbonates (Ordovician), Florentine Valley, Tasmania, Australia. *Sedimentary Geology, 66*(1-2), 83-97.

Rao, C. P. (1991). Geochemical differences between subtropical (Ordovician), cool temperate (recent and Pleistocene) and sub polar (Permian) carbonates, Tasmania, Australia. *Carbonates and Evaporites, 6*(1), 83-106.

Ratcliffe, K., Wright, M., & Spain, D. (2012). Unconventional methods for unconventional plays: using elemental data to understand shale resource plays. *PESA News Resources*, 89-93.

Rausch, R., Simon, T., Al Ajmi, H., & Dirks, H. (2014). The scarp lands of Saudi Arabia. *Arabian Journal of Geosciences, 7*(6), 2437-2450.

Reid, R. P., & Macintyre, I. G. (2000). Microboring versus Recrystallization: Further Insight into the Micritization Process: CURRENT RIPPLES. *Journal of Sedimentary Research, 70(*1).

Sandberg, P. A. (1983). An oscillating trend in Phanerozoic non-skeletal carbonate mineralogy. *Nature, 305*, 19-22.

Sarg, J. F. (1988). Carbonate sequence stratigraphy.

Schlager, W. (2005). Carbonate Sedimentology and Sequence Stratigraphy, SEPM Concepts in Sedimentology and Paleontology Series no. 8. *Society for Sedimentary Geology (SEPM-SSG), Tulsa, Oklahoma*.

Schlumberger. (2007). Schlumberger Market Analysis. Retrieved from http://www.slb.com/~/media/Files/industry_challenges/carbonates/brochures/cb_carbonate_reservoirs_07os003.ashx

Sharland, P.P., Archer, R., Casey, D.M., Davies, R.G., Hall, S.H., Heward, A.P., Horbury, A.D. and Simmons, M.D., (2001). Arabian Plate Sequence Stratigraphy. *GeoArabia, Special Publication 2*, p. 45-60, 97-102.

Standnes, D. C., & Austad, T. (2000). Wettability alteration in chalk: 2. Mechanism for wettability alteration from oil-wet to water-wet using surfactants. *Journal of Petroleum Science and Engineering*, *28*(3), 123-143.

Steineke, M., Bramkamp, R. A., & Sander, N. J. (1958). Stratigraphic relations of Arabian Jurassic oil: Middle East.

Tang, G. Q., & Morrow, N. R. (1996). *Effect of temperature, salinity and oil composition on wetting behavior and oil recovery by waterflooding* (No. CONF-961003--). Society of Petroleum Engineers (SPE), Inc., Richardson, TX (United States).

Tiab, D., & Donaldson, E. C. (2015). *Petrophysics: theory and practice of measuring reservoir rock and fluid transport properties*. Gulf professional publishing.

Treiber, L. E., & Owens, W. W. (1972). A laboratory evaluation of the wettability of fifty oil-producing reservoirs. *Society of petroleum engineers journal*, *12*(06), 531-540.

Tucker, M. E., & Wright, V. P. (1990). Carbonate mineralogy and chemistry. Carbonate *Sedimentology*, 284-313.

Vail, P. R. (1987). Seismic stratigraphy interpretation using sequence stratigraphy: Part 1: Seismic stratigraphy interpretation procedure.

Vaslet D, Brosse JM, Breton JP, Manivit J, Le Strat P, Fourniguet J, Shorbaji H (1988) Geologic map of the Shaqra quadrangle, sheet 25 H, Kingdom of Saudi Arabia: *Deputy Ministry for Mineral Resources Geoscience Map GM*-120C, p 29

Vaslet, D., Al-Muallem, M. S., Maddeh, S. S., Brosse, J. M., Fourniquet, J., Breton, J. P., & Le Nindre, Y. M. (1991). Explanatory notes to the geologic map of the Ar Riyad Quadrangle, Sheet 24 I, Kingdom of Saudi Arabia. *Saudi Arabian Deputy Ministry for Mineral Resources, Jeddah. Geosciences Map*, 121, 1-54.

Vaslet, D., Delfour, J., Manivit, J., Le Nindre, Y. M., Brosse, J. M., & Fourniguet, J. (1983). Geologic map of the Wadi ar Rayn quadrangle, sheet 23H, Kingdom of Saudi Arabia. *Saudi Arabian Deputy Ministry for Mineral Resources Geologic Map* GM-63-A, 1.

Veizer, J. (1983). Chemical diagenesis of carbonates: theory and application of trace element technique.

Vijapurapu, C. S., & Rao, D. N. (2003, February). SPE Paper 80273, presented at the SPE Int. In *Symposium on Oilfield Chemistry*, Texas, USA.

Vijapurapu, C. S., Rao, D. N., & Kun, L. (2002, January). The effect of rock surface characteristics on reservoir wettability. In *SPE/DOE Improved Oil Recovery Symposium*. Society of Petroleum Engineers.

Wang, W., & Gupta, A. (1995, January). Investigation of the effect of temperature and pressure on wettability using modified pendant drop method. In *SPE Annual Technical Conference and Exhibition*. Society of Petroleum Engineers.

Warren, J. (2000). Dolomite: occurrence, evolution and economically important associations. *Earth-Science Reviews, 52*(1), 1-81.

Whittaker, J. E., Jones, R. W., & Banner, F. T. (1998). Key Mesozoic benthic Foraminifera of the Middle East. The Natural History Museum, Department of Palaeontology, London, 1-237.

Wilson, J. L. (1975). Carbonate facies in geologic history. Springer Science & Business Media.

Winefield, P. R., Nelson, C. S., & Hodder, A. P. W. (1996). Discriminating temperate carbonates and their diagenetic environments using bulk elemental geochemistry: a reconnaissance study based on New Zealand Cenozoic limestones. *Carbonates and Evaporites, 11*(1), 19.

Xuetao Hu, Fayang Jin, Hu Shuyong and Huang Jing (2017) Physics of Petroleum Reservoirs; Springer-Verlag Berlin Heidelberg

Youssef, M., & El-Sorogy, A. S. (2015). Paleoecology of benthic foraminifera in coral reefs recorded in the Jurassic Tuwaiq Mountain Formation of the Khashm Al-Qaddiyah area, Central Saudi Arabia. *Journal of Earth Science, 26*(2), 224-235.

ZIAUDDIN, M. (2007). Fundamentals of Wettability. *Schlumberger Oilfield Review*.

Ziegler, M. A. (2001). Late Permian to Holocene paleofacies evolution of the Arabian Plate and its hydrocarbon occurrences. *GeoArabia, 6*, 445-504.

# Vitae


Name : Mahmoud Mohammed Samir Desouky Nour El Yamani

Nationality : Egyptian

Date of Birth : 02nd March 1991

Email : mms.elyamani@gmail.com

Address : Nasr City, Cairo, Egypt


Academic Background : Geosciences

## Experience

**Teaching Assistant (01/03/2012–31/08/2013)**

**Ain Shams University - Geoscience Department, Cairo (Egypt)**

- Teaching lab sessions of undergraduate courses (Sedimentary petrology, sedimentology, structure geology, optical mineralogy, engineering geology, geological maps, geomorphology, metamorphic rocks, geochemistry)
- Administrative work related to accreditation of geoscience department